

**Alma Mater Studiorum – Università di Bologna**

**DOTTORATO DI RICERCA IN  
INGEGNERIA CIVILE, CHIMICA,  
AMBIENTALE E DEI MATERIALI**

**Ciclo XXIX**

**Settore Concorsuale di afferenza:** 08 A2

**Settore Scientifico disciplinare:** ING/IND 28

***Geostatistical modeling of ore deposits with transitional boundaries***

**Presentata da: Sara Kasmaeeyazdi**

**Coordinatore Dottorato**

*Prof. Luca Vittuari*

**Relatore**

*Prof. Stefano Bonduà*

**Correlatori**

*Prof. Giuseppe Raspa*

*Prof. Roberto Bruno*

*Prof.ssa Chantal de Fouquet*

Esame finale anno 2017



# **Abstract**

In mineral resources and ore reserves estimation, a crucial point is the geological domains that will be used for the modelling, as well as the type of boundaries between these domains. The most common geostatistical techniques are based on the assumptions of stationarity of the variable within estimation domains considered hard boundaries (sharp contact between geological units). However, in most cases, the geological mechanisms that generate a deposit are transitional -overlapping in geological units- in nature. In transitional boundary deposits, each geological zone has its own mineral grade distributions and spatial variability, but with an overlapping between geological zones. Hence, any method for estimation models, affects the mine planning with a significant sensitivity particularly in transition areas. Due to this point, the identification of the exact boundaries of mineralization is essential for an accurate estimate of resources. The objective of this dissertation is to develop a methodological framework to be used in presence of transitional boundaries. The methodological framework is introduced and then explained through a case study with transitional boundaries. Moreover, through a mining case study, it will be shown how choosing appropriate methodology for modelling variables and for interpreting the deposit geology will help to optimize parameters identification. The methodological framework in general allows decreasing the uncertainty in resources estimation and reserves selection. The method is general and can be used in other field of geoscience that incorporate numerical modelling, such as environmental modelling, petroleum or mining industry where complex geology deposits should be characterized.



# Contents

<b>ABSTRACT.....</b>	<b>3</b>
<b>ABBREVIATIONS .....</b>	<b>17</b>
<b>INTRODUCTION.....</b>	<b>21</b>
<b>PART I.....</b>	<b>26</b>
<b>1 BACKGROUND.....</b>	<b>26</b>
1.1 MOTIVATION OF THE STUDY: SECAHUN IRON MINE, ANOMALY XI-SOUTH	
33	
<b>2 CASE STUDY INTRODUCTION: SECAHUN IRON ORE DEPOSIT .....</b>	<b>38</b>
2.1 GENERAL INFORMATION .....	38
2.2 GEOLOGY OF SECAHUN ORE BODY .....	39
2.3 EXCAVATION AND MINING PROCEDURES .....	43
2.4 AVAILABLE DATA.....	45
2.4.1 <i>Borehole data</i> .....	46
2.4.2 <i>Blast hole data</i> .....	49
<b>3 DIFFERENT DATA SUPPORTS .....</b>	<b>54</b>
3.1 COMPOSING SAMPLES WITH DIFFERENT SUPPORTS .....	56
3.1.1 <i>Regularization method</i> .....	58
3.1.2 <i>Aggregation method</i> .....	60
3.2 THE THEORETICAL PUNCTUAL MODEL.....	61
3.3 APPLICATION TO THE CASE STUDY .....	64
3.3.1 <i>Regularization method</i> .....	65
3.3.2 <i>Aggregation method</i> .....	70
3.3.3 <i>Theoretical punctual model</i> .....	73
3.4 CROSS-VALIDATION .....	80
3.5 CONCLUSION.....	84
<b>4 ESTIMATION METHODS IN TRANSITIONAL BOUNDARIES.....</b>	<b>87</b>

4.1 LOCAL MODEL .....	88
4.2 GLOBAL MODEL.....	94
4.2.1 <i>Hypothesis of modeling: trend.....</i>	95
4.3 INCORPORATE GEOLOGICAL INFORMATION .....	98
4.3.1 <i>Indicator kriging method .....</i>	100
4.3.2 <i>Spatial transitions .....</i>	108
4.4 TOOLS TO IDENTIFY TRANSITIONAL BOUNDARIES .....	113
4.4.1 <i>Preferential relationship schemes .....</i>	113
4.4.2 <i>Contact plots .....</i>	119
4.5 BORDER EFFECTS .....	122
4.6 PARTIAL GRADE .....	123
4.7 VALIDATION OF ESTIMATIONS .....	127
<b>5 CONCLUSION.....</b>	<b>135</b>
5.1 DISCUSSION.....	135
5.2 FUTURE DEVELOPEMENTS .....	138
<b>PART II.....</b>	<b>140</b>
<b>6 FEASIBILITY OF GEOSTATISTICAL STOCKPILE CHARACTERIZATION</b>	<b>140</b>
6.1 INTRODUCTION.....	140
6.2 INTRODUCTION OF THE CASE STUDY: CHOGHART IRON ORE MINE .....	144
6.3 ORE DEPOSIT MODELLING .....	147
6.4 STOCKPILE MODELING.....	151
6.5 CONCLUSION.....	153
<b>REFERENCES.....</b>	<b>159</b>



## List of Figures

Figure 1. Schematic figures showing hard (left) and soft (right) boundaries ....	27
Figure 2. Location of Sechahun Iron Mine and important anomalies in central part of Iran .....	39
Figure 3. Simplified geological map of the Sechahun deposit, showing Anomalies X and XI modified after (NISCO, 1975). The thick lines are the cross-sections shown in Figure 4. ....	41
Figure 4. Simplified cross-sections of Anomaly XI, southern ore body (modified after NISCO, 1975) .....	42
Figure 5. Picture of Sechahun mine open pit, anomaly south-XI.....	44
Figure 6. exploration profiles and bore holes of two Sechahun ore bodies, north-XI and south-XI .....	45
Figure 7. Pseudo histogram of borehole samples obtained from Fe (%) and the histogram of length of relating samples .....	47
Figure 8. Pseudo histograms of borehole samples obtained from P (%) (on the left) and S (%) (on the right).....	47
Figure 9. Distribution of borehole samples in each geological unit (on the left) and scatter of sample lengths in different geological units (on the right) .....	48
Figure 10. Scatter plot between Fe(%) and P(%) (on the left) and scatter plot between Fe(%) and S(%) (on the right).....	49
Figure 11. Elevation Z=1585 m:of blast holes, (white: waste (no grade), yellow: waste (grade), Orange: poor zone, red: rich Zone); classified by cut-of grades	50
Figure 12.Changing blast holes locations according to the multiple data (a): all blast samples that each two points have equal concentration value; (b): calculating coordinates in the middle of two equal values; (c): putting the concentration value for the identified point.....	51
Figure 13. Histograms of blast hole samples obtained from Fe (%) –Left- and P (%) – Right.....	51

Figure 14. Scatter plots of Fe and P –Left- and variation of Fe in vertical direction– Right.....	52
Figure 15. Variograms over two different supports $w$ (small length) and $W$ (long length) illustrating relationship between support size and changing sample variograms .....	57
Figure 16. Core samples aligned along a bore hole (Journel and Huijbregts, 1991).....	58
Figure 17. Schematic example of regularization borehole samples in a 2.0 meter support (colors only identify different samples) .....	59
Figure 18. Schematic procedure of aggregation of samples into 2.0 meters ....	61
Figure 19. Schematic procedure of sample aggregation to 2.0 meters .....	62
Figure 20. Bar chart shows difference of average obtained from Fe (%) between regularized to 2.0 and 4.0 meters .....	67
Figure 21. Scatter plots showing effect of regularization on average of iron concentration Fe (%) .....	68
Figure 22. Comparison of vertical and horizontal sample variograms of Fe (%) following 2.0 meter regularization .....	68
Figure 23. Comparison of vertical and horizontal sample variograms of Fe (%) after 4.0 meter regularization .....	69
Figure 24. Comparison of vertical sample variograms of Fe (%) from aggregation at 2.0 and 4.0 meters.....	70
Figure 25. Comparison of vertical and horizontal sample variograms of Fe (%) for 2.0 meter aggregation.....	71
Figure 26. Comparison of vertical and horizontal sample variograms of Fe (%) for 4.0 meter aggregation.....	72
Figure 27. Comparison of vertical sample variograms of Fe (%) for 2 and 4.0 meter aggregation .....	72

Figure 28.Comparison of histograms of iron concentration in 2.0 (left) and 4.0 meter (middle) selected samples with original samples (right) .....	74
Figure 29. Comparison of two vertical ore body sections with 2.0 meter (black) and 4.0 meter (white) samples, showing the non-homogeneity of sampling with different lengths in the geological units .....	74
Figure 30. Vertical experimental variograms (black dots) and models (red line) for justification of Point-variogram in 2.0 and 4.0 meter aggregation.....	76
Figure 31. Flowchart of procedure to deduce theoretical punctual model from variogram models of 2.0 and 4.0 meter aggregation.....	79
Figure 32. Variogram models fitted on vertical experimental variograms obtained from 2.0 and 4.0 meter aggregation and the deduced theoretical punctual model.....	80
Figure 33. Geological cross section illustrating use of bore holes and blast holes in 3D geological modelling.....	89
Figure 34. Geological model in 3D indicating poor zone (orange) and rich zone (red) .....	89
Figure 35. Histogram and Sample variogram (black points) and the variogram model (red line) for regularized 2.0 meter samples residuals- poor zone .....	90
Figure 36. Histogram and Sample variogram (black points) and the variogram model (red line) for regularized 2.0 meter samples residuals- rich zone .....	91
Figure 37. Histogram and Sample variogram (black points) and the variogram model (red line) for regularized 2.0 meter samples residuals- metasomatite zone .....	91
Figure 38. An example of a geological section of the mine and estimation results obtained from local models (upper Figure) and zoom of three specific areas ( lower Figure).....	93
Figure 39. Histogram and vertical sample variogram (black points) and variogram model (red line) for regularized 2.0 meter samples.....	94

Figure 40. Scatter plots showing the iron variation in 3 directions (North-South, East-West and vertical directions), from regularization 2.0 m data.....	96
Figure 41. Histogram of Fe(%) residuals and sample variogram (black points) and variogram model (red line) for regularized 2.0 meter samples residuals ...	97
Figure 42. Sample variograms of indicators and Fe (%) (direct and cross variograms): Regularized 2.0 m samples .....	102
Figure 43. Section 9 showing ICK results .....	103
Figure 44. Section 11 showing ICK results .....	103
Figure 45. Section 13 showing ICK results .....	104
Figure 46. Residual sample variograms of indicators and Fe (%) (direct and cross variograms) for regularized 2.0 m samples .....	107
Figure 47. Practical inference of the parameter .....	110
Figure 48. Different possible situations for the Preferentiality Values .....	112
Figure 49. Cross indicator variogram divided by a single indicator variogram along the North-South direction.....	114
Figure 50. Cross indicator variogram divided by a single indicator variogram along the East-West direction .....	115
Figure 51. Cross indicator variogram divided by a single indicator variogram along the vertical direction .....	116
Figure 52. Preferential relationship schemes obtained after classification of positive preferentiality values, transitions in North-South direction, upper part recalls units above cut-off ( $Fe > 20\%$ ) and lower part recalls units below the cut-off ( $Fe < 20\%$ ).....	118
Figure 53. Preferential relationship schemes obtained after classification of positive preferentiality values, transitions in east-west direction .....	118
Figure 54. Preferential relationship schemes obtained after classification of positive preferentiality values, transitions in vertical direction .....	118
Figure 55. The general form of contact plots for a hard and soft boundary ....	120

Figure 56. Contact plot showing the mean value of Fe (%) in rich domain (left) and poor domain (right) at a distance (a) and contact plot showing the mean value of Fe (%) in poor domain (left) and metasomatite domain (right) at a distance (b).....	121
Figure 57. Contact plot showing the mean value of Fe (%) in rich domain (left) and metasomatite domain (right) at a distance (a) and contact plot showing the mean value of Fe (%) in waste domain (left) and metasomatite domain (right) at a distance (b).....	121
Figure 58. Cross variogram between indicator and partial grade divided by indicator variogram .....	125
Figure 59. Cross variogram between indicator and partial grade divided by indicator variogram .....	126
Figure 60. Histogram of true block values obtained from mean of blast holes (Left) and histogram of number of blast holes used for averaging block values .....	128
Figure 61. Maps of real block values obtained from mean of blast holes with optimum estimation method .....	132
Figure 62. Maps of ICK results with optimum estimation method for two excavated levels .....	137
Figure 63. Simple chart of numerical modelling procedure of stockpiles .....	143
Figure 64. Choghart iron ore mine in Iran and the Google map of the ore deposit and stockpiles.....	144
Figure 65. HP and LG stockpiles .....	145
Figure 66. Base map of blast hole data for five panels, classified according destination (High Phosphorous stockpile: Red; Low Grade stockpile: Yellow; Crusher Feed: Blue).....	146
Figure 67. Histograms of Fe (left) and P (right) concentration (%) for blast hole data from 5 panels .....	147

Figure 68. Experimental and cross variograms of Fe and P obtained from blast holes of five panels.....	148
Figure 69. Structural analysis of HP (estimated) blocks from 5 panels .....	150
Figure 70. Structural analysis of LG (estimated) blocks from 5 panels .....	150
Figure 71. Simplified flowchart of piling modelling from ore deposit .....	151
Figure 72. Structural analysis of cells grades of simulated HP pile in two orthogonal directions, N0 and N90 .....	152
Figure 73. Structural analysis of cell grades of simulated LG pile in two orthogonal directions, N0 and N90 .....	152
Figure74. Scheme of stockpiling procedure from the panels .....	154
Figure 75. Map of Fe (%) variability in HP (left) and LG (right) stockpile obtained by construction piling procedure .....	156
Figure 76. Grade-Tonnage curve for two simulated stockpiles .....	157

## List of Tables

Table 1. Statistical data in all geological zones .....	48
Table 2. shows 10 excavation plans (from 1650 to 1560 in depth) .....	52
Table 3. Statistical information of original and regularized data (2.0 and 4.0 meters regularized data).....	66
Table 4. Statistical information for original and aggregated data.....	71
Table 5. Parameters of two vertical variogram models of 2.0 and 4.0 meter aggregation.....	76
Table 6. Parameters of theoretical punctual model deduced from two variogram models of 2.0 and 4.0 m aggregation .....	78
Table 7. Results of cross-validation using different models for 2.0 meter support.....	81
Table 8. Results of cross-validation using different models for 4.0 meter support.....	81
Table 9. Scatter plot of original data and estimated values using aggregation model (2.0 m and 4.0 m targets) .....	83
Table 10. Results of cross-validation using different models for OK and UK methods.....	97
Table 11. Cross-validation results for five classes of borehole samples .....	104
Table 12. Total results of Cross-validation using two methods of CK and comparison with OK cross-validation results .....	105
Table 13. Total results of Cross-validation using two methods of CK and comparison with OK cross-validation results .....	105
Table 14. Statistical parameters of cross-validation obtained from two CK and UCK.....	107
Table 15. Scatter plots of cross-validation between real values (boreholes) and Fe (%) estimated by different kriging methods .....	108

Table 16. Preferentiality values; each cell contains one value per direction from top to bottom: N-S, W-E and vertical directions .....	117
Table 17. Scatter plots between real values (obtained from blast holes) and Fe (%) estimated by different kriging methods .....	129
Table 18. Statistical parameters between real values (obtained from blast holes) and Fe (%) estimated by different kriging methods.....	130
Table 19. Comparison of number of blocks with optimum estimation methods for three main geological domains; poor, rich and waste (include metasomatite zone) .....	133
Table 20. Optimum estimation method (minimum error) for three main geological domains; poor, rich and waste (include metasomatite zone) .....	136
Table 21. comparison of variogram parameters of structured (spherical/spherical) components in stockpiles and deposit blocks .....	155



# **Abbreviations**

Co-Kriging, CK

Copper, Cu

3Dimensional, 3D

High Phosphorous Stockpile, HP

Indicator Kriging, IK

Iron Concentration, Fe

Kilometer, km

Linear Model of Coregionalization, LMC

Low Grade Stockpile, LG

Million tons, Mt

Ordinary Kriging, OK

Partial Grade, PG

Phosphorous Concentration, P

Universal Kriging, UK

Universal Co-Kriging, UCK

Uranium, U

Zinc, Pb

National Iranian Steel Corporation, NISCO



## **Acknowledgements**

I would like to thank my supervisors Professors Eng. Roberto Bruno and Eng. Stefano Bonduà from University of Bologna “Alma Mater” and special thanks to Professor Eng. Giuseppe Raspa from University of Rome “La Sapienza” without whom this thesis would not have been possible. I would also like to thank Professor Chantal de Fouquet from Mines ParisTech, France.

I am grateful to Professor Jacques Rivoirard and Professor Helen Beucher from Mines ParisTech for their help on the application work and their suggestions regarding method and improving results.

I would especially like to thank Eng. Francesco Tinti and Eng. Sara Focaccia and Eng. Mohamed Mohy Elkarmoty from University of Bologna “Alma Mater” for their thorough review of this thesis.

Finally, I could not have gotten this far without the encouragement of my parents.



# INTRODUCTION

In many geo-engineering applications, as hydrocarbon reservoir production, mineral extraction, tunneling and underground storage or disposal of hazardous wastes, a characterization of the geology of the earth is required. In the mentioned applications, at least in the planning stages, one of the direct accesses to geology is provided by boreholes, which must be kept to a minimum number for economic and/or physical reasons (Dowd and Pardo-Igúzquiza, 2005). Obtaining accurate geological boundaries-exact borders of geological units- and assessing the uncertainty of these borders are crucial steps for any study in georesource field. For instance, in the case of mining, the uncertainty in the extent of an ore body can be reflected in a low reliability level in ore resource estimation. The borders between different geological units are traditionally interpreted as hard boundaries and it can be difficult to quantify uncertainty in the boundary and its impact on ore tonnage (Dowd and Pardo-Igúzquiza, 2005). One of the evaluation methods used for ore reserve estimation and geological boundaries is geostatistical methods.

Geostatistics proposed by Matheron (Matheron, 1971) as a scientific estimation method taking account structure and randomness inherent in any deposit. It is important to note that the origin of geostatistical studies is from the field of mining engineering (Krige, 1951). For the first time, an interpolation technique named “Kriging” was used to estimate a gold mine grade. Following this first application, the basis of the theory has been developed for general application by Georges Matheron. Matheron used Krige's innovative concepts and set them in a single powerful framework with his Theory of Regionalized Variables (Matheron, 1971). Originally developed for solving ore reserve estimation

problems, the techniques of Kriging spread in the seventies into other areas of the earth sciences. They are nowadays popular in many fields of science and industry where there is a need for evaluating spatially or temporally data.

One of the main points in geostatistical evaluations is that prior to estimation of any spatial variable in georesource fields, it is necessary to construct the conceptual geological model and/or the domain model and to represent and identify the constraints and borders of mineralization zone to be estimated. This is usually a semi-automatic process, but generally requires a confining shape in which to estimate the mineralization zone. Hence, the determination of the boundary separating ore and waste/ or between geological units is an important aspect in ore reserve estimation because incorrect assumptions of stationarity can lead to a significant bias in the final resource estimation model. In statistics and geostatistics studies, stationary means that the distribution of a variable is invariant under translation. In the same way, a stationary random function is homogeneous and self-repeating in space, which means for any increment ( $h$ ) in the space, the distribution of the variable remains the same (Armstrong, 1998).

Estimation with hard boundaries is straightforward since only the samples within the domain are used. Hard boundaries mean that there is a sharp or abrupt between borders of geological units and therefore there is no continuity between variables in adjacent geological units. However, in many applications, the variables at either side of a boundary are not independent and there are some overlapping and continuity between them. Besides, the boundary may be defined by a change in the local mean grade, which is usually gradational rather than abrupt, and named soft or transitional boundaries<sup>1</sup>.

Soft boundaries allow variables from multiple domains to be used in the estimation of each domain. Common practice is to share samples within a given

---

<sup>1</sup> Two expressions of soft and transitional boundaries have the same meaning in this dissertation

zone of influence of one domain over the other (Larrondo and Deutsch 2004). Samples from different domains are treated equal to those within the domain, that is, the same mean; variance and covariance model from samples within the domain are assumed. This generally has the effect of changing the representative statistics of the domain of interest. This corruption of the final variables, especially in the transition zones, often dissuades practitioners from using soft boundaries. Therefore, for deposits with soft boundaries, the geological constraints are gradual and a much more careful treatment is required when estimating using geostatistical tools (Larrondo and Deutsch 2004). However, the following features of modelling soft boundary deposits have not been dealt with an accomplished model in the literature in depth. Hence, the milestones given below are the major contributions from this study:

- Segmentation, defining domains and choosing the best input data set for global/local estimations;
- Testing and proposing methods to face the problem of integrating samples and non-homogenous data, as we are dealing with samples with different supports;
- Testing different variogram models to reflect accurately global/local uncertainty (proposing the theoretical punctual model in addition to the sample variogram models);
- Comparison of different methodologies for prediction of the best result in a specific deposit and investigate the best locally/global adaptive methodology;
- Prediction of the optimum parameters to produce the best efficiency in each process based on the geostatistical modelling;
- Assessment of sensibility of each sector and indicating the best model for mine design and planning.

All the mentioned steps are essential for the understanding and development of geostatistical models for the particular case of transitional boundaries.

This work has developed a framework for estimation in case of transitional boundaries. A case study of a metasomatite iron ore deposit, with complex geology and transitional boundaries, is estimated using the developed framework. The developed framework is integrated with methodologies introduced in recent literature and some novel approaches are proposed. In this case, the variable modelling is adapted by the geological modelling. Domains are defined by a combination of geostatistical means. In addition, by testing different models in the estimation methodologies through transitional boundaries, the investigation of the most coherent model is possible.

In each part of this work, the theory is explained and then applied through the case study. Although, generally, each case study is distinguished by its specific geology and particular distribution of variables, the procedure considered for geostatistical modelling and proposed methods and tools in this work can be used in any other application (mining, petroleum environmental, etc.).

This thesis is structured through two parts. In part one; it starts with a background Chapter, where the topic of the research is described. Chapter 2 describes the case study and provides some general information about the iron mine, about the difficulties occurred in geological interpretations and reserve estimation, and the necessity of deepening the studies. Chapter 3 describes the first step of geostatistical modeling for reserve estimation particularly with transitional boundaries: data analysis, integrating samples for variable spatial analysis, statistical studies and their importance on variogram modelling and finally choosing the appropriate variogram model. All steps are developed through the mentioned case-study demonstrating applicable points through the

procedures. The procedures in this Chapter are done with programming in FORTRAN (FORTRAN software, n.d).

In Chapter 4 different methods are applied to estimate the ore body and particularly transition areas using ISATIS software (ISATIS software, n.d), and the results are validated using blast hole data, considered as “true data”. In Chapter 5 the conclusions of this research are discussed.

Part two of the thesis is described in Chapter 6, as a small work on the geostatistical characterization of stockpile with an example on an iron stockpile.

# **Part I**

## **1 BACKGROUND**

To generate a geological model in ore reserve estimation, the determination of the exact lithological and mineralogical domains is fundamental. Identification of geological domains should represent the estimator's best knowledge of the genesis of the deposit. Consequently, researcher focused to develop geostatistical methods to decrease the geological model uncertainty nearby boundaries.

Geostatistical modelling depends on the type of variable to be estimated. In general, in different fields of geoscience, we can resume it in several steps: (Chiles and Delfiner, 2012, Journel and Huijbregts, 1991, Clark, 1977, Armstrong, 1998, Wackernagel 2003).

- I) Preliminaries and statistical studies: collecting data and available information, uni/multivariate statistical studies, trend analysis etc.;
- II) Structural analysis: study of the main features of the regionalization, preliminary checking of the data and deep study of the problem, calculation of the experimental variogram and fitting of a mathematical model, cross-validation, and choose of the best model to evaluate the variable;
- III) Kriging using different methods: choosing appropriate geostatistical tools such as ordinary kriging, simple kriging, indicator kriging, disjunctive kriging, etc.;
- IV) Validating results: in the case of availability real data, the estimated results can be validated with real data.

In many applications, it is possible to define geological domains for resource estimation, considering several types of boundary conditions. However, in many literatures (Larrondo and Deutsch, 2004), domain boundaries are often referred to as either ‘hard’ or ‘soft’ (Figure 1). As mentioned, hard boundaries are considered when an abrupt change in average grade or variability occurs at the contact between two domains, such as coal seams or sedimentary zinc deposits. In deposits where the disseminated mineralisation has a gradational nature, such as some porphyry Cu-Au deposits or massive iron deposits, grades change transitionally across a boundary and the contact is referred to as a soft boundary (Larrondo and Deutsch, 2004).

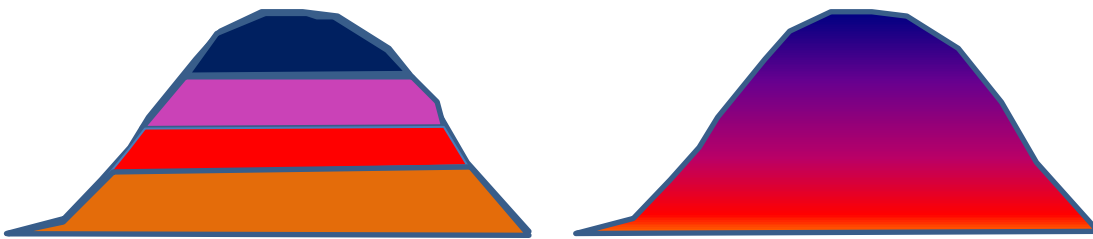


**Figure 1.** Schematic figures showing hard (left) and soft (right) boundaries

Soft boundaries are found in several types of deposits due to the transitional nature of the geological mechanisms involved in the formation of a deposit. There is often some degree of overlapping between geological domains. Nevertheless conventional grade estimation usually treats the boundaries between geological units as hard boundaries. This is primarily due to the limitations of current evaluation methods and procedures. So, considering the transitional boundaries fields -as an example- lead to investigate appropriate modelling approaches.

When considering resource estimation and reserve selection with a geostatistical block model, there are two main sources of uncertainty due to sparse sampling:

- The uncertainty in the mineral variable distribution which controls the quality of ore found within each block of the model, and
- The uncertainty in ore-body boundaries identification, which discriminates mineralized ore from un-mineralized waste.

A number of techniques currently exist for boundary modelling. A brief review is provided in the following; however, the literature is vast and encompasses many case studies. Note that in any case study, the used methods of modelling and estimation are according to the available data, genesis and geological information of the regarded area and the target point of the study.

Beyond the linear basic geostatistical methods used for reserve evaluations such as ordinary kriging (OK), some probabilistic tools (such as indicators) are exploited in some applications to develop the geological and mineralised models (Dimitrakopoulos and Dagbert, 1993; Soares 1992). In mentioned researches, the use of indicators (the means to model qualitative variables) such as multiple lithology types was studied. Lithology types as indicator variables are defined sequentially. As a result, indicator type modelling approach was implemented to sequentially generate models of qualitative variables, using both indicator kriging and indicator conditional simulation (Dimitrakopoulos and Dagbert, 1993). In geostatistics, simulation is the realization of a random function that has the same statistical features as the sample data used to generate it (Chiles and Delfiner, 2012). In their work, Chiles and Delfiner introduced two examples: (i) estimating the lithology of a mineral deposit; (ii) simulating the lithofacies of a reservoir (Dimitrakopoulos and Dagbert, 1993). As another example, Gossage (1998) has used indicator kriging (IK) in an

application for a mesothermal gold deposit, which was interpreted as being both structurally complex and having multiple controls on the distribution of the gold mineralization. The geological data investigated includes lithology, alteration and veining, which had been reviewed both independently and in conjunction with geochemical drilling data. The results of the IK studies have been compared with the geological/mineralisation model and the advantages of the IK approach have also been briefly discussed (Gossage, 1998). In some other case studies, based on a probability criterion, IK methods have performed to objectively model the geometry of geological zones (Marinoni, 2003, Gholamnejad et al., 2010, Kameshwara and Narayana1, 2015). Gholamnejad (2010) suggested the use of geostatistical method of IK to determine the boundary of ore body in Choghart iron mine of Iran. However, in this study the cut-off grade is assumed in terms of the iron content mode and to identify boundaries. Cut-off grade is the lowest grade of the mineralized material considered economically exploitable and depends on many parameters (Cairns and Shinkumab, 2004).

The estimated probability according to the selected cut-off identified the blocks inside the ore body and the wastes (Gholamnejad et al., 2010). Hence, in the presented applications the estimation results of different geological units could be improved using IK, but with no exact consideration of overlapping between units.

Larrondo and Deutsch (2004) proposed to use a Linear Model of Coregionalization (LMC) to evaluate grades using data from adjacent rock types. The LMC approach assumes the linear model of variogram in the case of multivariate variables. Although the LMC is traditionally used to characterize the spatial variability of several petro-physical parameter of one rock type, it has shown that can be applied to model the spatial variability of one property

across the boundary between several rock types (Larondo and Deutsch 2004). The proposed methodology was applied to a synthetic deposit and compared to the conventional approach of modelling, using hard boundaries. The method has provided an appealing alternative to capture grade distribution for deposits where complex contacts between different rock types exist. Furthermore, it has improved the resource estimation by reducing the uncertainty in transitional zones around boundaries. This method was showed using a synthetic deposit.

Ortiz and Emery (2005, 2006) proposed to estimate grades within geological domains, using several methods and compared them through a case study on a copper mine. For instance: OK considering hard boundaries between geological domains; OK omitting the geological boundaries; traditional ordinary Co-Kriging (CK) of the grades assayed in different domains; OK within dilated geological domains, that is, incorporating samples from adjacent domains up to a given radius from the boundary of the domain being considered. In their case study, the estimations are performed using a set of exploration data (drill hole samples) and results are validated using a set of production data (blast hole samples collected for grade control).

Results of their research has indicated that kriging with dilated domains has more coherent results than OK using hard boundaries or no boundaries and better than the CK approaches. It therefore appears as a simple alternative to global kriging (without considering the geological domains) and allows accounting for changes in the grade average, dispersion and spatial continuity with the geological characteristics of the deposit.

Besides estimation approaches, another approach for soft boundaries deposits is plurigaussian simulation (Emery et al. 2008). Simulation is simply a realization of a random function selected in the set of all possible realizations (Chiles and Delfiner, 2012). Plurigaussian simulation allows constructing lithofacies or rock

type models that reproduce the contacts between facies in accordance with the geologist's interpretation. Its implementation requires inferring the local facies proportions. There is a variation of the plurigaussian models, in which the facies proportions are represented by random fields. The realizations can be made conditional to soft geological information to account for local changes in the facies proportions. The model is illustrated via a case study of a porphyry copper deposit where four gaussian random fields are simulated conditionally to drill hole data and to constraints on the probability of finding a given facies at specific locations (control points) in the deposit. Then two fields of the copper deposit are truncated using the random thresholds defined by the last two, generating a three-facies model. The proposed random proportion model proves to be simple to use and to account for spatial variations of the geological characteristics and for the uncertainty in the facies proportions. As mentioned approaches have performed only on copper deposits, testing other types of deposits with different genesis and mineralogy can show the benefits of each method.

The potential field method is another approach to build geological models (Calcagno et al. 2008) and can be helpful for interpretations from the geologist (Fitzgerald et al. 2009). The original method has been developed to model geology using the location of the geological interfaces and orientation data. The orientation data, i.e. dip measurements, are not necessarily located on the geological interfaces. The orientation data can represent stratifications or foliations related to the contacts. Both types of data are Co-Kriged to estimate a continuous 3dimensional (3D) potential-field scalar function used to describe the geometry of the geology. Nonetheless, this method explains separate geological series with no referring to the particular case of transitional series.

Séguret (2011, 2012) in his work focused on mineral deposits consisting of geological bodies whose metal grades have different characteristics in space in terms of distribution and variogram. He mentioned that in such deposits estimating grades by OK may produce unrealistic spatial continuity. His paper proposes a method based on the indicators of the geological objects (in his work called units) and their multiplication with the metal grade. He illustrated his approach by an application to a porphyry copper deposit. According to the existence of border effect phenomena and transition analyses between geological domains (Rivoirard 1994), by multiplying indicator functions and metal grades, the concept of the Partial Grades (PG) method is developed (Séguret 2011).

The method is based on the CK of partial grades variables, allowing for unit specificities coherently. The case study on the copper deposit showed some improvement compared to kriging, depending on the partial grades between geological units and the spatial behaviour of the grades inside each unit. Séguret mentioned that the partial grade approach should be tested in a deposit that presents important border effects. The partial grade method is tested on the three porphyry copper deposits (Cu), and on a zinc deposit (Pb) in Peru. However, none of the tested case studies have encountered an important border effect phenomena where this method has been applied so far (Séguret 2012).

Lillah and Boisvert (2012) have referred to the uncertainty in the geological boundaries as a critical point for effective ore resource and reserve estimation. They have introduced the Local Varying Anisotropy field to consider stochastic modelling of the ore boundary with a distance function. Implementing locally varying anisotropy kriging retains the geologically realistic features of a deterministic model while allowing for a stochastic assessment of uncertainty (Lillah and Boisvert, 2012).

Due to the presented methods and tools, techniques have applied in various case studies with different purposes. However no specific method highlighted a methodological framework able to guarantee a correct and efficient method, necessary for getting the best estimation of a variable distribution in case of a complex geological deposit with transitional boundaries.

## 1.1 MOTIVATION OF THE STUDY: SECHAHUN IRON MINE, ANOMALY XI-SOUTH

In all georesource fields, it is necessary to define the geometric dimensions of resources prior to design and economic planning. For instance, in the mining projects definition of the geological units are based on the geological knowledge of the ore body and on sample information. Sample information can be obtained from two main sources: indirect methods (such as geophysics) and direct methods such as exploration-drilling grid. The first step in resources estimation is an exploratory analysis aimed at understanding the characteristics of the available data and identifying homogeneous geological domains within the deposit, according to the spatial continuity of grades and the geological features such as lithology, mineralogy and alteration. Once the geological model is as complete as the available data and knowledge of the setting and genesis of the mineralization allow, the data should be classified according to its domain.

For the Sechahun iron anomalies, geological studies and reserve estimation researches are done by geologists and mining engineers of the mining sector in Iranian Central Company. The ZaminKav Company (2010-2013) did reserve estimation of the Sechahun iron mine and their results were published in 2014.

Geological domains were defined by a combination of statistical and geostatistical means, in addition IK by using the cut-off grade method (Kasmaee et Torab, 2014). In Sechahun iron ore deposit as a result of metasomatic replacement of host rock by iron-rich hydrothermal fluids (Moore and Modabberi, 2003), the geological boundaries can be considered as gradual or soft boundaries, requiring the use of a specific approach.

The 3D geological model and reserve estimation of Sechahun iron ore were constructed by drill holes at 50 m average core drilling spacing and also available 3 m.4 m.10 m (length) blast hole data set from 10 benches within the open pit. According to the recent studies published for reserve estimation of the Sechahun iron mine, borehole samples with different lengths were composited into 2.5 m sample lengths (Kasmaee et Torab 2014). Then, borehole samples are mixed with blast hole samples which have 10 meters sample lengths.

In the mentioned study (Kasmaee et Torab, 2014), the reserve estimation of anomalies was done by using borehole data and available blasthole samples and by applying OK for the two main geological units, Poor and Rich zones. Due to the bimodal distribution of Fe % data, the two main geological units (Poor and Rich) are estimated separately with two different variogram models. However, for indicating the Sechahun iron ore boundaries some difficulties raised. The main difficulty emerged when estimating recoverable resources for poor and rich ore zones especially near the grades measured at either side of boundaries.

Comments present in the mentioned work (Kasmaee et Torab, 2014) about this ore body demonstrate the necessity of a deep research study in this dissertation. In particular:

- 1) The two groups of data with different volumes (supports) (boreholes with composited length of 2.5 m and blast holes with 10 m length) are

mixed in the reserve estimation of anomaly XI south. This mix is not acceptable according to the geostatistical studies, which need data with the same volumes (support).

- 2) Geostatistical estimation is done for the two main geological units (Poor and Rich zones) using two local variogram models (Poor and Rich variogram models). In this way, two nearby blocks near the boundaries can have remarkable difference in the estimated values. This is because of considering hard boundaries between geological units and so using independent models, which for this ore body seems not working properly. This comment is according to the final comparisons with blast holes data from 10 excavation benches (Kasmaee et Torab, 2014).
- 3) To face with the second uncertainty of the estimation results, developing the geological model and a comparison with the traditional geological model (defined by geologists according to the geological constraints) was performed. Multiple indicator kriging for iron grade as the main variable was shown to be a viable approach to estimate poor and rich resources in Sechahun deposit, especially when boundaries are not sharp and show a gradational transition. This technique provides a novel method for increasing the productivity of senior geoscientists leading to a faster and better 3D modelling of ore bodies. In this work, MIK was used in order to determine the ore-waste and also the poor-rich contacts in Sechahun iron deposit (Kasmaee et Torab, 2014). However, the cut-off grade is considered as threshold to choose final boundaries. Moreover, there is no deep study on boundaries and their characteristic on grade variability.

Hence, due to lack of studies for Sechahun deposit, re-estimation of the ore body would be a benefit not only as a complex example for a dissertation to develop the geostatistical modelling, but also as an economic aspect to improve

the geological interpretations and mining procedures in Bafgh district. The methods and approaches proposed in each step of this work can be used for any other case with similar geological formation or in any case of transitional boundaries.

According to the mining plan and available data in Sechahun iron mine, the XI-south anomaly is studied in this dissertation.

The first motivation is deepening the studies on the borehole samples and facing with general problems of data. Data with different supports as a general problem in many examples should be studied. Then through to the structural analysis, different methods for focusing on transitional boundaries should be developed.

Blast hole data as an added value can be used for validating estimation and methods used for ore body evaluations. Considering blasts averaged in each block as the real values, the estimation results can be validated.



## **2 CASE STUDY INTRODUCTION: SECAHUN IRON ORE DEPOSIT**

### **2.1 GENERAL INFORMATION**

There are more than 80 identified magnetic anomalies in the Bafq mining district, and the region is believed to host over two Giga tons of iron oxide ore (Daliran, 1999). An anomaly is a geologic feature or structure that departs markedly from its surrounding environment with respect to composition, texture, or genesis (Xinbiao and Pengda, 1998). The Bafq mining district is in central Iran, 12 kilometer (km) northeast of Bafq town and 125 km southeast of Yazd city. Most of the deposits are unexploited or only partially mined (Moore and Modabberi, 2003) and among these magnetic anomalies, Choghart, Chadormalu, Sechahun and Esfordi are mined. The Sechahun iron deposit is located 50 km northeast of Bafq and 170 km east of Yazd in central Iran (Figure 2). The Sechahun anomaly is blind, covered by conglomerate, young terraces, and gravel fans. Geophysical methods and extensive drilling have explored this deposit. The deposit is divided into two parts (north and south ore bodies) with a total reserve of about 140 Million tons (Mt) low-grade iron ore with an average grade of 36% iron concentration (Fe).

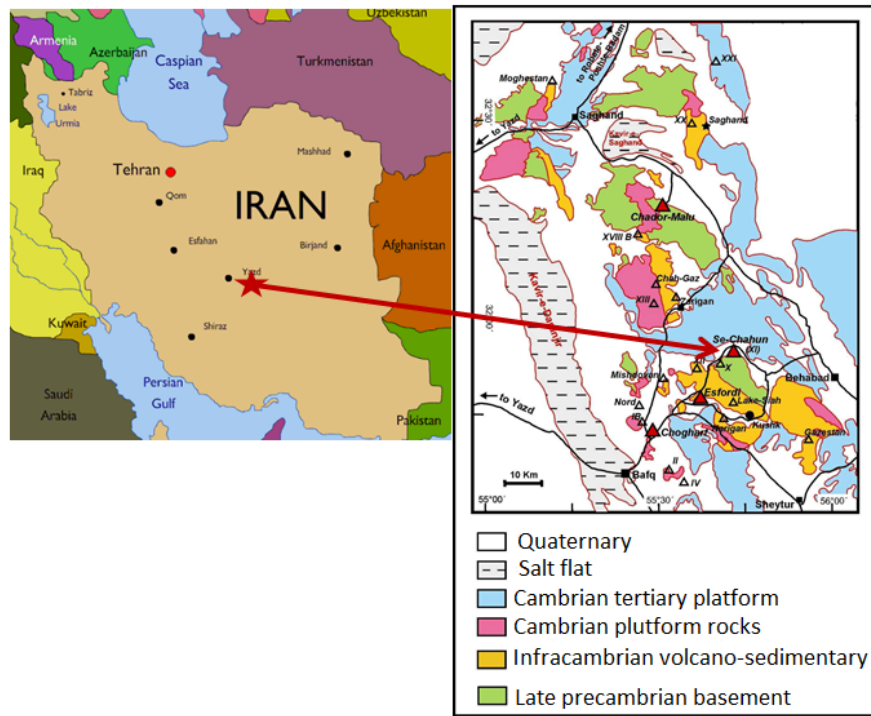


**Figure 2.** Location of Sechahun Iron Mine and important anomalies in central part of Iran

## 2.2 GEOLOGY OF SECHAHUN ORE BODY

The origin of Sechahun iron deposit and other similar iron oxide deposits in the Bafq mining district is like their counterparts in the rest of the world. This has been the subject of continuing controversy for local geologists with the difference that the controversy has been fuelled by the lack of absolute age determinations, accurate isotopic and fluid inclusion studies, and reliable analytical data. Magnetite is the main mineral in most of important iron ore bodies in Bafq (Moore and Modabberi, 2003). The central Iran consists of a complex set of volcano-sedimentary rocks (rocks consists of volcanic and sedimentary material), which hosts the most important iron oxide-apatite, Pb-Zn (lead and zinc) and U (uranium) ore deposits in Iran (Bonyadi et al. 2011).

The iron ore deposits of the Bafq district are associated with volcano-sedimentary rocks and high-level intrusions, and have a sulfide-poor mineral assemblage of low-titanium magnetite with varying but characteristic amounts of fluorapatite and actinolite. This assemblage is similar to the iron ore deposits of the Kiruna district in northern Sweden, whence such ores are known as “Kiruna-type” (Moore and Modabberi, 2003).

The origin of these deposits, similar to their counterparts of the Kiruna-type systems, is controversial (Borook et al., 1998, Frietsch, 1978, Nyström and Henriquez, 1994). Several different genetically models, from carbonatic, to iron ore magma (intrusion or volcanic) to metasomatic replacement were proposed (see e.g., Samani, 1993; Daliran, 1999; Förster and Jafarzadeh, 1994; Mücke and Younessi, 1994; Daliran, 2002). Metasomatic process is a chemical composition of a rock, which involves the introduction and/or removal of chemical components as a result of the interaction of the rock with aqueous fluids (solutions) (Zharikovetal., 2004). These different interpretations may firstly derive from the complexity of the ore deposit system, but can also come from the lack of accurate dating of the ore, and insufficient geochemical investigations. For instance, it is not exactly clear in which geotectonic regime these deposits formed, and which the relationship of geotectonic setting and ore formation could be.

The Sechahun deposit is composed of two major groups of ore bodies called the X and XI anomalies (National Iranian Steel Corporation: NISCO, 1975). Anomaly XI occurs 3 km northeast of Anomaly X (Figure 3). Each anomaly consists of two or three smaller tabular to lens shaped ore bodies (Figure 3) in association with many other small bodies.

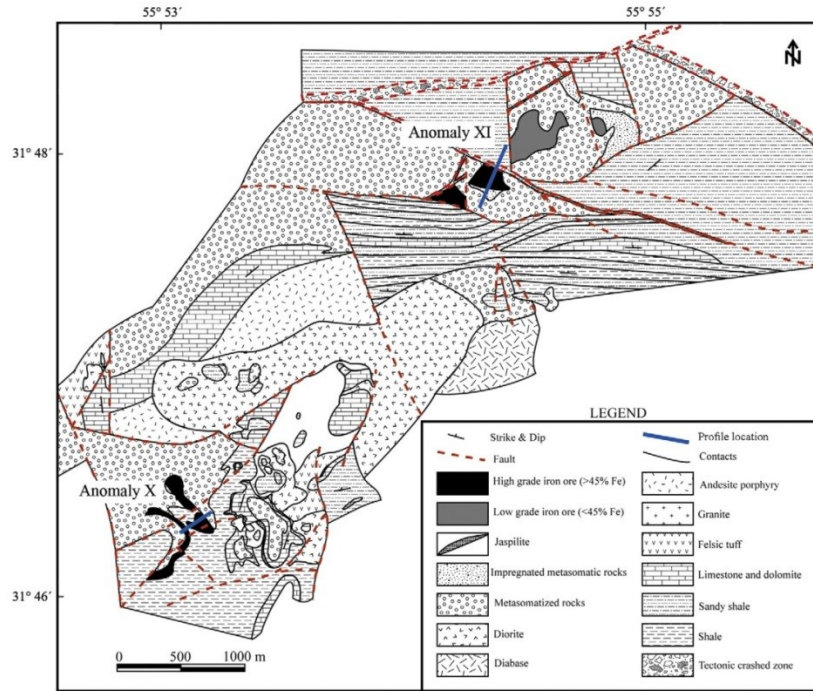


**Figure 3.** Simplified geological map of the Sechahun deposit, showing Anomalies X and XI modified after (NISCO, 1975). The thick lines are the cross-sections shown in Figure 4.

The mineralization is hosted by altered rhyolitic tuff (extrusive igneous rock) and intercalated shallow-water sandstone, dolomitic limestone and shale, representing the middle succession of the Saghand Formation (Samani, 1993). A persistent jaspilite horizon (banded compact siliceous rock) is present in the east of Anomaly X. Most mineralization occurs in sedimentary rocks that are stratigraphically 200 m below this jaspilite, and a relict, variably brecciated, sedimentary banding persists in parts of Anomaly X. The host rocks and the ore bodies are cross cut by E–W-trending normal faults. In addition, late E–W-oriented, unaltered dolerite and dioritic dikes locally crosscut the ore bodies and the alteration (Bonyadi et al., 2011) which is shown in Figure 4.

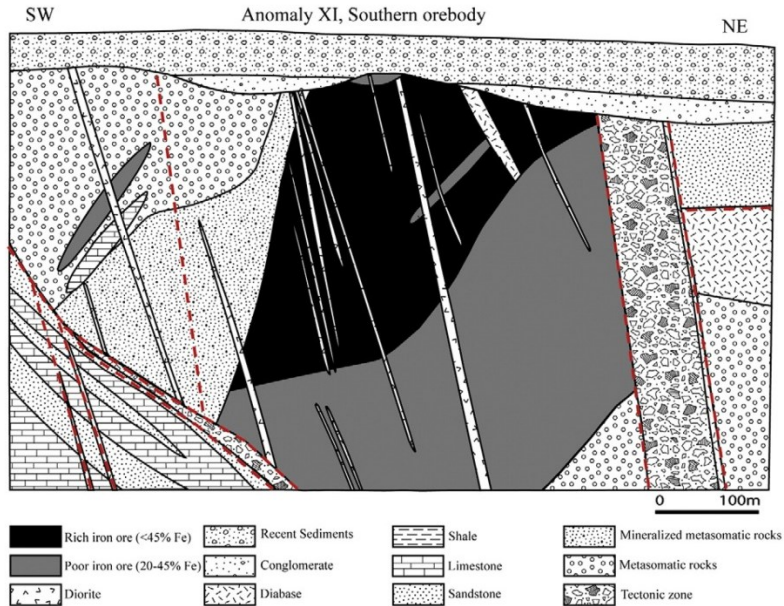


**Figure 4.** Simplified cross-sections of Anomaly XI, southern ore body (modified after NISCO, 1975)

The Anomaly XI ore bodies contain 89% of the ore reserves (average grade of 36–37% Fe), although the massive (with minor banded) magnetite–actinolite ore in Anomaly X has a higher grade (up to 67% Fe; NISCO, 1975; Förster and Jafarzadeh, 1994). The ore in Anomaly XI has a lower phosphorus content (0.08 wt.% P) than that of Anomaly X (0.13 wt.% P).

The main iron mineral is magnetite, however all gradations towards hematite (martitization) can be recognized. The volcano-sedimentary host rocks have been pervasively altered and the original chemistry of these rocks is strongly modified by metasomatic alteration. These strongly altered rocks which are locally named metasomatite are widespread at the deposit and show a gradual transition toward poor iron ore. Several diabasic dikes cut the ore body and the metasomatite country rock. The plain that surrounds the ore body and its metamorphosed intrusive and volcanic country rocks are composed of Quaternary formations and recent alluvium, of fine grained sand and gravel, magnetite boulders, gypsum and intrusive fragments.

Based on previous studies and documents, the different types of Sechahun iron ore are:

- 1) High-grade magnetite or rich iron ore ( $(\text{Fe}) > 45\%$ );
- 2) Oxidized high-grade magnetite (hematitized);
- 3) Low-grade magnetite or poor iron ore ( $(\text{Fe}) < 45\%$ ).

## 2.3 EXCAVATION AND MINING PROCEDURES

Sechahun anomalies are located at about 1700 m above sea level. Anomaly XI is divided into two parts (north-XI and south-XI ore bodies) with a total reserve of about 140 Mt iron ore with an average grade of 36% for Fe. The mine is designed on the basis of two separate open pits (north and south pits). The south pit applies selective mining method; due to thick overburden, the north pit has a relatively high stripping ratio (the amount of waste material that should be removed to extract a given amount of iron in this mine) and it still is not excavated. The mineable reserve of the Sechahun deposit (both pits) has been classically estimated to be 106 Mt with a stripping ratio (W/O) equal to 2.48/1. South ore body is more complex geologically and discrimination between boundaries is highly sophisticated; for these reasons, it is the object of this study (Figure 5). This anomaly has the length of about 1200 meter and contains 89% of the ore reserves (Bonyadi et al., 2011).



**Figure 5.** Picture of Sechahun mine open pit, anomaly south-XI

The exploration on the deposit has been performed by vertical boreholes at 50 m average core drilling spacing through 10 parallel profiles orthogonal to the extension of the ore body (Figure 6). The estimated geological reserve is 64 Mt based on a 20% cut-off grade which 51.3 Mt is mineable. Conventional open pit mining methods are used to extract at the rate of 3 million tons of iron concentration (Fe) rocks per year. The open pit mine is a truck-and-shovel operation using advanced mining equipment. The blasted rock is loaded by shovels and transferred via 30 ton trucks into the rock crushing plant bin that has a capacity of 250 m<sup>3</sup>. A primary crusher has been installed at Sechahun and the ore is transported to Choghart after primary crushing. Hence, Sechahun deposit is one of the important iron ore producers of Iran Steel Industry with a process line in Choghart iron mine, with the feed capacity of 3.4 Mt/y and feed quality of Fe>32% to produce 1.6 Mt/y of fine concentrate (Torab, 2008).

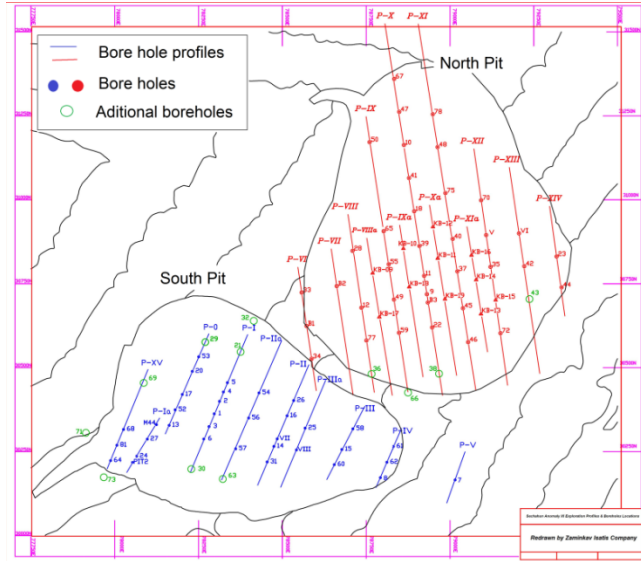


**Figure 6.** exploration profiles and bore holes of two Sechahun ore bodies, north-XI and south-XI

The bench height is 10 m and the overall pit slope angle ranges between 48 to 53 degrees depending on the rock mass characteristics. Blocks of rocks are excavated by blasting in a grid of 3m (width)  $\times$ 4m (length)  $\times$ 10m (height) and 10 benches (excavation horizontal levels: Z(m)) are already excavated within the open pit which includes the five stages of drilling, blasting, loading, hauling and crushing. The mining depth at the time of received data (2013) was to Z=1550 m above sea level and mining will be continued down to an elevation of Z=1407 m.

## 2.4 AVAILABLE DATA

All input data for this case study are provided from the geological office of the mine. Data is coming from exploration boreholes and blast holes.

### 2.4.1 Borehole data

Available data of the anomaly XI south of Sechahun are mainly from exploration boreholes and blast holes. Available samples of bore holes (up to 2013) are mainly from 42 vertical bore holes with 50 m average core drilling spacing, including iron (Fe %), Phosphorous (P %), and Sulphur (S %) concentrations. The main variable in this dataset is the iron concentration (Fe %). As the phosphorous and sulphur have low concentration in this ore body based on the processing plant of the mine, their distributions are not important and so they are not studied in this work. Statistical studies, about phosphorous and sulphur data, were applied to assess if there is a correlation between iron and phosphorous concentration. In addition to the data concentrations, there is geological information from which geological units each sample is taken. Note that there are some samples with geological information but without the iron concentration. This can be highlighted in histograms of the data, showing a different number of samples, for the several variables.

A very important point relating to the borehole exploration data is the different lengths of the samples. Borehole exploration samples in Sechahun Iron Mine, have lengths from 0.4 to 7.3 meters (Figure 7).

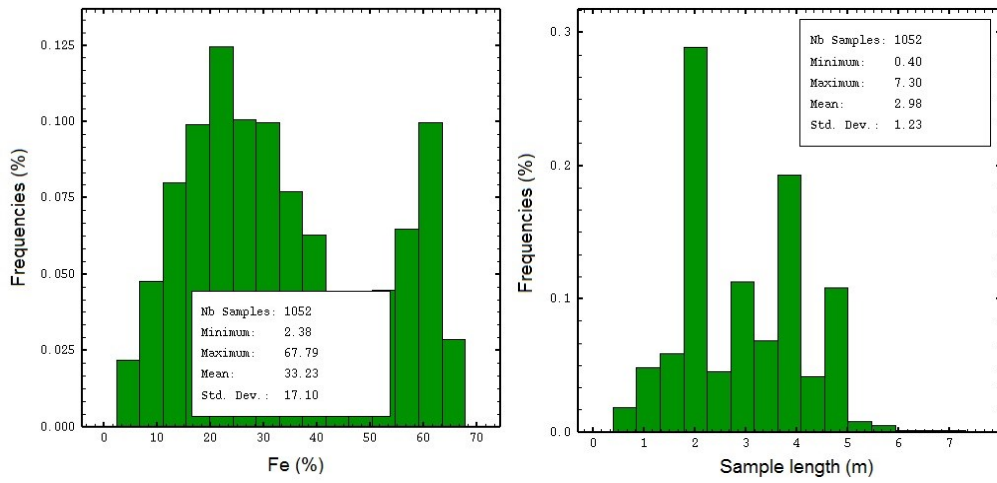


**Figure 7.** Pseudo histogram of borehole samples obtained from Fe (%) and the histogram of length of relating samples

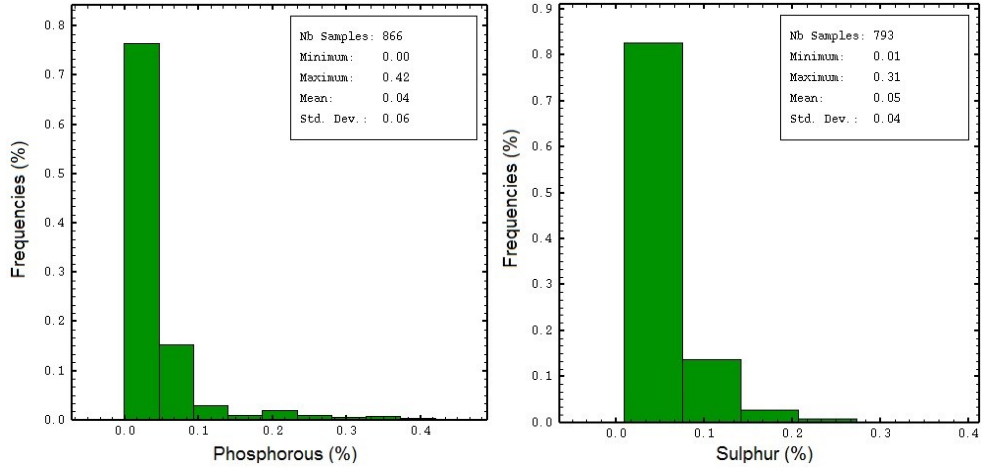


**Figure 8.** Pseudo histograms of borehole samples obtained from P (%) (on the left) and S (%) (on the right)

As showed in Figure 8, there are fewer samples with a measurable content of phosphorous and sulphur. Geological information of the Sechahun ore body is provided through different geological units (Figure 9). The maximum number of samples is related to the poor unit while the minimum number is related to

the waste unit. In any case, the length of samples largely varies in all geological units.

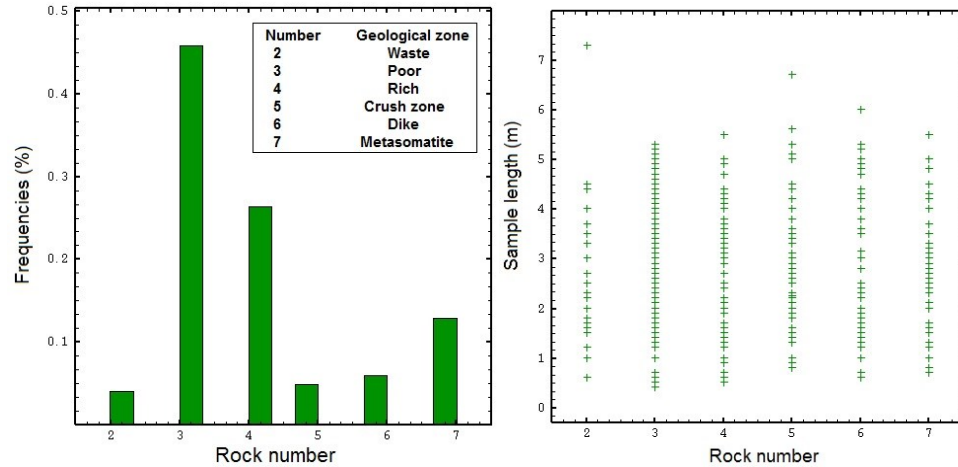


**Figure 9.** Distribution of borehole samples in each geological unit (on the left) and scatter of sample lengths in different geological units (on the right)

More details about borehole samples in each geological unit with the average of the iron concentration is shown in the Table 1.

**Table 1.** Statistical data in all geological zones

Six geological zones of the iron deposit	Number of data	Length of Samples (m)			Grade Fe (%)		
		Mean	Min	Mode	Mean	Min	Max
Waste	5	2.6	1.8	2.0	8.5	2.4	14.7
Poor	477	3.2	0.4	2.0 and 4.0	30.4	15.4	53.2
Rich	285	2.5	0.5	2.0	56.7	14.2	67.8
Crush	50	2.7	0.8	2.0	15.1	3.0	31.0
Dike	84	3.1	0.6	2.0 and 3.0	14.9	4.9	46.4
Metasomatite	138	3.5	0.7	5.0	15.1	4.1	40.6

The statistical correlation between Fe, P and S are shown in the Figure 10 to assess if there is a statistical correlation between iron, phosphorous and sulphur. Figure 10 shows that there is no important correlation between Fe, P and S.

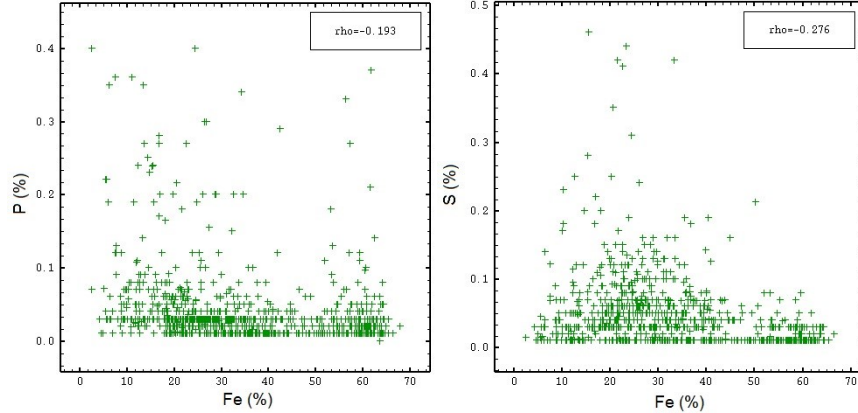


**Figure 10.** Scatter plot between Fe(%) and P(%) (on the left) and scatter plot between Fe(%) and S(%) (on the right)

#### 2.4.2 Blast hole data

There are 20985 Blast hole data from the 10 levels of excavations, with the grid of sampling of  $3 \times 4 \times 10 \text{ m}^3$ . The length of all the samples is 10 meters, however without any geological information. Figure 11 shows the location of blast holes at level  $Z=1585 \text{ m}$  of excavation. For applying the classification of geological units for blast holes, a cut-off grade and a threshold are considered according to the mining plans:

- 1) Waste zone:  $\text{Fe} < 20\%$
- 2) Poor Zone:  $20\% \leq \text{Fe} < 45\%$

### 3) Rich Zone: $\text{Fe} \geq 45\%$

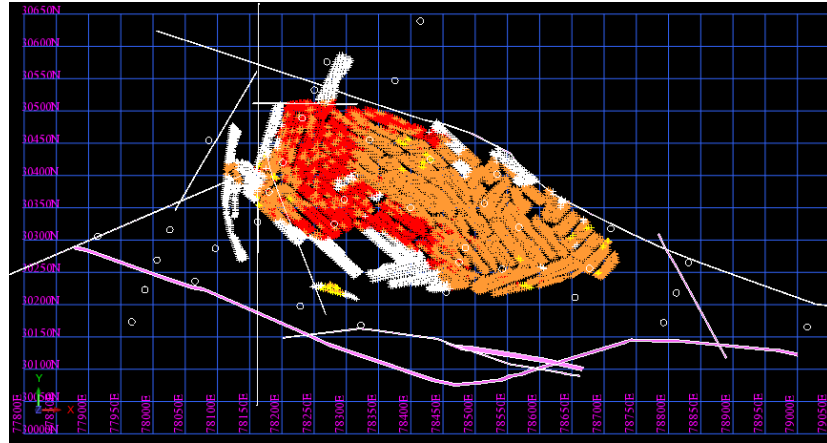


**Figure 11.** Elevation  $Z=1585$  m:of blast holes, (white: waste (no grade), yellow: waste (grade), Orange: poor zone, red: rich Zone); classified by cut-of grades

One important point about blast holes is multiple data in the database. While analyzing blast hole samples, two samples in neighborhood are mixed and analyzed as one sample, and then putting the result of its content (Fe (%) and P (%)) for the two locations. This might be due to the large number of analyzing samples. Hence, data processing was performed by removing duplicate concentration of samples. To clarify the removing duplicate data process, a simplified scheme with a regular grid is shown in Figure 12. For example, considering that concentrations are equal in points  $X_1$  and  $X_2$ ,  $X_3$  and  $X_4$ , etc. ( $X_1=X_2$ ,  $X_3=X_4$ ,  $X_5=X_6$ , etc. in Figure 12.(a)), duplicate data are removed and the coordinate in the middle of two samples in the neighborhood, (with equal Fe (%) and P (%)) is calculated (Figure 12.(b)). Therefore, the concentration is considered for a point in the middle of two equal samples (Figure 12.(c)). Statistical analysis about processed borehole data is shown in Figure 12.

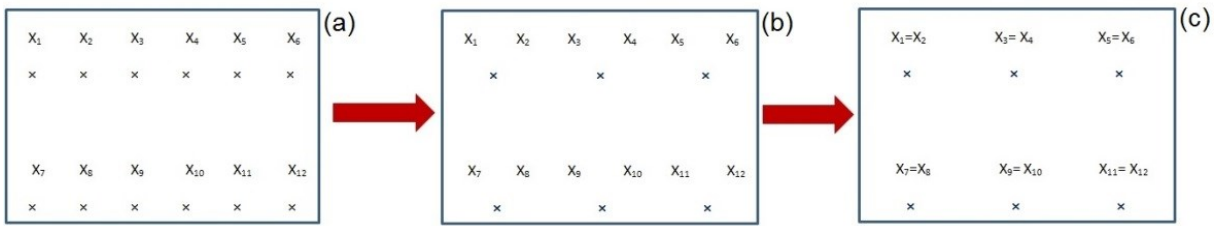


**Figure 12.** Changing blast holes locations according to the multiple data (a): all blast samples that each two points have equal concentration value; (b): calculating coordinates in the middle of two equal values; (c): putting the concentration value for the identified point

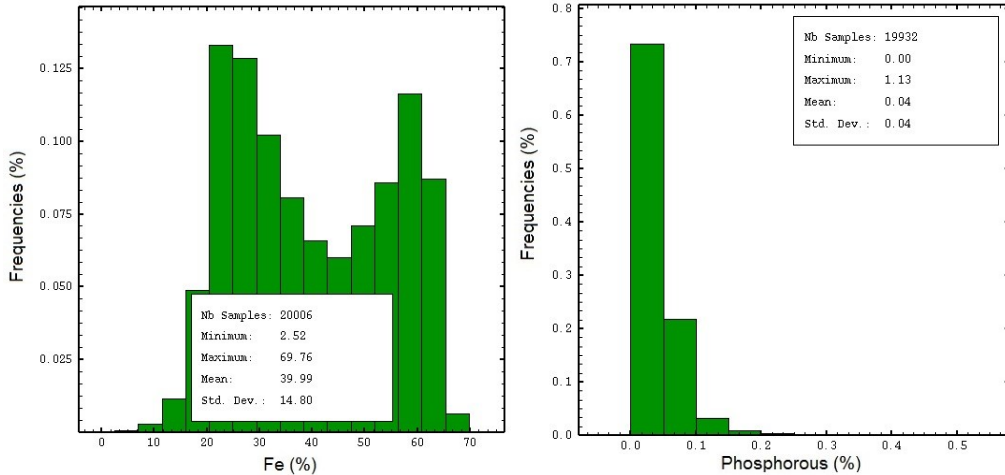


**Figure 13.** Histograms of blast hole samples obtained from Fe (%) –Left- and P (%) – Right

Histogram of iron concentration in blast holes (Figure 13) shows the similarity of bi-modality in the two distributions (obtained from blast holes and bore holes). Moreover, correlation between iron and phosphorous obtained from blast holes confirm that there is no statistical correlation between iron and phosphorous concentrations (Figure 14).

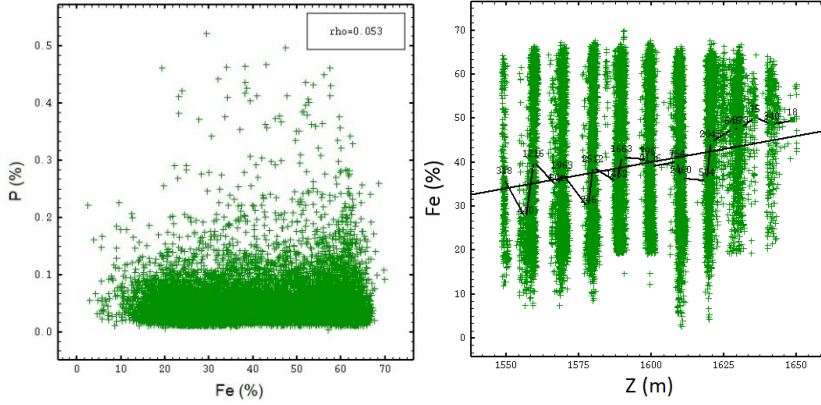


**Figure 14.** Scatter plots of Fe and P –Left- and variation of Fe in vertical direction– Right

According to the decrease of iron concentration with depth (Figure 14) there is a possibility to have a mild trend (presence of space-varying mean) in vertical direction. Statistical parameters are resumed in Table 2 from blast hole samples, from different excavation levels. However, as the number of samples in each excavation level is varying, the variation of the mean from first level to depth in Table 2 is not trustable to consider a trend. Hence, more detailed studies of geostatistical structural analysis is applied in the next chapters.

**Table 2.** shows 10 excavation plans (from 1650 to 1560 in depth)

Blast Hole Levels	Number of Data	Min (Fe%)	Max (Fe%)	Mean (Fe%)	St. Deviation	Mean (P%)	Mean (FeO%)	Mean Ratio
Z <sub>mean</sub> =1550	1656	7.28	66.20	36.49	16.48	0.036	12.98	3.05
Z <sub>mean</sub> =1560	2464	7.22	67.13	36.88	15.66	0.033	12.93	3.03
Z <sub>mean</sub> =1570	2789	8.33	67.46	38.32	15.58	0.038	13.29	3.09
Z <sub>mean</sub> =1580	3284	8.65	69.76	37.01	14.91	0.042	12.46	3.23
Z <sub>mean</sub> =1590	3025	8.32	67.45	38.84	14.57	0.052	12.97	3.26
Z <sub>mean</sub> =1600	3216	2.52	66.24	37.27	14.91	0.052	11.72	3.52
Z <sub>mean</sub> =1620	2405	4.14	67.42	42.39	13.78	0.055	12.29	3.96
Z <sub>mean</sub> =1630	1672	2.00	66.55	47.08	12.27	0.055	11.08	4.64
Z <sub>mean</sub> =1640	423	5.44	63.89	48.25	11.21	0.048	7.76	6.66
Z <sub>mean</sub> =1650	54	4.00	58.46	49.48	8.28	0.910	6.63	7.96



## 3 DIFFERENT DATA SUPPORTS

Geostatistical analysis includes statistical studies and the analysis of the spatial variability of a variable considered as the realization of a random function (Armstrong 1998). The tool used to analyze the spatial variability is the variogram (Equation 1). Spatial covariance and correlation of sample values at two points in space can be used, as well for characterization the spatial variability (Chiles and Delfiner, 2012). In any case, the variogram is the simplest way to relate uncertainty with distance:

$$\gamma(h) = \frac{1}{2} E[(Z(x+h) - Z(x))^2] \quad (1)$$

Where  $Z(x)$  is the variable value at point  $x$  (location, time, etc.) and  $Z(x+h)$  is the variable value at point  $x+h$  (at a distance of  $h$ ).

One of the main difficulties arising in the structural analysis is how to consider the variogram of a variable value at point  $x$ . Measured samples usually have a volume (based on their dimension), which is defined in geostatistics as “support”. Spatial variability analysis must be applied to data with the same support. The problem of the sample with different support was a topic of research that remains still open (Guarascio and Raspa, 1974, Clark, 1977, Atkinson and Tate, 2000, Carrasco et al., 2008, Kasmaee and Torab, 2014, Bassani and Costa., 2016). One frequently used solution in the case of samples with different support is to composite samples into the same volume (support). One of the simplest methods of processing data in order to use sample with the same support is averaging. (Armstrong, 1998; Chiles and Delfiner, 2012; Wackernagel, 2003). Another method, though rarely used, is to perform a theoretical punctual model that allows the use of samples with different supports (Guarascio and Raspa, 1974). This method requires modifying the

kriging system, which must be built using average covariances to account for the different sample supports (Bassani and Costa, 2016). Using average covariances in the kriging system also has the added value whereby instead of using a variogram model of composited samples (Bassani and Costa, 2016), a theoretical punctual model can be used, providing a more precise model with greater coherency with samples having different supports.

To test the coherency of models obtained from mentioned methods, Cross-validation techniques can be used. Cross-validation is a powerful model validation technique to check the performance of the model for kriging (Chiles and Delfiner, 2012). The principle underpinning cross-validation is to omit in turn a sample point  $x_\alpha$  from the set of variables  $Z(x)$  and then predict it by kriging with the proposed model from neighboring data  $Z(x_\beta)$ ,  $\alpha \neq \beta$ . Accordingly, at every sample point  $x_\alpha$  the kriging estimate  $Z_\alpha^*$  and the associated kriging variance  $\sigma_{K_\alpha}^2$  are available.

Since the true value  $Z_\alpha = Z(x_\alpha)$  is known, it is therefore possible to compute the kriging error  $E_\alpha = Z_\alpha^* - Z_\alpha$  and the standardized error:  $e_\alpha = E_\alpha / \sigma_{K_\alpha}$ .

To study the quality of the fitting,  $s = \frac{1}{N} \sum_{\alpha=1}^N e_\alpha^2$  can be considered as an appropriate parameter, and should be close to 1 (Chiles and Delfiner, 2012). This technique can show which model is more reliable. This helps understanding of the effect of integrating data, the efficiency of each method and their effect on the kriging results.

### 3.1 COMPOSITING SAMPLES WITH DIFFERENT SUPPORTS

In many geo-resource applications, punctual data  $z(x)$  are rarely available. Available data  $z_v(x)$  are defined on a support  $v$ , centered on a point  $x$ . For example,  $v$  is the volume of a core sample, or more generally, the volume of the sample. The support of a regionalized variable is the average volumes of samples for the measured data. As the size of the samples changes, the histogram of the samples varies. However, it is possible to predict distribution change when passing from one size of support to another, generally point to block (Journel and Huijbregts, 1991).

The variable  $z_v(x)$  of a sample is the mean value of the point variable  $z(x)$  in volume  $v$

$$z_v(x) = \frac{1}{v} \int_v z(x) dx \quad (2)$$

Where the variable value  $z(x)$ , and  $z_v(x)$  are said to be the integrated of the point variable  $z(x)$  over volume  $v$ .

Integrating data significantly impacts geostatistical variability. To show this effect, the relation between variogram of  $z(x)$  and  $z_v(x)$  (for instance regularized variograms  $2\gamma_v(h)$ ) are shown in Figure 15. The Figure shows how the variogram changes when samples are integrated in a small volume ( $w$ ) or into bigger volume ( $W$ ). If we refer to a core samples of the same diameter, then the support can be considered as the length of the core samples.

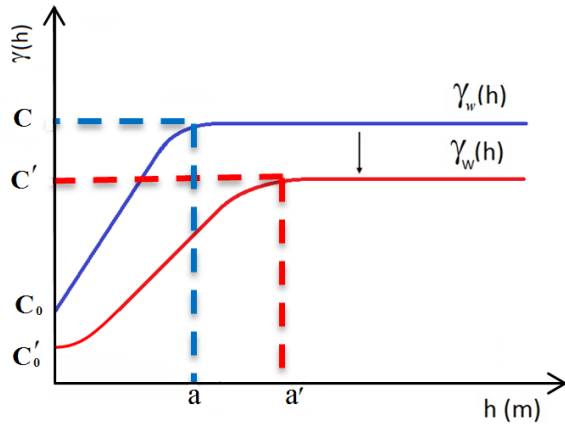


**Figure 15.** Variograms over two different supports  $w$  (small length) and  $W$  (long length) illustrating relationship between support size and changing sample variograms

Therefore (Journel and Huijbregts, 1991):

$$C' = \frac{C_0}{W}, \quad a' = a + (W-w), \quad C' = C + \bar{\gamma}(w, w) - \bar{\gamma}(W, W) \quad (3)$$

Where  $\gamma_w(h)$  is the variogram of support  $w$  (small length),  $C_0$  the nugget effect,  $a$  the range and  $C$  the sill and

$\gamma_W(h)$  is the variogram of support  $W$  (long length),  $C'$  is the nugget effect,  $a'$  the range and  $C'$  the sill

Hence, any transformations induced by integrating data generally have effects on the spatial variability and can be analyzed using the variogram: at a large distance, they impart more regular behavior on the small scale (Chiles and Delfiner, 2012). As shown in Figure 15 and Equation 3, when samples are coming from a small support (e.g. small length) and are processed, composing sample into a larger support, the range of the variogram increases due to the subtraction of two supports (e.g. the subtraction of two lengths), giving rise to a decreased variogram nugget effect and sill.

### 3.1.1 Regularization method

The most used method of processing data for obtaining samples with the same support is regularization. Regularization is a weighted averaging method to estimate the average value for a defined support. This method is based on construction of a variogram of the mean values of samples along their length or volume. For example for a core sample along a bore hole length, it is assumed that all core samples have the same length  $L$  and the same cross-sectional area  $A$  (Figure 16).

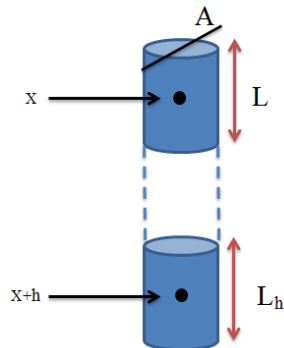


**Figure 16.** Core samples aligned along a bore hole (Journel and Huijbregts, 1991)

Equation (2) can be used to perform the regularization method on support  $v$  of core samples ( $v=A \cdot L$ ). When the diameter of the core is small compared to sample length  $L$ , only the length of the samples can be considered, and the cross-sectional area  $A$  of the core sample may be considered as constant value:

$$Z_v(x) \cong Z_L(x) = \frac{1}{L} \int_L z(x) dx \quad (4)$$

According to this equation, the regularized variogram can then be written:

$$\gamma(h) = \frac{1}{2} E[(Z_L(x+h) - Z_L(x))^2] \quad (5)$$

Regularization of samples with different supports is a useful means of analyzing nested structures (Chiles and Delfiner, 2012). Figure 17 shows the schematic example of regularization for four samples with different supports (here, length). In this example, as the selected support length for structural analysis was chosen equal to 2.0 meters, samples are therefore weighted averaged to 2.0 meters (regularized into 2.0 meters with a tolerance of 0.5 meter).

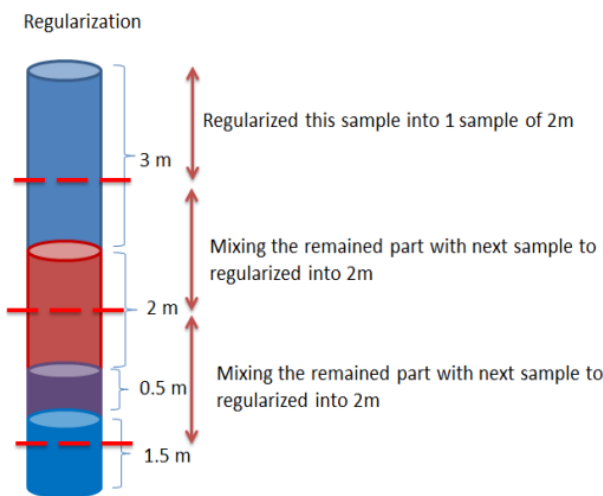


**Figure 17.** Schematic example of regularization borehole samples in a 2.0 meter support (colors only identify different samples)

As shown in Figure 17, regularization permits the use of all available samples. However, compositing data by regularization change the measured values of the data, even when they are exactly of the same length as the support selected. For example, in the second sample in Figure 17, a 2.0 meter sample is integrated with the first 3.0 meter sample and so its measured value is changed.

Compositing the two initial samples create two new data, both with a length of 2.5 meters. This leads to a reduction of dataset variance, with the result that regularized data will always have a smaller variance than measured data. This impact is significant when samples of larger lengths than the selected support length are used. To reduce this effect, another method named aggregation is proposed. The advantage of the regularization method is that most data may be used to perform the sample variograms, with the result that the more data used, the more accurate geostatistical modelling and evaluation become (Oliver and Webster, 2014).

### 3.1.2 Aggregation method

The regularization method applied into a very long length causes loss of some data, in other words, a loss of information. In contrast, regularizing to a short length entails splitting a large sample into equal variable pieces, which is, however, also inaccurate, since it reduces short-scale variability (Bassani and Costa, 2016). In order to reduce these effects on data, the aggregation method is proposed. This method entails setting a similar sample length tolerance as in the regularization method (for example, 0.5 m). The weighted average is then calculated using the same equation used for regularization but on selected data and depending on the lengths of the samples to be integrated. For instance, if the length selected for the support is 2.0 meters (similar to the regularization example with a tolerance of 0.5 m), then all samples of more than 2.5 meters must be removed from the input data. Samples exactly 2.0 meters long will be used unchanged and only samples of less than 2.0 meters will be integrated with the weighted average. Figure 18 shows the proposed method of aggregation in comparison with regularization. In summary, in the aggregation

method the smaller samples are composited into the appropriate support length as a weighted average (Figure 18) while the longer samples are not included.

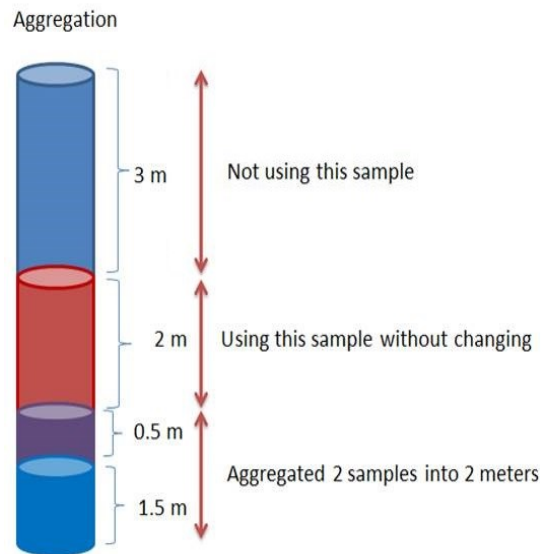


**Figure 18.** Schematic procedure of aggregation of samples into 2.0 meters

When removing samples larger than the selected support in order to apply the aggregation method, it is fundamental to check whether the remaining data are representative of the spatial variety of area in question. In an application where sampling with different supports has been carried out on the basis of preferential criteria (for example, small samples in the richest zones and large samples in poor zones), removing large samples can lead to a substantial loss of information about the area. This is one of the disadvantages of the method.

### 3.2 THEORETICAL PUNCTUAL MODEL

The theoretical punctual model  $\bar{\gamma}_p(v_i, v_j)$  is calculated as the average of point variograms  $\gamma(x'_i, x'_j)$  defined between any discretizing point  $x'_i$  of data  $v_i$  and any discretizing point  $x'_j$  of sample  $v_j$ :

$$\bar{\gamma}_p(v_i, v_j) = \frac{1}{N_i N_j} \sum_{i=1}^{N_i} \sum_{j=1}^{N_j} \gamma(x'_i, x'_j) \quad (6)$$

Where  $N_i$  and  $N_j$  are the number of discretizing points of data  $v_i$  and  $v_j$ .

To clarify this discretizing procedure in the kriging system, Figure 19 shows the same example as the previous sections.

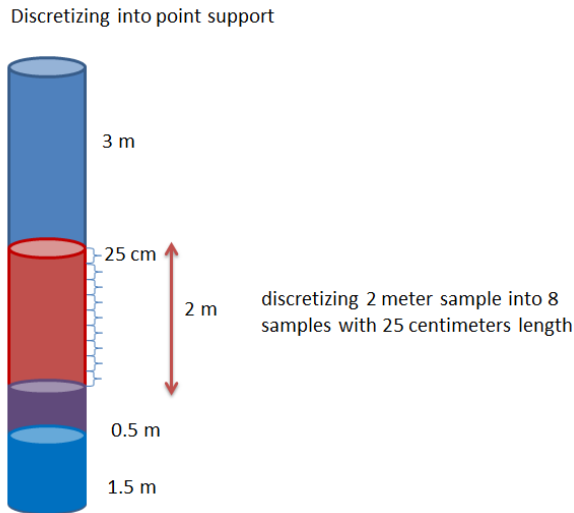


**Figure 19.** Schematic procedure of sample aggregation to 2.0 meters

The theoretical punctual model is applicable when the available data are defined on a non-point support  $v$ , and no constant support volume (length) can be considered with which to integrate the measured data. In many applications, when data are integrated, for example, by the regularization procedure, as shown in the previous sections (3.1.1 and 3.1.2), the regularized data differ

from the raw measured data values. In addition, the aggregation method may not be able to include all samples, which again might impact data distribution and variogram modeling. Figure 19 shows the same example in order to demonstrate how, when using the theoretical punctual model for samples with different supports, in the kriging system, data would be discretized into a very small support, close to zero, in this case, 25 centimeters.

The theoretical punctual variogram model has the advantage of using all raw data without transformation. The parameters of theoretical punctual model  $\gamma_p(h)$  must be consistent with the observed integrated (regularized or aggregated) variogram  $\gamma_l(h)$  parameters. In fact, deducing the theoretical punctual model  $\gamma_p(h)$  from the composited model  $\gamma_l(h)$  amounts to a “de-convolution” of the model  $\gamma_l(h)$ . The theoretical punctual model is not an experimental variogram model obtained from samples but is deduced from passing  $\gamma_l(h)$  to  $\gamma_p(h)$ , that is an approximation by calculating parameters. An approximation expression is used because if the punctual variogram  $\gamma_p(h)$  is of a certain model - for instance spherical – in the regularized variogram  $\gamma_l(h)$  may not be exactly of the same model (Figure 15). However, in practice the theoretical punctual model is an acceptable approximation of the regularized/aggregated variogram  $\gamma_l(h)$ . Thus, if the regularized/aggregated variogram is spherical  $\gamma_l(h)$  with range  $a$  and sill  $C$ , the point variogram  $\gamma_p(h)$  can be deduced from Equation 3 (for distances  $|h| \geq l$ ) to a spherical model (Journel and Huijbregts, 1991):

- I) a sill  $C = C_l + \bar{\gamma}(l, l);$
- II) a range is equal to  $(a_l - l)$  if the regularization or aggregation is done by support  $l$ .

Once the variogram model of the integrated data is determined, the theoretical expression for the punctual model can be deduced. The kriging system is modified when using the theoretical punctual model. In the kriging system, the estimated value  $z^*(x)$  at point  $x$  in the OK is calculated (Matheron, 1971):

$$Z^*(x) = \sum \lambda_i Z_{V_i}(x_i) \quad (7)$$

Where  $\lambda_i$  is the ordinary kriging weights associated with data  $Z_{v_i}(x_i)$  that have the constant support of  $v$  at each point  $x_i$  under the following conditions:

$$\begin{cases} \sum_{j=1}^n \lambda_i \gamma(v_i, v_j) + \mu = \gamma(v_i, v_0) & i=1,2,\dots,n \\ \sum \lambda_i = 1 \end{cases} \quad (8)$$

Where  $\mu$  is the Lagrange multiplier and  $\gamma(v_i, v_j)$  is the variogram of point to point between data  $v_i$  and  $v_j$ , and  $\gamma(v_i, v_0)$  is the variogram between the estimated point and data  $v_i$ . In the kriging system, all samples should have and are considered with the same support used for the variograms. With the theoretical punctual model, samples can have different supports in the kriging system. In this case all samples must be discretized to a very small length (the punctual support is usually assumed to be close to zero length support) (Bassani and Costa., 2016):

$$\sum_{j=1}^n \lambda_i \bar{\gamma}_p(v_i, v_j) + \mu = \bar{\gamma}_p(v_i, v_0) \quad (9)$$

### 3.3 APPLICATION TO THE CASE STUDY

The available measured data are coming from 42 vertical borehole samples, as showed in the second Chapter; The baseline for investigation of the methods described in the previous Chapter are applied in this case study.

The selected variables are the iron concentration (Fe %) and the geological information for the six geological units. Statistical studies and structural analysis of data are presented as the primary step of the study (Table 1). The study included a total of 953 samples with varied iron ore concentration from different geological units. The distribution of the samples in each geological unit is not constant and so the number of samples for each geological unit is different. For economic reasons, there are more samples in poor and rich geological units and very few in the waste unit. The sample support length according to the mode of sample lengths in different geological units was mainly 2.0 meters (Table 1). The histogram of the sample lengths in all geological units (Figure 7) provides detailed raw data. Given the particular features of the geological units of the ore body and the existence of post-processing geological structures such as dikes and faults, samples corresponding to the dike units and some crush zones were removed from the dataset, in order to have a homogeneous area of study. The scatter plot of sample lengths in all geological units in Figure 9 shows that different length samples are present in almost all the geological units. To choose the support length for all samples and integrating data for a global variogram model, the mode of sample lengths covering all geological units was considered. The lengths of 2.0 and 4.0 meters, according to the histogram of the sample lengths in Figure 7, were chosen. The above-mentioned theoretical methods were used to process the data. In addition, the theoretical punctual model was used to compare results obtained with the previous models.

### 3.3.1 Regularization method

The case is summed up in Table 1, and the histogram of sample lengths in Figure 7 show that over 25% of all samples are 4.0 meters long, while more than 35% are 2.0 meters long. It follows that the support length with the largest number of samples has to be used as the selected support.

As shown in Figure 17, borehole samples were regularized by weighted average over sample length considering a 0.5 tolerance for 2.0 and 4.0 meters.

Minimum length is an important parameter for regularization, since it has a significant effect on the number of regularized samples (particularly on the number of samples, mean and variance) and experimental variograms (shown in Table 3). For instance, if the support selected is 2.0 meters, with a minimum length of 1.0 meter (Table 3), samples smaller than 1.0 meter will be excluded from the regularization process.

**Table 3.** Statistical information of original and regularized data (2.0 and 4.0 meters regularized data)

Input Data	Minimum Length of samples considered (m)	Iron concentration		
		Number of data	Fe Mean (%)	Fe Standard deviation (%)
Original data	0.3	953	35.1	16.7
Regularization 2m	0.5	1477	33.5	15.9
Regularization 2m	1.0	1436	33.4	15.9
Regularization 2m	1.5	1378	33.4	15.8

Input Data	Minimum Length of samples considered (m)	Iron concentration		
		Number of data	Fe Mean (%)	Fe Standard deviation (%)
Original data	0.3	953	35.1	16.7
Regularization 4m	0.5	784	33.5	15.8

<b>Regularization 4m</b>	1.5	742	33.3	15.6
<b>Regularization 4m</b>	3.0	665	33.5	15.5
<b>Regularization 4m</b>	3.5	638	33.4	15.4

As it is possible noting from the table, regularization modifies the information available since: a) it excludes some samples so that the mean values change (for example, the local means), and b) it generates a more regular, less scattered population, with a lower variance (Table 3). The bar charts in Figures 20 and 21 show the different average Fe (%) concentrations obtained from regularized 2.0 and 4.0 meters as well as the scatter plots between the real and regularized borehole mean. The scatter plots show how the mean value change of some boreholes can affect local estimation results (Figures 20 and 21).

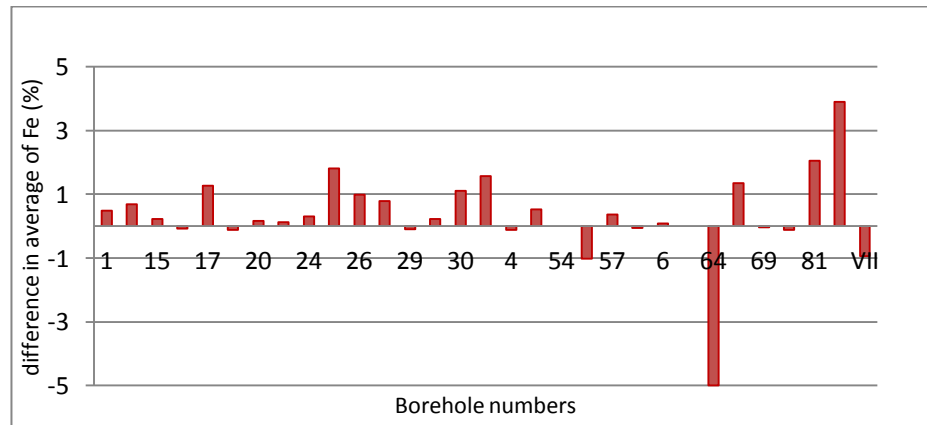


**Figure 20.** Bar chart shows difference of average obtained from Fe (%) between regularized to 2.0 and 4.0 meters

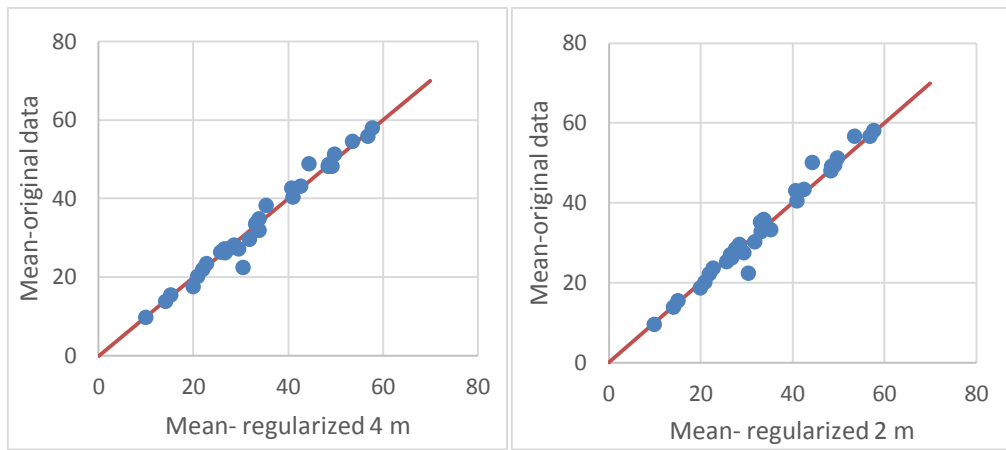


**Figure 21.** Scatter plots showing effect of regularization on average of iron concentration Fe (%)

Regularization also has a vertical and horizontal effect on structural analysis as shown by the variograms in Figures 22 and 23:

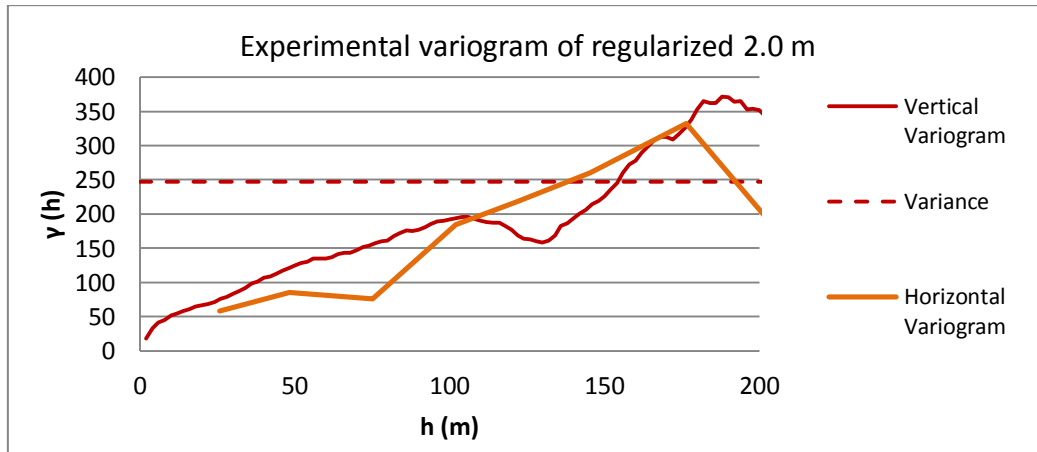


**Figure 22.** Comparison of vertical and horizontal sample variograms of Fe (%) following 2.0 meter regularization

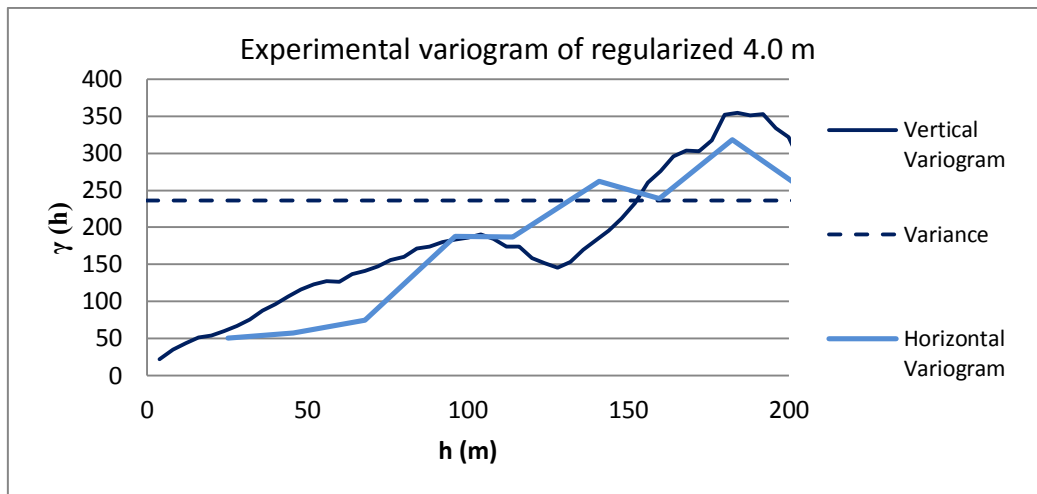


**Figure 23.** Comparison of vertical and horizontal sample variograms of Fe (%) after 4.0 meter regularization

As the behavior of sample variograms in vertical and horizontal directions are the same, (Figures 22 and 23) it is possible to consider the variable as almost isotropic (which means similar variogram behavior in different direction).

The two regularized variograms (Figure 24) were compared in order to check the coherency between the sample variogram parameters obtained from two different supports (Equation 3). The comparison between the two support lengths, shows that the theoretical coherency between the two sample variograms is not strictly obeyed. In fact, the experimental variogram for 4.0 m regularization should show a lower variance/sill (<5%) and a larger range (+2 m), whatever the structure considered, between 50 and 100 meters or over 150 m.

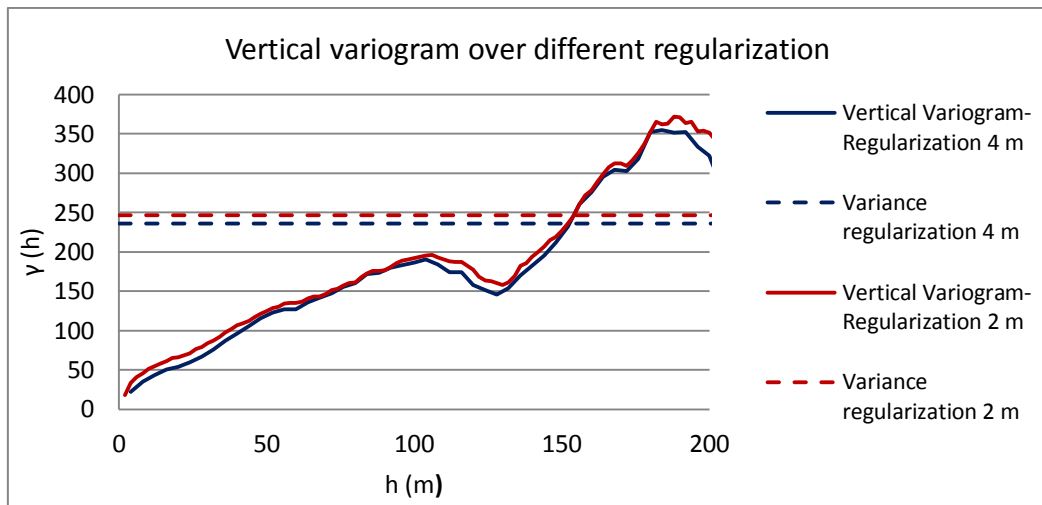


**Figure 24.** Comparison of vertical sample variograms of Fe (%) from aggregation at 2.0 and 4.0 meters

### 3.3.2 Aggregation method

The same support lengths were used to perform the aggregation method. To apply aggregation, a tolerance of 0.5 meters was considered, with the result of the following application of the proposed aggregation method to the borehole sample lengths were as follows:

- for 2.0 meter aggregation support: [1.5 m - 2.5 m];
- for 4.0 meter aggregation support: [3.5 m - 4.5 m].

If aggregation adopts a support length of 2.0 meters, it follows that only samples of less than 2.0 meters will be used and a weighted average will be applied to the samples from 1.5 to 2.5 meters. Similarly, aggregating at 4.0 meters will consider only samples of less than 4.0 meters and the weighted average of samples from 3.5 to 4.5 meters. It should be noted that with this method, samples with an original length of 2.0 and 4.0 meters respectively are

not changed or smoothed while aggregating. Sample statistics are shown in Table 4:

**Table 4.** Statistical information for original and aggregated data

Input Data	Iron concentration			
	Minimum Length of samples considered	Number of data	Fe Mean (%)	Fe Standard deviation (%)
Original data	0.3	953	35.1	16.7
Aggregation 2 m	1.5	371	42.0	17.5
Aggregation 4 m	3.5	426	37.5	16.2

Table 4, shows the mean and standard deviation of 4.0 meter aggregated samples are close to the statistical parameters of raw data. In addition, in comparison with the regularization method, the statistical parameters in samples of aggregation 4.0 meter have more similarity with the original data. The structural analyses in Figures 25 and 26 show the isotropic behavior of sample variograms (comparison of horizontal and vertical variograms) in 2.0 and 4.0 meter aggregated sample variograms.

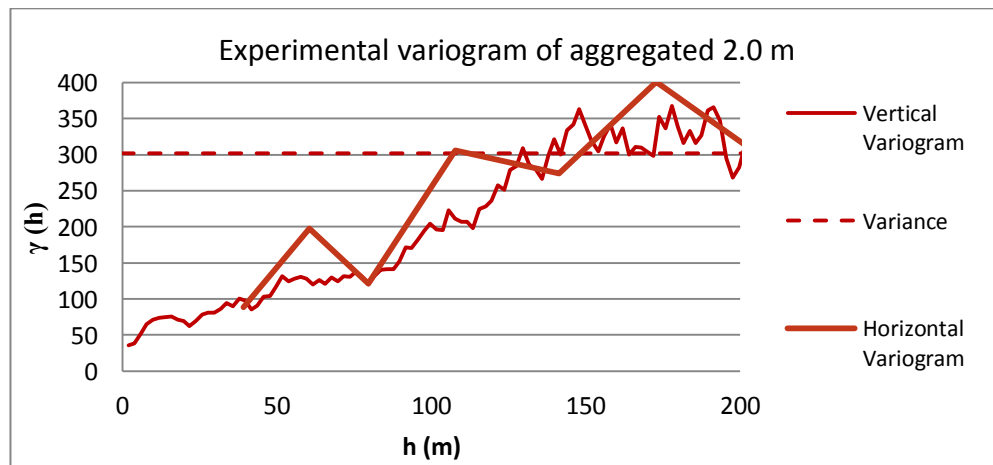


**Figure 25.** Comparison of vertical and horizontal sample variograms of Fe (%) for 2.0 meter aggregation

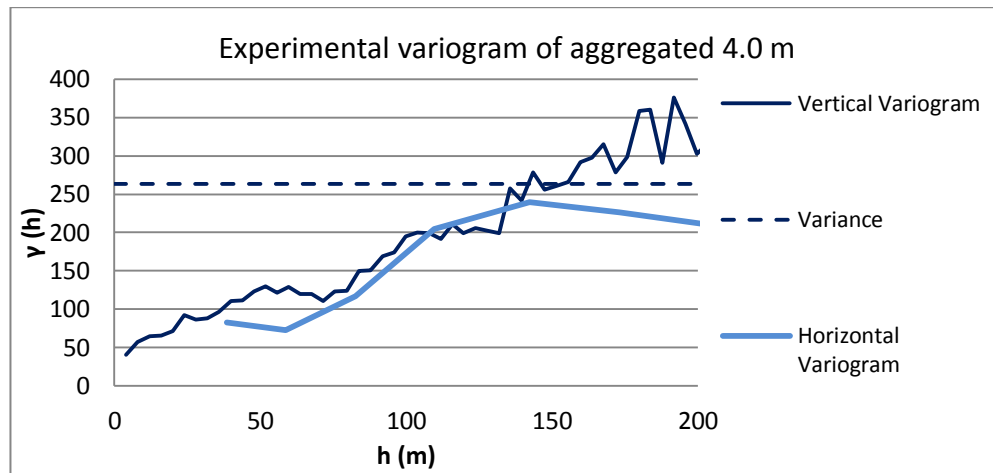


**Figure 26.** Comparison of vertical and horizontal sample variograms of Fe (%) for 4.0 meter aggregation

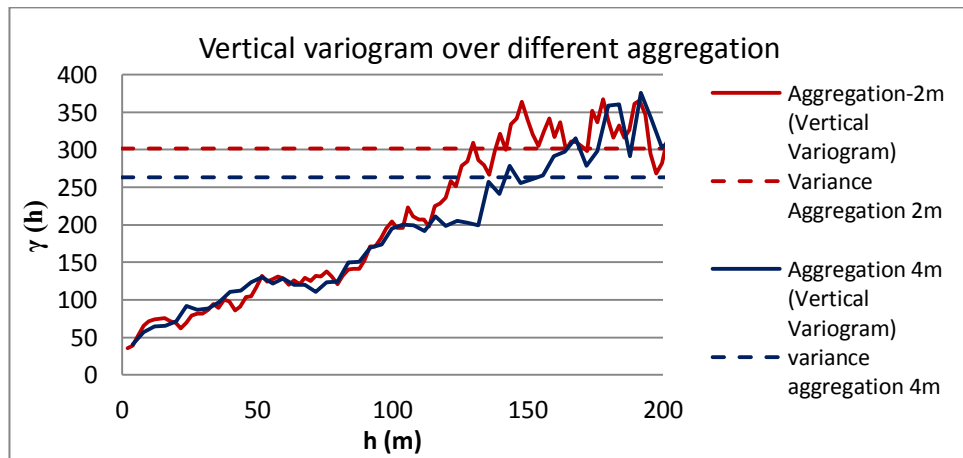


**Figure 27.** Comparison of vertical sample variograms of Fe (%) for 2 and 4.0 meter aggregation

Comparison of two sample variograms obtained from aggregated supports (2.0 and 4.0 meters) (Figure 27), similar to the regularized sample variograms, shows that the theoretical coherency between the sample variograms (Equation 3) and the two different supports is not exactly obeyed. This could be due to non-homogenous data in the two classes of input data (2.0 and 4.0 meter

supports). To demonstrate this hypothesis, in-depth studies into the original data and their distribution in different geological units are required.

### 3.3.3 Theoretical punctual model

The theoretical punctual model uses all raw samples with their lengths with no need for transformation. The theoretical punctual model can be deduced on the basis of the coherency between two variogram models obtained from two supports of 2.0 and 4.0 meters. To gain more information on original data, particularly in two selected classes of samples 2.0 and 4.0 meters long, univariate statistic studies were performed on original data with the exact lengths of 2.0 and 4.0 meters and with a tolerance of 0.5 meter. Histograms of the two selected classes are shown in Figure 28. The lengths of the raw samples used for the histograms are:

- Class of 2 m: [1.5 m - 2.5 m];
- Class of 4 m: [3.5 m - 4.5 m].

Comparison of the original data histograms in the two classes (Figure 28) with the pseudo-histogram of Fe (%) in shows that despite there being fewer 4.0 meter than 2.0 meter samples, distribution is more similar to the total data pseudo-histogram.

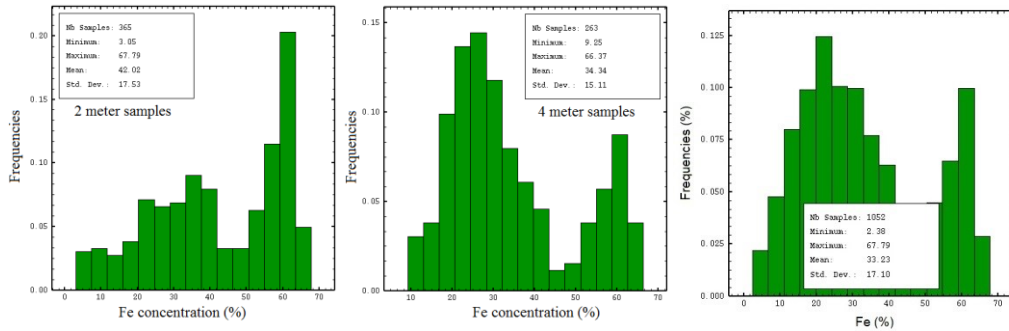


**Figure 28.**Comparison of histograms of iron concentration in 2.0 (left) and 4.0 meter (middle) selected samples with original samples (right)

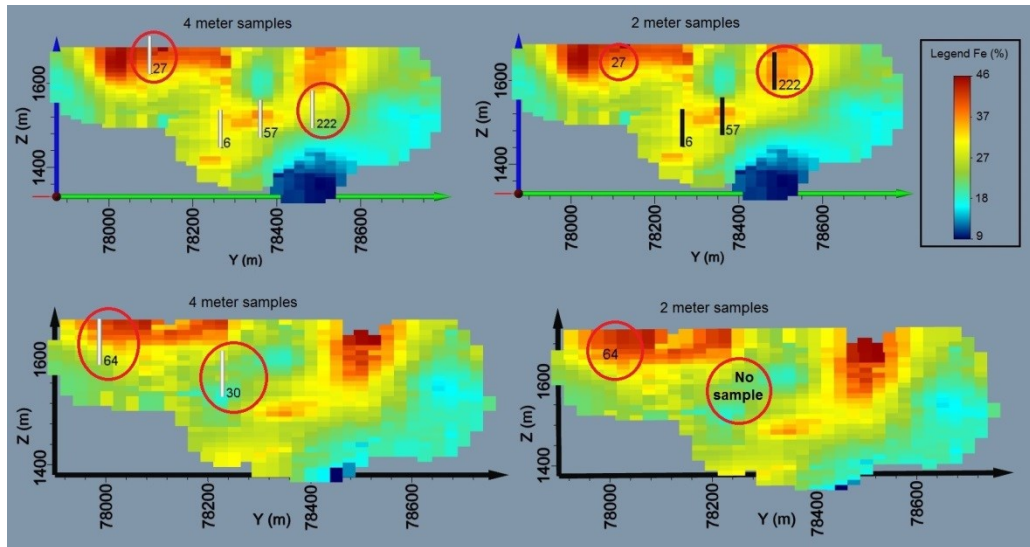


**Figure 29.** Comparison of two vertical ore body sections with 2.0 meter (black) and 4.0 meter (white) samples, showing the non-homogeneity of sampling with different lengths in the geological units

Moreover, Figure 29 shows the non-homogenous sampling of the measure. For instance, borehole number 222 (red circle) shows the 2.0 meter support samples to be in the upper part of the ore body while the 4.0 meter samples are in the lower part (2.0 and 4.0 meter samples are not in the same geological unit). In another example, borehole number 30 has only 4.0 meter and no 2.0 meter

samples. The non-homogenous samples between two classes of data (2.0 and 4.0 meters) led to non-consistency between the two sample variograms obtained from supports of 2.0 and 4.0 meters. Using the theoretical punctual model might be a solution for the geostatistical modeling in this case study. In the theoretical punctual model, aggregated supports of 2.0 and 4.0 meters are used in order to avoid sample transforming and smoothing. Approximation of the punctual variogram can be derived indirectly from aggregated data on the basis of the parameters of two variogram models obtained from two aggregated supports (Clark, 1977).

The mathematics of the process are explained by Matheron (Matheron, 1971). The appropriate length for the theoretical punctual model can be chosen on the basis of the minimum length of samples ( $l \leq l_{min}$ ). In this case study, the minimum length of data is 0.4 meter and so the length of the theoretical punctual model is considered to be 0.25 meter (close to zero). Hence, in the kriging system, samples can be discretized into 0.25 meter using the theoretical point variogram model. This model is indirectly deduced from the variograms of 2.0 and 4.0 meter aggregated samples.

Two spherical models with the nugget effect are chosen for modeling the sample variograms obtained from aggregation of 2.0 and 4.0 meters;

The spherical model is expressed as:

$$\begin{cases} \gamma(h) = C \left\{ \frac{3h}{2a} - \frac{h^3}{2a^3} \right\} & h \leq a \\ C & h \geq a \end{cases} \quad (10)$$

Where  $C$  is the sill of the sample variograms (once for 2.0 meter aggregation and then for the 4.0 meter aggregation) and  $a$  is the range. The sill of the aggregated variograms obviously will be lower than the sill of the corresponding point model (Equation 3).

As data from two classes of 2.0 and 4.0 meters are not homogenous (Figure 29), the coherency between aggregated sample variograms of 2.0 and 4.0 meters is not strictly obeyed, with the result that fitting a model on sample variograms obeying Equation 3 becomes difficult (Figure 30). After performing the best fit of sample variogram parameters, the theoretical punctual model can be deduced. Note that because of the isotropic behavior of variograms (coherency of the vertical and horizontal sample variograms), parameters of the vertical sample variograms were considered to deduce the theoretical punctual model.

### 3.3.3.1 Range of the theoretical punctual model

Punctual model range is calculated from the vertical variogram model range for the 2.0 (or 4.0) meter aggregation shown in Equation (3). The fitted models on sample variograms of 2.0 and 4.0 meter aggregation are shown in Figure 30 and Table 5 with a notice of following the coherency of the theory in Equation 3.

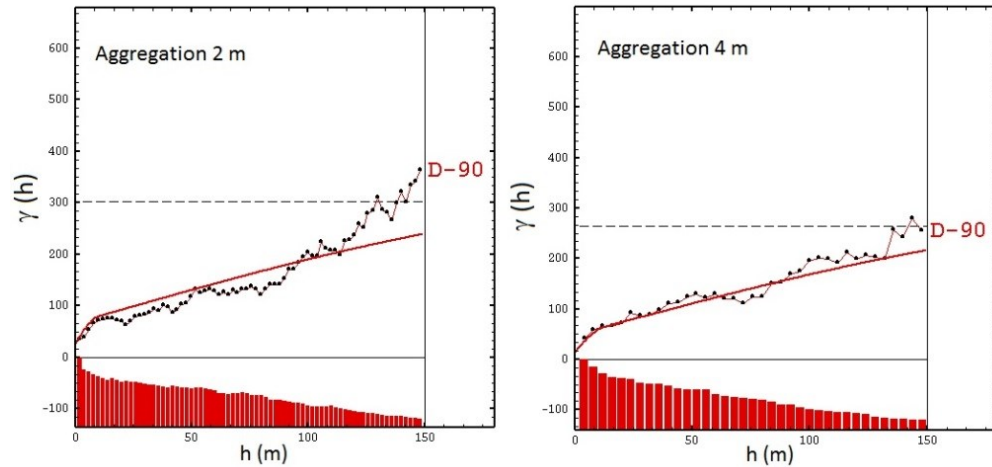


**Figure 30.** Vertical experimental variograms (black dots) and models (red line) for justification of Point-variogram in 2.0 and 4.0 meter aggregation

**Table 5.** Parameters of two vertical variogram models of 2.0 and 4.0 meter aggregation

Variogram	Nugget Effect $C_0$ (%) <sup>2</sup>	Structure 1 (Spherical)		Structure 2 (Spherical)	
		Range ( $a_1$ ) (m)	Sill ( $C_1$ ) (%) <sup>2</sup>	Range ( $a_2$ ) (m)	Sill ( $C_1$ ) (%) <sup>2</sup>
Aggregation 2.0 m	16	8	48	260	223
Aggregation 4.0 m	8	10	39	262	222

According to Equation 3, the range of the theoretical punctual model is:

$$a_{\text{aggregated } 2m} = a_{\text{punctual}} + (W_{\text{aggregated } 2m} - w_{\text{punctual}})$$

$$16 = a_{\text{punctual}} + (2 - 0) \quad \rightarrow \quad a_{\text{punctual}} = 6$$

This relation can be reached also from a 4.0 meter aggregation

### 3.3.3.2 Sill of the theoretical punctual model

The sill of the punctual model can be deduced from the relationship between the sill of  $\gamma_1(h)$  – variogram of aggregated data (2.0 or 4.0 meters) and that of  $\gamma_p(h)$  – theoretical punctual variogram, with 25-centimeter long samples. The theoretical value of sill  $C_p$  (sill of the punctual model) is deduced from the spherical model (Journel and Huijbregts, 1991):

$$C_{\text{Aggregated}} = C_{\text{punctual}} \left[ 1 - \frac{l_{\text{Aggregated}}}{2a_{\text{punctual}}} + \frac{l_{\text{Aggregated}}^3}{20a_{\text{punctual}}^3} \right] \quad (11)$$

This procedure can be carried out using the variogram of 2.0 or 4.0 meter aggregation from the Equation 7:

$$C_{\text{punctual}} = \frac{C_{\text{Aggregated } 2m}}{1 - \frac{2}{2a_{\text{punctual}}} + \frac{2^3}{20a_{\text{punctual}}^3}} = \frac{C_{\text{Aggregated } 4m}}{1 - \frac{4}{2a_{\text{punctual}}} + \frac{4^3}{20a_{\text{punctual}}^3}}$$

$$C_{punctual} = \frac{48}{1 - \frac{2}{2 * 6} + \frac{2^3}{20 * 6^3}} = \frac{39}{1 - \frac{4}{2 * 6} + \frac{4^3}{20 * 6^3}} = 57$$

### 3.3.3.3 Nugget effect of the theoretical punctual model

To calculate the nugget effect of the punctual model the appropriate equation is:

$$A_{punctual} = C_0(l) \cdot \frac{l_{aggregated}}{l_{punctual}} \quad (12)$$

Where  $C_0(l)$  is the nugget effect of the composited variograms (2.0 or 4.0 meter aggregation) and  $l_{punctual}$  is 25-centimeters. A is calculated from aggregated variogram models, which is 128 for this case study.

**Table 6.** Parameters of theoretical punctual model deduced from two variogram models of 2.0 and 4.0 m aggregation

variogram	Nugget Effect $C_0 (\%)^2$	Structure 1 (Spherical)		Structure 2 (Spherical)	
		Range ( $a_1$ ) (m)	Sill ( $C_1$ ) (%) <sup>2</sup>	Range ( $a_2$ ) (m)	Sill ( $C_1$ ) (%) <sup>2</sup>
Aggregation 2 m	16	8 vertical	48	260	223
Aggregation 4 m	8	10 vertical	39	262	222
Punctual	128	6	57	258	224

The parameters for the theoretical punctual model deduced from variogram models of 2.0 and 4.0 meter aggregation are shown in Table 6. Figure 31 shows the simplified procedure of deducing the theoretical punctual model parameters.

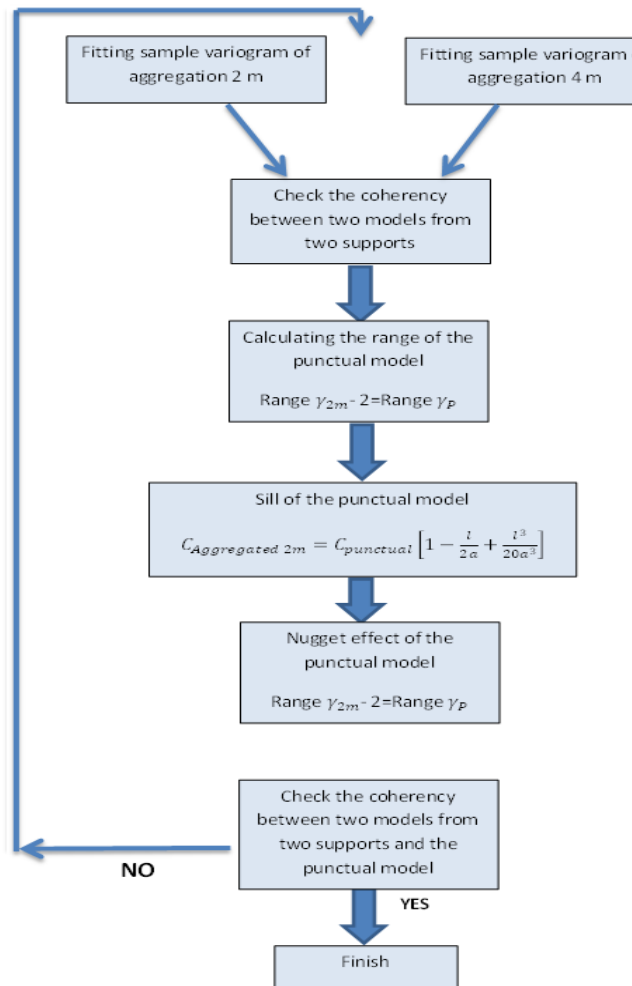


**Figure 31.** Flowchart of procedure to deduce theoretical punctual model from variogram models of 2.0 and 4.0 meter aggregation

Given the parameters deduced from the variogram models of 2.0 and 4.0 meter aggregation (Table 6), the theoretical punctual model can be compared to the aggregated variogram models (Figure 32). The approximate theoretical coherency between three variogram models is seen to be obeyed, with the theoretical punctual model having a smaller range (-2.0 m) than the variogram model of aggregated 2.0 m and a higher sill with the same structure as the aggregated sample variograms.

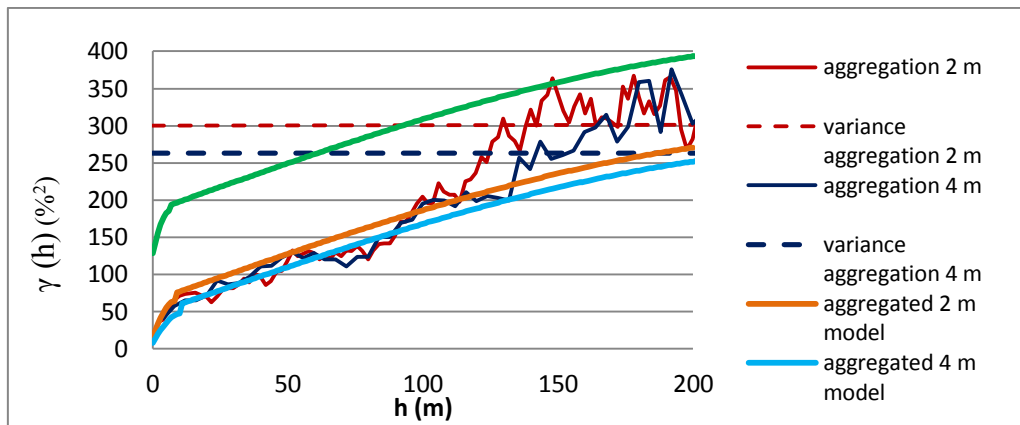


**Figure 32.** Variogram models fitted on vertical experimental variograms obtained from 2.0 and 4.0 meter aggregation and the deduced theoretical punctual model

The parameters obtained for the theoretical punctual model can be used in the kriging system, using an estimation that considers all raw sample values without any transformation.

### 3.4 CROSS-VALIDATION

To choose the appropriate model obtained from methods applied in the case study, cross validation is performed. Tables 7 and 8 show a comparison of the cross validation results. In the first column is reported the method of support change, (input), in the second column the number of samples. According to Table 7, the theoretical punctual model has a smaller variance of errors than the aggregation model, with the variance of standardized error closer to one. This seems to show the potential benefit of using the theoretical punctual parameters. The regularization method provides values close to the theoretical punctual model. However, as shown in Table 7, on account of the variance of standardized error, the model has a more precise fitting in the case of 2.0 meter

regularization because the standardized error is closer to one. The reason is the weak coherency between the two supports (2.0 and 4.0 meters) obtained from aggregated samples, which influences the theoretical punctual model deduced from the two above-mentioned variogram models. Therefore, as showed in Figures 29 and 30, it is not easy to have a precise fitting because samples are not homogenous in the ore body.

The slope of regression, as shown in Tables 7 and 8, is a parameter to select the optimum neighborhood for performing kriging. It means identifying the maximum distance of the neighborhood and the number of samples used for kriging. An optimum neighborhood has a slope regression close to one (Rivoirard 1987).

**Table 7.** Results of cross-validation using different models for 2.0 meter support

Input data	Number of Input data	Minimum Length (m)	Variogram	Slope regression	Estimation variance (%) <sup>2</sup>	Variance of error (%) <sup>2</sup>	Variance of Standardized error (%) <sup>2</sup>	Number of target points
Raw data	944	0.25	Theoretical Punctual model	1.00	141.37	109	0.78	346
Aggregation 2.0 m	370	1.50	Aggregated	0.96	149.82	110	0.74	346
Regularization 2.0 m	1378	1.50	Regularized	0.95	138.77	109	0.81	346
Regularization 2.0 m	1436	1.00	Regularized	0.95	139.00	109	0.81	346
Regularization 2.0 m	1477	0.50	Regularized	0.95	138.53	109	0.81	346

**Table 8.** Results of cross-validation using different models for 4.0 meter support

Input data	Number of Input data	Minimum Length (m)	Variogram	Slope regression	Estimation variance (%) <sup>2</sup>	Variance of error (%) <sup>2</sup>	Variance of Standardized error (%) <sup>2</sup>	Number of target points
------------	----------------------	--------------------	-----------	------------------	--------------------------------------	------------------------------------	---	-------------------------

<b>Raw data</b>	<b>944</b>	<b>0.25</b>	<b>Theoretical Punctual model</b>	<b>1.00</b>	<b>145.20</b>	<b>141</b>	<b>0.94</b>	<b>234</b>
<b>Aggregation 4.0 m</b>	426	3.50	Aggregated	1.00	146.17	131	0.87	234
<b>Regularization 4.0 m</b>	638	3.50	Regularized	0.91	162.05	127	0.76	234
<b>Regularization 4.0 m</b>	665	3.00	Regularized	0.91	161.29	129	0.76	234
<b>Regularization 4 m</b>	742	1.50	Regularized	0.91	161.04	141	0.85	234
<b>Regularization 4 m</b>	<b>784</b>	<b>0.50</b>	<b>Regularized</b>	<b>0.91</b>	<b>160.53</b>	<b>143</b>	<b>0.86</b>	<b>234</b>

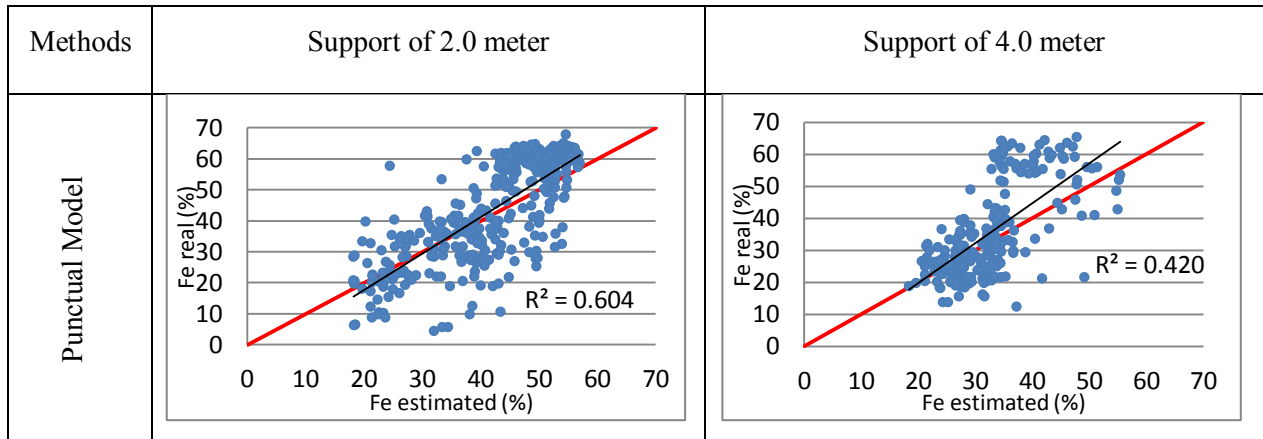
In the case of a 4.0 meter support (Table 8), the variance of standardized error is closer to one on account of the precise fit of the variogram model (Figure 29). Nonetheless, the theoretical punctual model has a lower variance value error compared to the regularized model (whose minimum length is 0.5 meter).

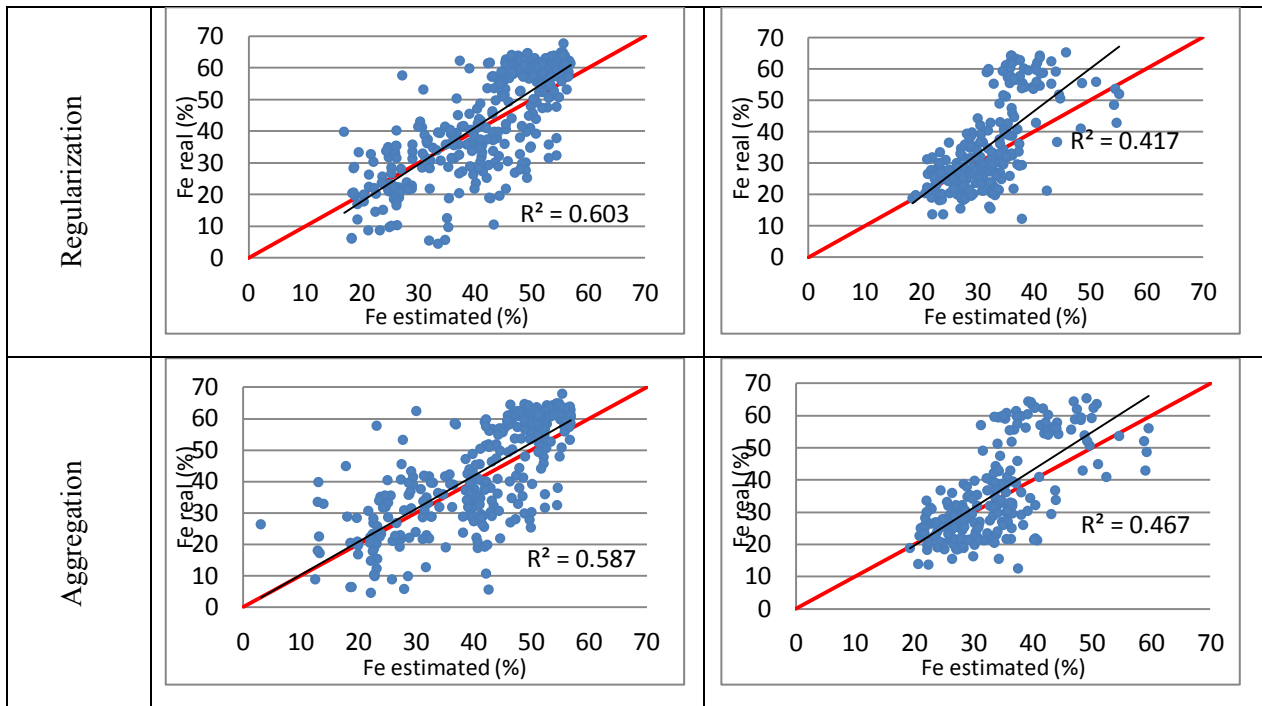
In addition, the cross-validation results clarify how minimum sample length influences the estimation results. Considering different minimum lengths leads to considerable input data differences, which will have an important effect on estimation results (Oliver and Webster, 2014). For example, in the case of 4.0 meter regularization with a minimum length of 3.0 (or 3.5) meters, some parts of samples with lengths of under 3.0 (or 3.5) meters are not regularized, with the result that the variance of error will be small, and the results not comparable with the results of the theoretical punctual model. This must also be considered in the case of aggregation, i.e. that some parts of data are used while integrating samples. Therefore, while performing cross validation and comparison, all effective parameters, which influence models (such as number of samples), should be considered in order to avoid ambiguous results. In this case study, the theoretical punctual model with the lower variance of error has a value of standardized error variance near to one and is one giving the most accurate estimation model, compared those obtained using other variogram models. To assess the correlation between the unprocessed measure data and estimated values, the scatter plots between estimated vs. measured data are shown in

Table 9. The scatter plots can be examined in the context of the properties of the kriging estimator, highlighting data that are poorly explained by their neighbors. In this case study, the theoretical punctual model (in a 2.0 meter support) shows a higher correlation between measured data and estimated values. The result is the same for the 4.0 meter example, and the variogram model obtained from regularized data (minimum length 0.5 m). As mentioned above, the aggregation method does not use some of the samples; consequently, the aggregation results in the case of the 4.0 meter support can only be compared with regularization for a minimum length of 3.5 meters, which presents the same situation with similar input data.

In Table 8, the cross validation results of aggregated data are compared with 4.0 meter regularization with a minimum length of 3.5 meters, showing that the aggregation method has a smaller estimation variance and a variance of standardized error closer to one.

**Table 9.** Scatter plot of original data and estimated values using aggregation model (2.0 m and 4.0 m targets)





### 3.5 CONCLUSION

As illustrated in this Chapter, measured data rarely present the same support, a prerequisite for the geostatistical modeling. The data integration method for changing the support has a significant effect on variability analysis, and consequently, on estimation results. In addition to the commonly used regularization method to integrate data, the ‘Aggregation’ method is proposed for homogenizing samples and constructing datasets for variogram modeling using sample with the same support. Each sample-compositing method has advantages and drawbacks, which affect subsequent spatial analysis and structural identification. Although all samples may be used in the regularization data-integration method, data will be smoothed, which decreases the variance. With the aggregation method, on the other hand, although compositing possibly

omits some of the data, it allows to consider all samples at their length. The regularization method uses a minimum regularization length and it has not only an important influence on the number of input data but also may change the local mean of samples. Besides the regularization and aggregation methods, theoretical punctual modeling is a further method allowing inclusion of all raw samples without transformation. Using all samples provides greater coherency with input data and an appropriate approximation of data spatial structures. Comparison of cross validation results shows the advantage of deducing the theoretical punctual model. Even so, the regularization method has similar results to the punctual model in this case study. The similarity of results is due to the fitting difficulties of the aggregated sample variograms and the knock-on negative effects on the deduced punctual model. In this case study, the fitting difficulties of the variogram model are due to different subsets of original data (as shown in the geological cross sections). However, in the case of a 4.0 meter support, the theoretical punctual model is more accurate than the regularized variogram model (with minimum length of 0.5 m).

Non-homogeneous data and complex geological units (Figure 29) show the necessities of deep studies of the geostatistical methods for the selected case study. According to the cross-validation results and scatter plots, the regularized 2.0 meter samples can be considered as an appropriate input data and related model (regularized 2.0 meter model) can be used in the next Chapter. Because of the low variance of standardized error and high correlation coefficients similar into the theoretical punctual model in scatter plots, regularized 2.0 meter model can be chosen for ore body estimation in case of transitional boundaries.



## **4 ESTIMATION METHODS IN TRANSITIONAL BOUNDARIES**

Kriging is the main geostatistical estimation method that gives the unbiased linear estimates of point values or of block averages with the minimum variance. Different types of kriging estimators were developed, according to the available source of information and spatial variability of the variable of interest (Armstrong 1998):

Simple kriging (SK) assume known mean, Ordinary Kriging (OK) assume unknown mean, Co-Kriging (CK) allows for estimation using information coming from multivariate variables. Indicator Kriging (IK) estimate indicators (binary-transformed variables), Universal Kriging (UK) incorporate trend (space-varying mean called trend). The literature about Kriging methods is vast and among the others, it is worth to mention (Armstrong, 1998; Chiles and Delfiner, 2012; Journel and Huijbregts, 1991; Wackernagel, 2003). In this study, an explanation of the kriging method adapted for the specific case study will be detailed. like CK, the use of geological information as auxiliary variable, makes possible to produce a coherent model between geological units in transitional areas and grade. The aim of this work is to test different geostatistical approaches and particularly different tools to identify the transitional areas such as contact plots and preferential relationship schemes (Séguret, 2012.).

## 4.1.LOCAL MODEL

Geological domains are usually determined according to the spatial continuity of grades and the geological features, such as lithology, mineralogy and alteration (Ortiz and Emery, 2006). The local estimation is using spatial variability models and input data (only data within a specific geological unit) for each geological unit independently to estimate variables for each geological unit. In this work, based on the characterization studies done by the exploration office of Sechahun iron mine, the construction of the geological model (3D) was performed. To construct the geological ore model, geologists used the polygon interpolation method to represent the volume of mineralization in each geological unit. The geological ore model is given by a 3D model (poor and rich geological constrains). These geological models are generated by geological sections (Figure 33). The geological ore models (3D) have been constructed by geology office of the mine, according to mineralization units for the local ordinary kriging (Figure 34). Two models (with orange and red colors in Figure 34) identifying the rich and poor units are used to estimate the grade using only samples within rich and poor geological units (Kasmaee and Torab 2014). The local OK estimation is performed by three sample variograms and their models obtained from three set of samples: poor, rich and metasomatite (Figures 35, 36 and 37), considering a unique block model (25 m. 25 m. 10 m). Mining engineers of the Sechahun iron mine have performed the local OK for three main geological units of the ore body considering hard boundaries: poor unit inside the orange model, rich unit inside the red model and metasomatite with a neighbourhood outside the mentioned models (Figure 34). In this study, the work is reconstructed, with the geological models provided and the exact block model.

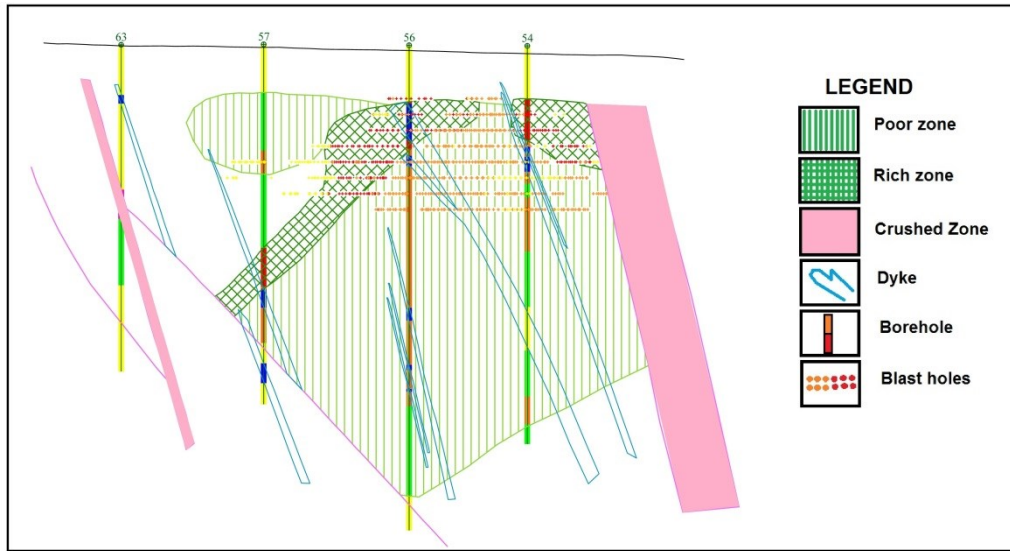


**Figure 33.** Geological cross section illustrating use of bore holes and blast holes in 3D geological modelling

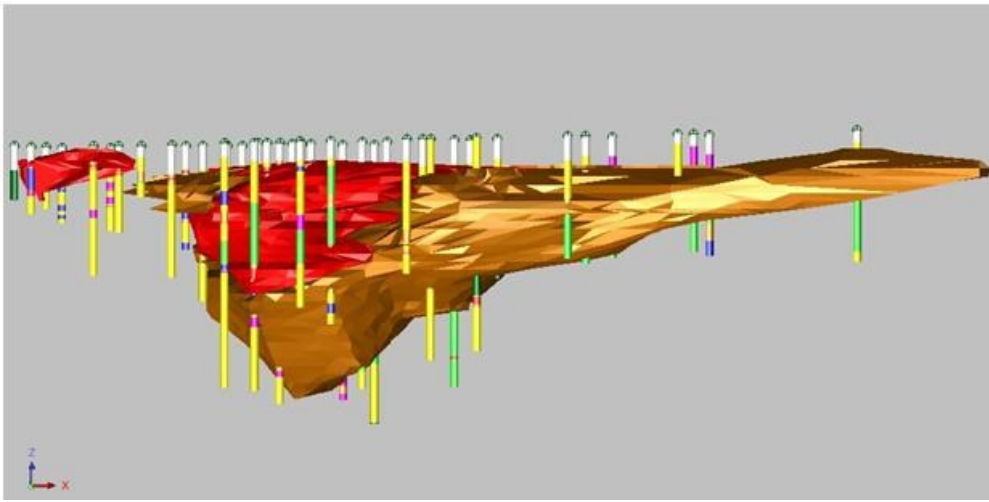


**Figure 34.** Geological model in 3D indicating poor zone (orange) and rich zone (red)

However, through this procedure some problems arise:

- 1- The definition of geological domains relies on the subjective interpretation of the mining geologists and on their understanding of the genetic

processes causing the mineralization. Various interpretations are therefore possible;

- 2- The description of the geological units is always subjected to errors, since only fragmentary information is available through a finite set of samples drilled in the deposit. For instance in Figure 36, in rich geological unit recognized by geologists, after analysing samples there are some data with very low iron concentration that might be an error;
- 3- Delineating the domains must be done carefully, accounting for geological knowledge about the deposit genesis and the type of geological boundaries. The boundaries that define the contact between adjacent geological domains are seldom ‘hard’, the grades measured at either side of a boundary are not independent. Besides, the boundary may be defined by a change in the local mean grade, which is usually gradational rather than abrupt.

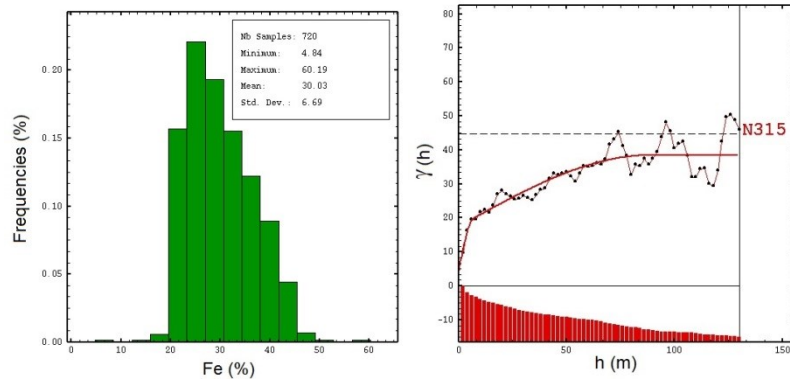


**Figure 35.** Histogram and Sample variogram (black points) and the variogram model (red line) for regularized 2.0 meter samples residuals- poor zone

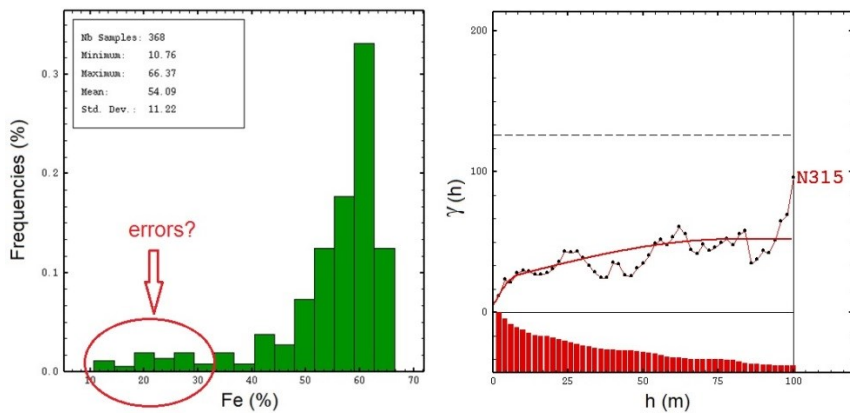


**Figure 36.** Histogram and Sample variogram (black points) and the variogram model (red line) for regularized 2.0 meter samples residuals- rich zone

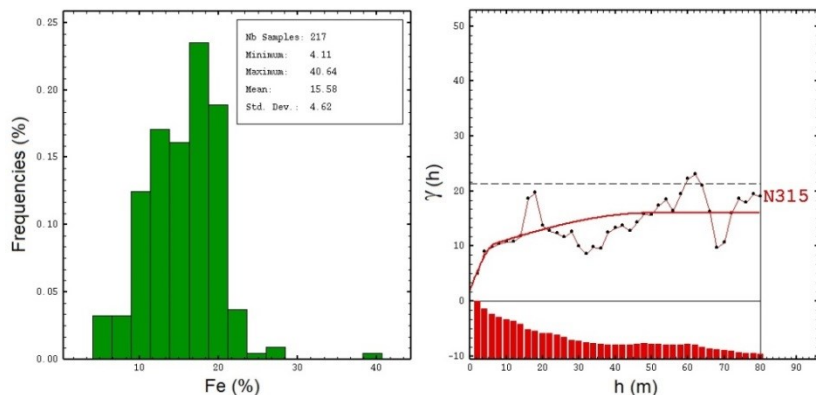


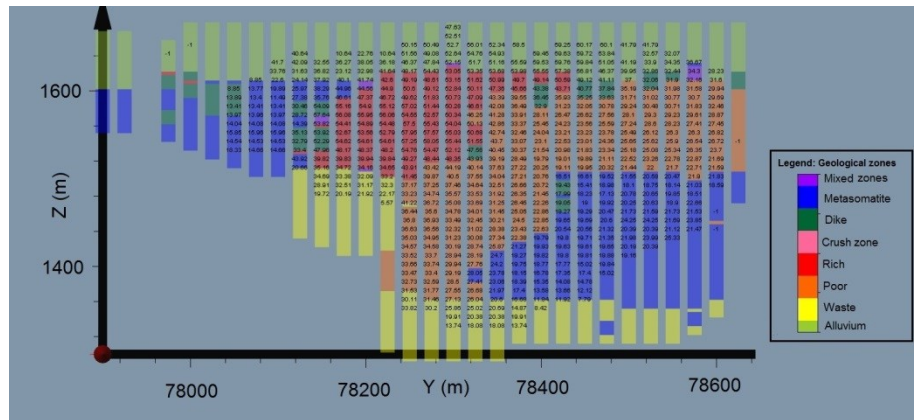
**Figure 37.** Histogram and Sample variogram (black points) and the variogram model (red line) for regularized 2.0 meter samples residuals- metasomatite zone

According to the models used for local estimations showed in Figures 35, 36 and 37, OK is used to estimate iron concentration within each domain. To perform the OK method on the case study, the input data and the variogram model selected from the previous Chapter is regularized 2.0-meter samples. This is according to the conclusion of the Chapter 3, which results had the minimum variance of error and the maximum correlation between the estimated

values and real values. To estimate the ore body in this method three domains were identified. For each domain a variogram model is used, as follow:

- Poor model (Figure 35) for estimating the poor unit (samples only inside the domain) considering hard boundaries;
- Rich model (Figure 36) for estimating rich unit (samples only inside the domain) considering hard boundaries;
- Metasomatite model (Figure 37) for estimating outside of the poor and rich units with a neighbourhood distance coherent with the range of variogram model

After estimation by local OK method, the grade variability in three main geological units is showed on geological sections (including all geological units) to highlight problems of this method, especially in the transition zones showed in geological sections (Figure 38).



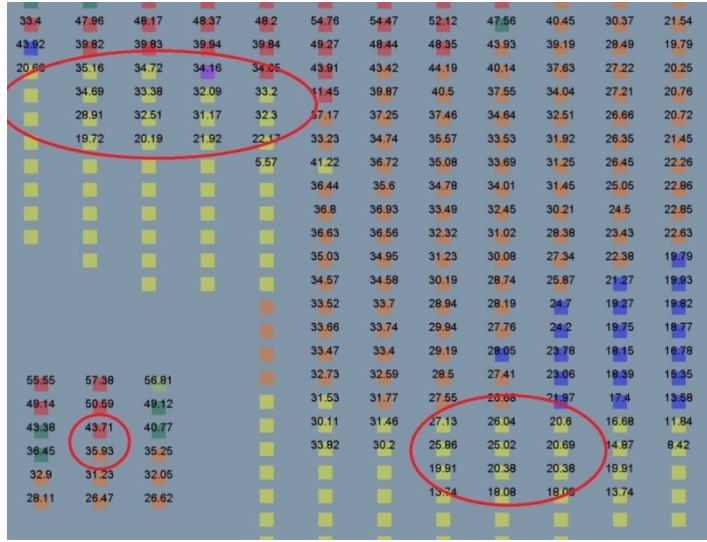


**Figure 38.** An example of a geological section of the mine and estimation results obtained from local models (upper Figure) and zoom of three specific areas ( lower Figure)

As shown in Figure 38, some estimated areas of the ore body have iron concentration higher than cut-off while are identified by geologists as “waste” unit, which can be used for excavation. Moreover, in areas between poor and rich units there are some estimated blocks with a big difference in iron concentration (about 8%) in comparison to other blocks (about 2-3%) (Figure 38). This can be interpreted because of considering hard boundaries in this method and using only the data inside one geological unit (but not samples in neighbourhood from other geological units) the continuity of grades cannot be followed by local estimations. To address these problems, one must know if the boundaries can be called soft or hard and, if a soft boundary exists, how to incorporate information from across this boundary to estimate the grades in a particular geological domain. Hence a global model is suggested with deeper studies of boundaries.

## 4.2 GLOBAL MODEL

To incorporate all available geological information and borehole samples the global model was performed. It means one variogram model for all borehole samples from all geological units. Several geostatistical methods were used to perform estimation and then a comparison of the results and with the local model is presented.

The spatial variability model (Figure 39) is obtained from regularized 2.0 meter-samples with minimum length of 0.5 meter according to the results obtained in Chapter 3.

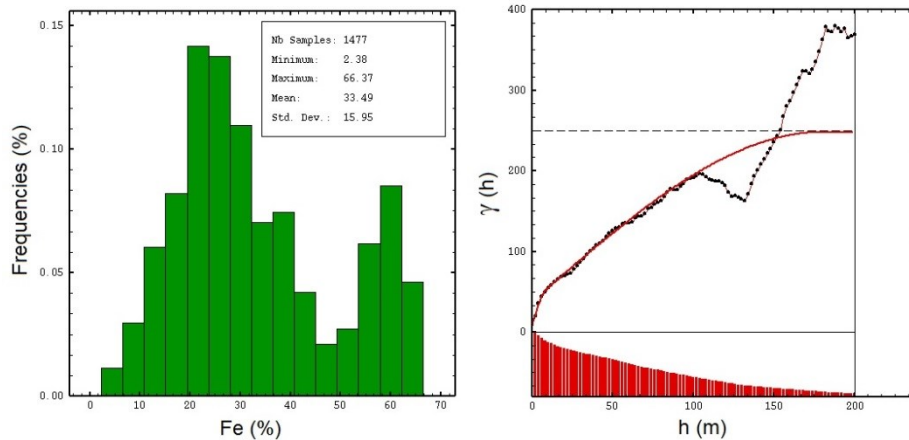


**Figure 39.** Histogram and vertical sample variogram (black points) and variogram model (red line) for regularized 2.0 meter samples

Due to vertical sample variograms and complexity of the ore body shown in section 3.3.3, a deeper study for the hypothesis of vertical trend was performed. The values of the variogram after 150.0 m were higher than the variance and they were keeping increasing that was a possibility of a vertical trend in the ore body.

#### 4.2.1 Hypothesis of modeling: trend

Perhaps the most critical decision in geostatistical modeling is choosing the stationary domains or populations for reserve estimations. The boundaries between the stationary domains should be modeled and the correlations of variables and trend analysis across these boundaries should be used in modeling. When a trend is present one generally turns to the universal kriging (UK) model (Chiles and Delfiner, 2012). In UK model the random function is considered as the sum of a deterministic trend ( $a(x)$ )

$$F(x) = (a(x) + b) + R(x)$$

where  $a(x)$  is the trend,  $x$  is the location in space,  $(a(x) + b)$  is as a polynomial with unknown coefficients ( $b$ ) and a zero mean stationary or intrinsic random residual  $R(x)$  (Chiles and Delfiner, 2012).

Then it is possible to perform UK estimation, when the residuals subtract from the original data:  $R(x)$ , which are assumed to be random. The mean of all  $R(x)$  is zero. Conceptually, the variogram modeling can be performed on residuals and then kriging applied on raw data and the variogram models of residuals.

$$Z(x_1, x_2, x_3) = a(x_3) + b + R(x_1, x_2, x_3) \quad (13)$$

The hypothesis of trend is from the sample variograms (in this study regularization 2.0 meters) which showed the upward behavior after 150.0 meters. To study deeply the presence of the trend, scatter plots are shown for three directions of Fe (%) variations. As it is shown in Figure 40, there is a decrease from top to bottom of the ore body (in vertical direction), and in North-South ( $Y$ ) direction.

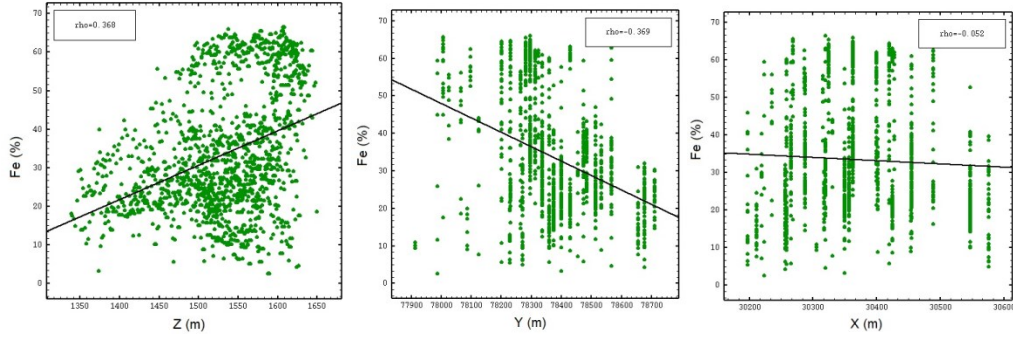


**Figure 40.** Scatter plots showing the iron variation in 3 directions (North-South, East-West and vertical directions), from regularization 2.0 m data

To test the hypothesis, by fitting a polynomial on data, residuals are calculated with the average of zero from Equation 13:

$$R(x_1, x_2, x_3) = Z(x_1, x_2, x_3) - a(x_3) + b$$

Where in this case study according to the Figure 40 and vertical trend,  $(a(x_3) + b)$  is a linear function in vertical direction, and by performing this linear regression function on data  $(Z(x_1, x_2, x_3))$ , residuals calculated  $(R(x_1, x_2, x_3))$ . Variogram is calculated for residuals (Figure 41).

The variogram model is fitted on residual variogram and then it is used in UK estimation.

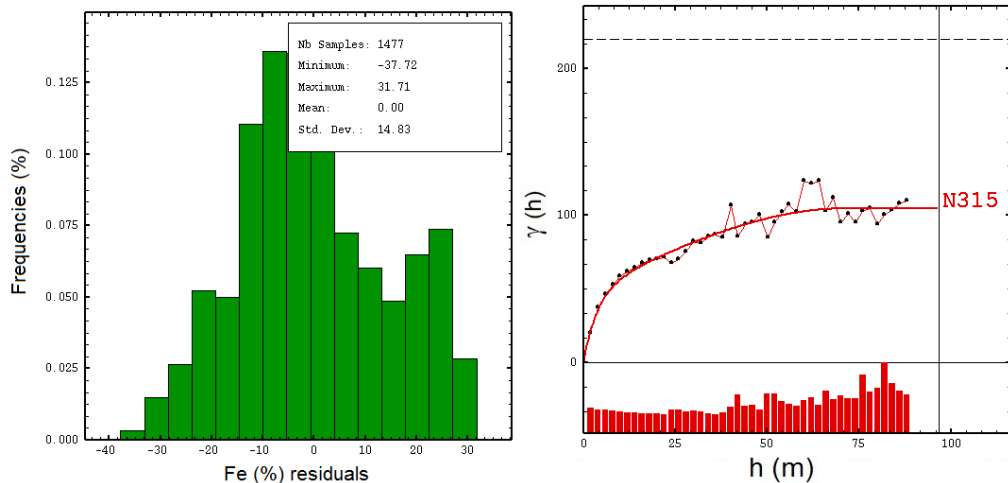


**Figure 41.** Histogram of Fe(%) residuals and sample variogram (black points) and variogram model (red line) for regularized 2.0 meter samples residuals

A comparison between OK and UK using cross-validation is presented in (Table 10). Moreover, scatter plots between true data (borehole samples) and estimated values are shown in Figure 42.

**Table 10.** Results of cross-validation using different models for OK and UK methods

Method	OK	UK
<b>mean-error (%)</b>	-0.14	-0.14
<b>variance-error (<math>\%^2</math>)</b>	26.45	26.73
<b>variance-standardized- error (<math>\%^2</math>)</b>	0.89	0.91

Results show that the model used for OK has the smaller variance of error, but the variance of standardized error in UK is closer to one that shows a more coherent fit of the variogram model.

## 4.3 INCORPORATE GEOLOGICAL INFORMATION

To include geological information into reserve estimation, geological units (or zones) can be interpreted as realizations of random sets (Matheron, 1982).

Indicator Kriging (IK) is a kriging analysis performed on a binary-transformed sample population. This approach firstly proposed by Journel (1983) can be used if the spatial correlation of a parameter is difficult to describe by raw data. Other applications of the IK are the modeling of categorical variables, e.g., if a sample belongs to a certain rock type, or if a variable lies above or below a defined cutoff value (Glachen and Snowden, 2001). Defining indicators for categorical variables would lead to the following transformation:

$$\forall x, i, 1_i(x) = \begin{cases} 1 & \text{if } x \in \text{unit } i \\ 0 & \text{otherwise} \end{cases} \quad (14)$$

When  $x$  (a point at the location of  $x$ ) belongs to just one unit,  $i$  is the indicator transform and the sum of the indicator functions is 1

$$\sum_{i=1}^n 1_i(x) = 1 \quad \forall x \quad (15)$$

The same notation  $i$  is used for unit indices and the sets themselves. It is important to distinguish between the independency of two random sets  $i$  and  $j$ , where in particular

$$P(x \in i, x \in j) = P(x \in i)P(x \in j) \quad (16)$$

And disjoined sets defined by

$$i \neq j, i \cap j = \emptyset \Leftrightarrow \forall x, 1_i(x)1_j(x) = 0 \quad (17)$$

Equation 16 expresses a spatial link between the sets making disjoined sets dependent and Equation 17 is defined for disjoined sets. In the following,  $i$  and  $j$  are disjoined sets.

As the indicator function is defined by Equation 14, its mathematical expectation is the probability for  $x$  to belong to  $i$ . When the indicator function  $I_i(x)$  is sampled in  $n$  locations, its mathematical expectation  $p_i$ , a probability, is interpreted as a spatial unit proportion and approximated by  $\frac{n_i}{n}$ , ( $n_i$  is the number of samples coded  $i$ ).

The indicator variogram is defined as in Serra (1982) by the variance of indicator increments and equals:

$\gamma_i(h) = 0.5[P(x + h \in i, x \notin i) + P(x + h \notin i, x \in i)]$ . Assuming the symmetry in  $h$  of the probabilities leads to:

$$\gamma_i(h) = P(x \in i, x + h \notin i) \quad (18)$$

If the indicator variogram is stationary, the variance becomes its sill: for large distances  $h$ , and the probability of the pair of events is the product of their probabilities

$$\text{Sill of } \gamma_i(h) = P_i(1 - P_i) \quad (19)$$

The indicator cross variogram  $\gamma_{ij}(h)$  is defined as:

$$\gamma_{ij} = -E[I_i(x)I_j(x + h)] = -P(x \in i, x + h \in j) \quad (20)$$

For  $h$  close to 0, the absolute value of the cross variogram gives the probability of direct contact between  $i$  and  $j$  and practically, represents the counting of pairs of adjacent samples  $(i,j)$ .

If the cross variogram is stationary, the events  $\{x \in i\}$  and  $\{x + h \in j\}$  for  $h >$  range become independent and the probability of the pair of events equals the product of their probabilities

$$\text{Sill of } \gamma_{ij}(h) = -P_i P_j \quad (21)$$

As  $i$  and  $j$  are disjoined,  $\{x + h \in j\} \Rightarrow \{x + h \notin i\}$  when  $i \neq j$  and we have

$$\gamma_{ij}(h) = -P(x \in i, x + h \in j, x + h \notin i) \quad (22)$$

Taking the absolute value of Equation (22) divided by Equation (18) and by definition of the conditional probability, we have

$$\left| \frac{\gamma_{ij}(h)}{\gamma_i(h)} \right| = P(x + h \in j | x \in i, x + h \notin i) \quad (23)$$

Equation 22 gives the probability of reaching  $j$  when leaving  $i$ . In case of stationary direct and cross variograms, this ratio is bounded by a sill given by Equation (21) divided by Equation (19)

$$\left| \frac{\gamma_{ij}(h)}{\gamma_i(h)} \right| = \frac{P_j}{1 - P_i} \quad (24)$$

This is the probability of belonging to  $j$  related to what is not  $i$ .

#### 4.3.1 Indicator kriging method

The use of IK involves calculating and modeling indicator variograms at each geological unit. Applying this method to the case study, each geological domain of Sechahun iron mine is defined as an indicator and with the combination of statistical and geostatistical means, geological units can be estimated.

According to the selected input data in Chapter.3, all following studies are done by the use of the regularized 2.0 meter samples with the minimum length of 0.5 meter.

Geological information as Indicators is as follows:

$$\text{Example: } \text{Poor Zone } (PO) \begin{cases} x \in PO & : 1 \\ x \notin PO & : 0 \end{cases}$$

Geological information through indicators can be used as a spatial variable to be entered in the geostatistical modeling.

Once all indicators have been defined, the structural analysis of the geological units in each of these areas should be described direct and cross sample variograms reveal important details of the geological interaction since they provide analytical means to quantify the anisotropy and the range of the underlying forming process (Figure 42). After establishing a model for the spatial correlation, the next step in a kriging analysis of blocks over the study area.

In Figure 42, in the histogram of data, the Fe (%) data relating to each geological unit is highlighted in blue color.

According to the available samples Fe(%) and indicators, it is possible to perform three estimations:

- I) Co-Kriging of indicators (ICK) to identify the probability of each geological domain in the ore body;
- II) Co-Kriging of indicators and Fe (%) to evaluate the iron concentration of the ore body, considering to have indicators as auxiliary variables, even at target points;

III) Co-Kriging of indicators (as auxiliary variables) and Fe (%) to evaluate the iron concentration of the ore body, considering not having indicators at target points.

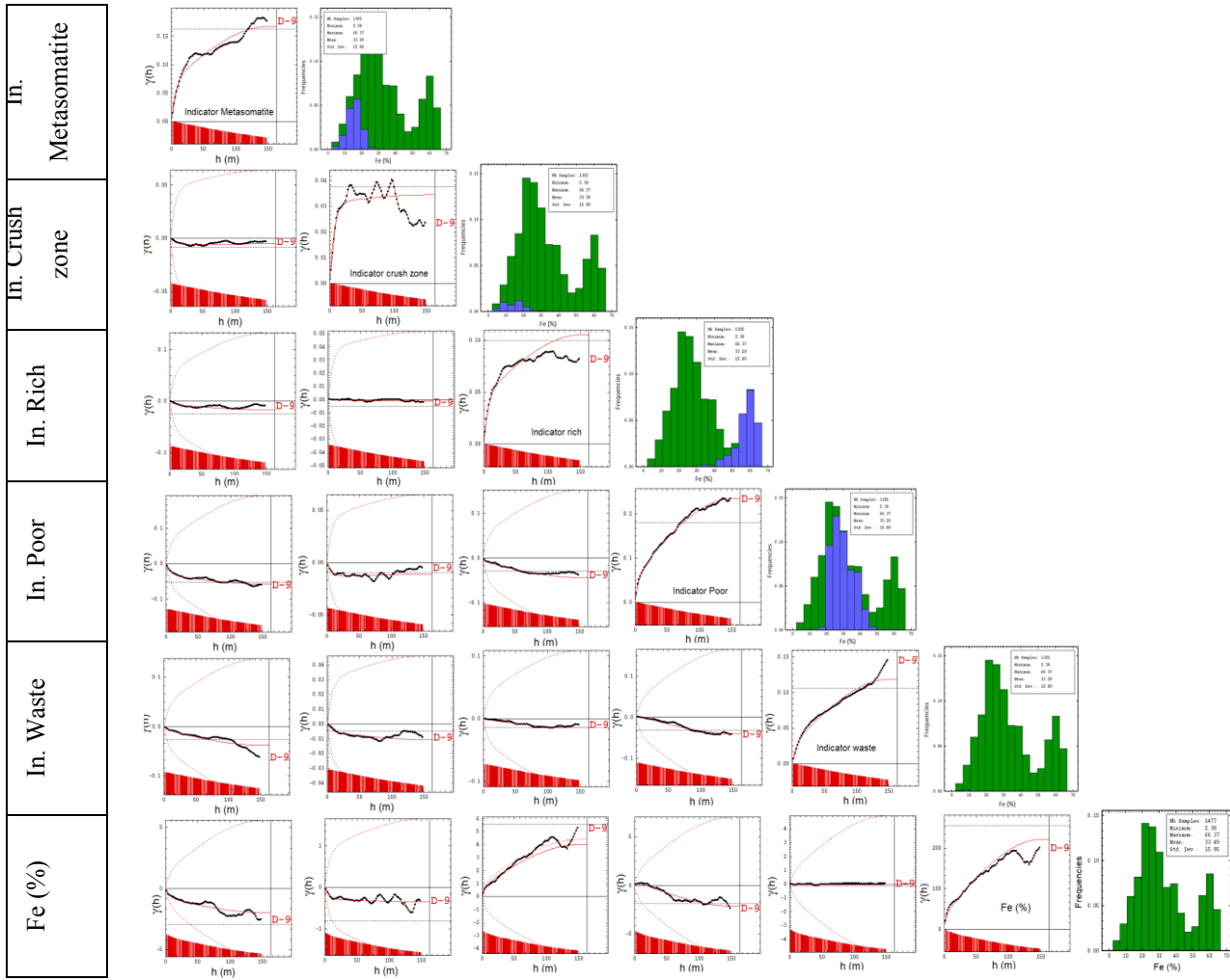


**Figure 42.** Sample variograms of indicators and Fe (%) (direct and cross variograms): Regularized 2.0 m samples

Moreover, through ICK of all indicators, it is possible to have an imagination from different geological domains and their interaction in different parts of the

ore body. Direct and cross sample variograms and models fitted are shown in Figure 42.

Figures 43, 44 and 45 show three examples of geological sections obtained from the ICK of indicators.

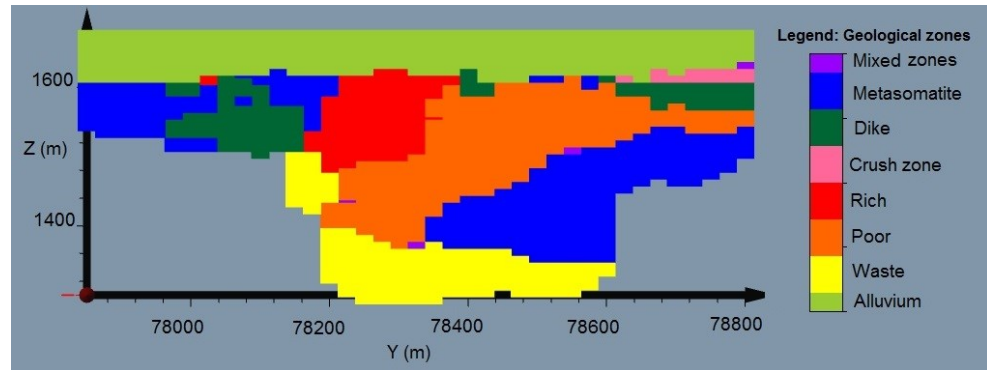


**Figure 43.** Section 9 showing ICK results

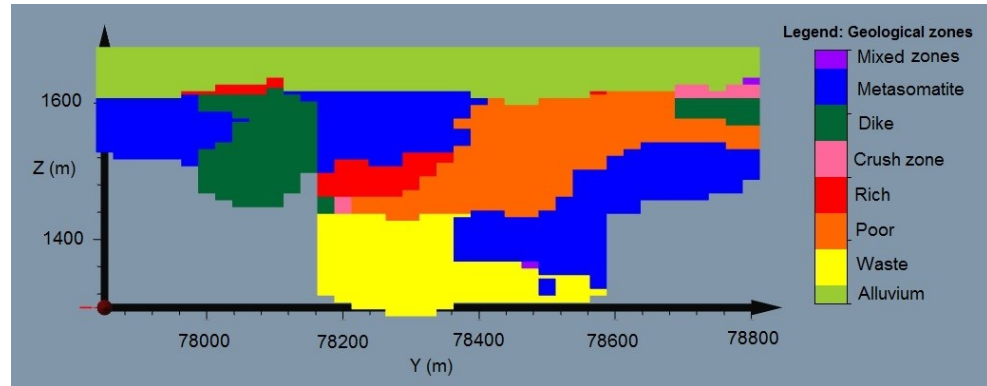


**Figure 44.** Section 11 showing ICK results

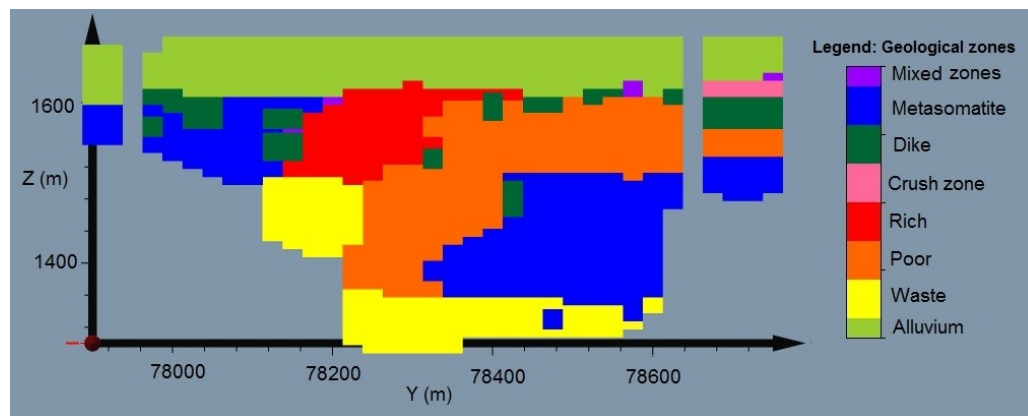


**Figure 45.** Section 13 showing ICK results

As it is shown, in this case study the ore body has a complex geological interaction between different domains, which calls for further studies for estimating the Fe (%).

To compare results of CK between indicators and Fe (%), cross validation is applied for each method. To perform cross validation, borehole samples are divided into five uniform distributed classes. Then cross validation is applied for each class, by removing data of one class and estimating borehole samples by the adapted spatial variability model using remaining samples. Results of cross validation are shown in Table. 11. Note that in all cases the input data are regularized 2.0 meter samples with the minimum length of 0.5 meter.

**Table 11.** Cross-validation results for five classes of borehole samples

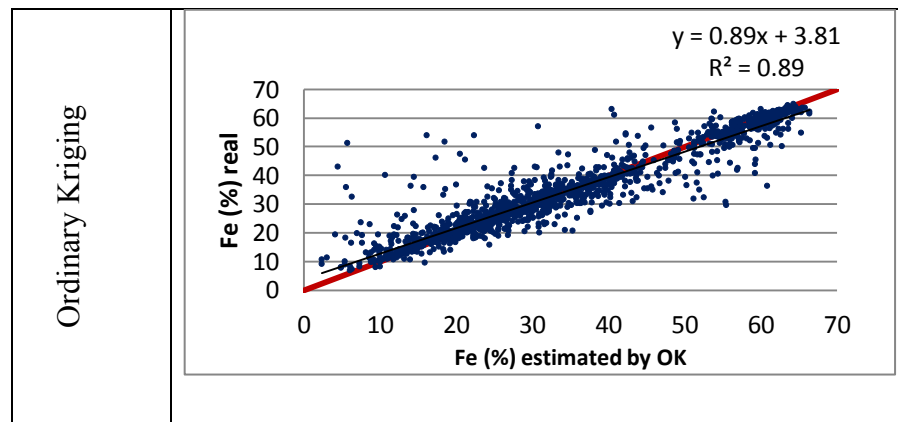
Borehole classes	Estimation method- Correlation coefficients (%)/(%)		
	OK- model	CK-without-Indicators	CK-with-Indicators
part1	0.95	0.95	0.97
part2	0.93	0.95	0.96
part3	0.93	0.93	0.95
part4	0.87	0.89	0.92
part5	0.96	0.96	0.98

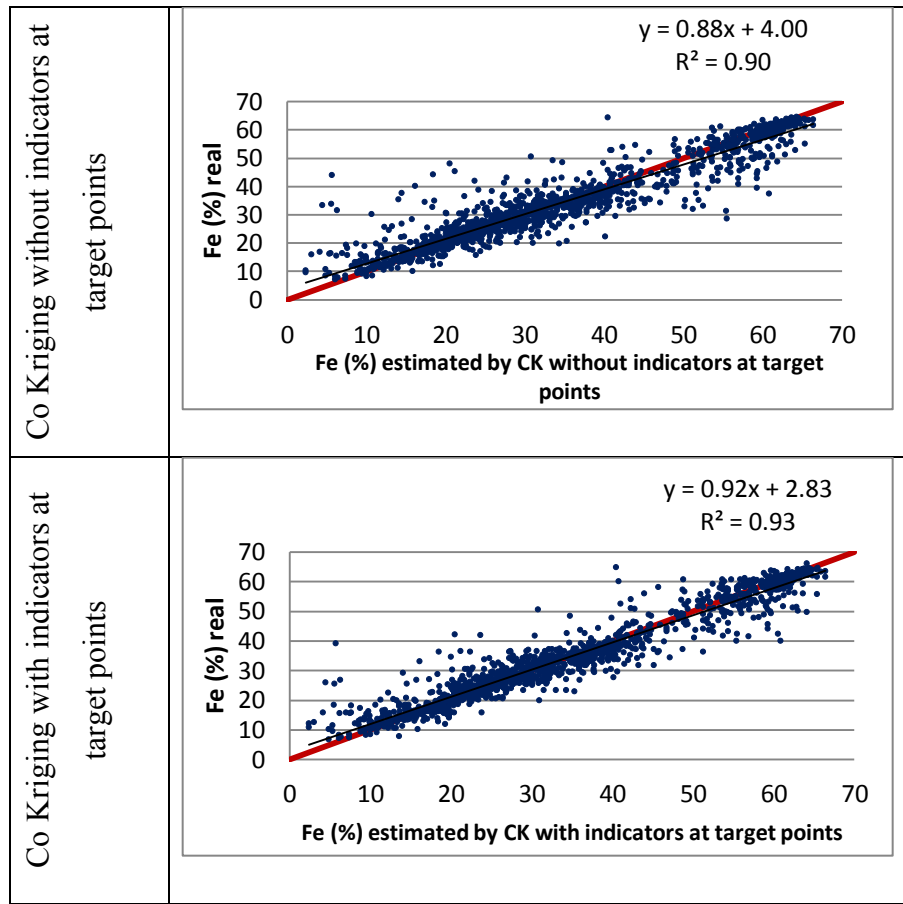
It is possible to combine all cross validation results to conclude from statistical parameters of errors and scatter plots (Table.12, Table.13) which show the coherency of each method.

**Table 12.** Total results of Cross-validation using two methods of CK and comparison with OK cross-validation results

Methods	CK- indicators at target points	CK- without indicators at target points	OK
mean-error (%)	-0.02	0.12	-0.09
variance-error(% <sup>2</sup> )	17.90	26.08	28.22
Variance of standardized error (% <sup>2</sup> )	0.82	0.99	1.04

**Table 13.** Total results of Cross-validation using two methods of CK and comparison with OK cross-validation results





As showed in Table.12, considering geological information leads to more coherent model for estimation. This shows that the model used for CK of indicators and Fe (%) when indicators are present at target points, gives reduced errors. To focus more on transitional boundaries and study the behavior of a variable within transitional areas, different methods are used.

The vertical trend hypothesis is studied for the all variables (Fe(%) and indicators) with the same function used before in the section of OK (in this study regularization 2.0 meters) which showed the upward behavior after 100.0 meters. Direct and cross sample variograms obtained from residuals are shown in Figure 46.

Universal co-kriging (UCK) can be used in this condition, considering indicators variables.. Results of cross-validation for the residual models are shown in Tables.14 and 15.

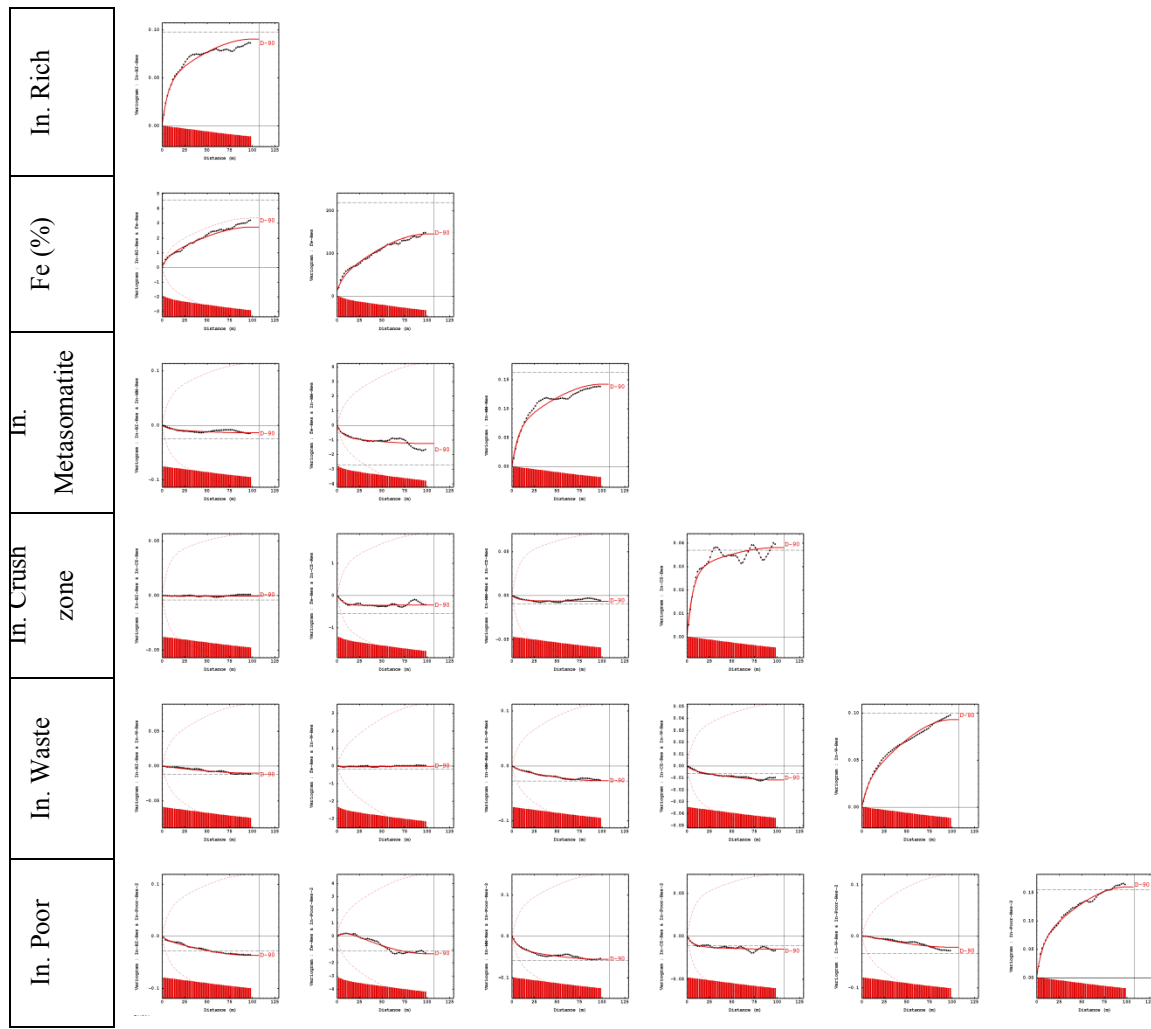


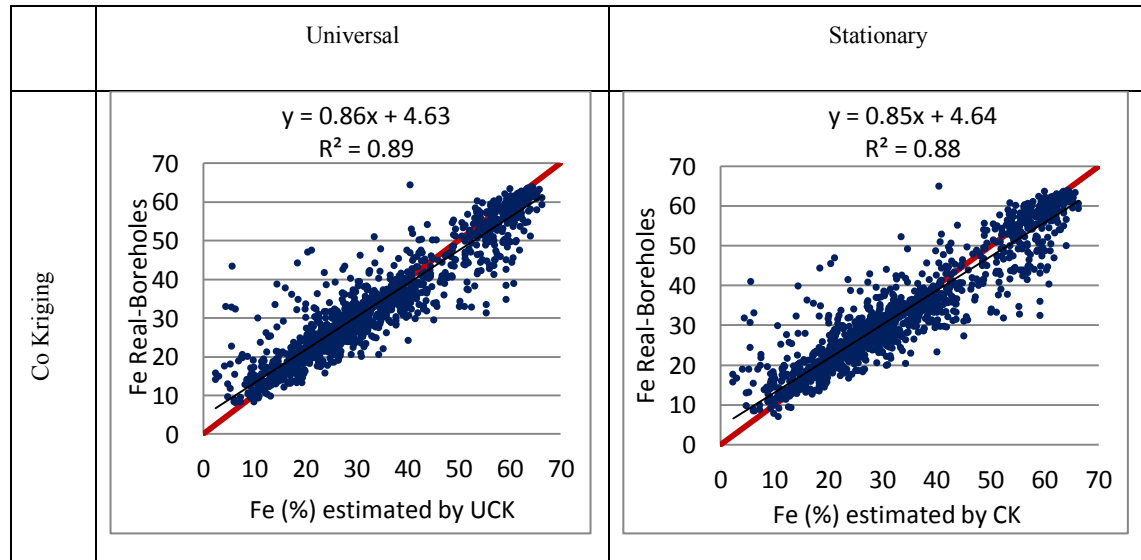
**Figure 46.** Residual sample variograms of indicators and Fe (%) (direct and cross variograms) for regularized 2.0 m samples

**Table 14.** Statistical parameters of cross-validation obtained from two CK and UCK

Statistical parameters	CK	UCK
------------------------	----	-----

mean-error (%)	0.28	0.20
variance-error (% <sup>2</sup> )	29.76	28.66
variance-standardized- error (% <sup>2</sup> )	1.12	0.97

**Table 15.** Scatter plots of cross-validation between real values (boreholes) and Fe (%) estimated by different kriging methods



According to the results shown in the Tables 14 and 15, the UCK results are very close to the CK results. However, cross-validation is used for the coherency of different models. For the comparisons of estimation methods, results are compared through validation methodology.

#### 4.3.2 Spatial transitions

Using indicators of data, it is possible to study the spatial transitions between different geological units. Using indicator samples, through Equation (17) indicator variograms are calculated and analyzed. (Figure 47)

According to the indicator variogram and the ratio ( $\left| \frac{\gamma_{ij}(h)}{\gamma_i(h)} \right|$ ) with cross-variogram (Equation 24), a new curve (variogram ratio) was calculated and analyzed. There are two quantities characterizing the curve (Seguret 2012):

1.  $P(\rightarrow j | i \rightarrow)$ , the value of the ratio for  $h$  close to 0 which represents the probability of encountering  $j$  while leaving  $i$  (i.e., practically the counting of pairs of samples  $(i,j)$  directly in contact divided by the total number of samples  $i$  involved in the calculation),
2. The sill of the variogram ratio (Figure 47), equal to  $\frac{P_j}{1-P_i}$  when the deposit is stationary and large compared to the range.

As it is,  $P(\rightarrow j | i \rightarrow)$  has no meaning for detecting preferential contacts because if the unit  $j$  into which we enter is omnipresent in the domain, upon leaving any  $i$ ,  $j$  will be encountered often. However, it has to be compared to something. Can it be the proportion of  $j$ ? Not exactly, because the contacts between  $i$  and itself have no interest, so the reference is the proportion of  $j$  relative to the proportion of what is not  $i$  and this gives  $\frac{P_j}{1-P_i}$ , the sill of the ratio variogram.

Finally, to quantify the preferential contacts, the interesting magnitude is the “Preferentiality value” from  $i$  to  $j$

$$\text{Pref}(i \rightarrow j) = P(\rightarrow j | i \rightarrow) - \frac{P_j}{1-P_i} \quad (25)$$

Preferential contact counting cannot be distinguished from the transition behavior. The physical interpretation is that if two units are more often in contact than they should be with regard to their proportions, their bodies share complementary shapes so their indicator functions are spatially linked.

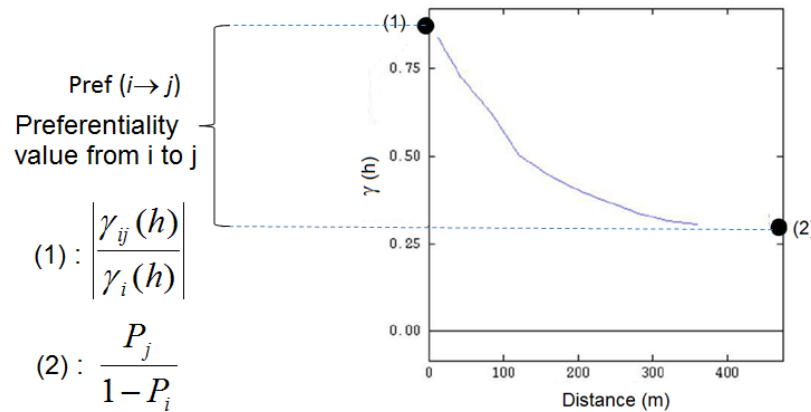


**Figure 47.** Practical inference of the parameter

The variogram ratio is calculated, as defined by Equation (23). Behavior close to 0 represents the contact probability of encountering unit  $j$  when leaving  $i$ , the sill (if any) represents the same probability but when the events {entering  $j$ } and {leaving  $i$ } are independent (assuming that the dimension of the deposit is large compared to the range of the ratio). The difference between the two quantities is defined as the Preferentiality Value defined by Equation (25).

There are four cases concerning the behavior of Equation (23) along  $h$ :

- 1-  $P(\rightarrow j | i \rightarrow) = 0$  The units  $i$  and  $j$  are never in direct contact, the contact starts at  $h > h_0$  (Figure 48(a)). Imagine that there are only 3 units  $i, j$  and  $k$ . If  $P(\rightarrow j | i \rightarrow) = 0$ ,  $k$  separates  $i$  from  $j$ . There will be a preferential contact between  $i$  and  $k$ , and between  $j$  and  $k$  and  $h_0$  represents the minimum width of  $k$  that has to be crossed in order to travel from  $i$  to  $j$ ;

2-  $P(i \rightarrow j) < 0$  The probability  $(\frac{P_j}{1-P_i})$  is smaller than it should be regarding  $P_i$  and  $P_j$ . (Figure 48(b)). This case is similar to the previous one. The range of the ratio is linked to the average width of the units to be crossed before a return to the situation where  $I_i(x)$  and  $I_j(x+h)$  become spatially independent;

3-  $P(i \rightarrow j) = 0$  The ratio  $(\frac{P_j}{1-P_i})$  is flat. There is no spatial transition and no preferential contact (Figure 48(c)).  $\gamma_{ij}(h)$  is proportional to  $\gamma_i(h)$ . If the reverse situation is true  $I_i(x)$  and  $I_j(x)$  are in intrinsic correlation, and knowledge of one unit provides no information of the second one. If the reverse situation is false, the geometry of  $j$  is subjected to the geometry of  $i$ , leading to an indicator residual model where indicator  $j$  is expressed as a linear function of indicator  $i$  plus a spatially independent residual;

4-  $P(i \rightarrow j) > 0$  The contact probability decreases with the distance (Figure 48(d)). Units  $i$  and  $j$  are preferentially in contact and it is the latter case that is exploited to build preferential relationship schemes.

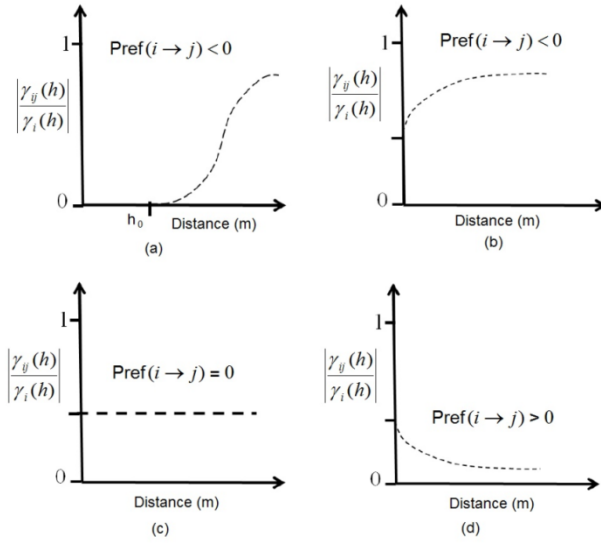


**Figure 48.** Different possible situations for the Preferentiality Values

As shown in Figure 48. (a) Units  $i$  and  $j$  are never in direct contact before  $h_0$ , which is the minimum width of the bodies that have to be crossed to reach  $j$  when leaving  $i$ . (b) Units  $i$  and  $j$  are in direct contact but less than they should be considering their proportions in the domain. (c) The Preferentiality Value is 0, the transition does not depend on the distance, the cross variogram between  $i$  and  $j$  is proportional to the indicator variogram of unit  $i$ , (d)  $i$  and  $j$  have a preferential contact with regard to their proportions in the domain.

Spatial transition analyses and the proportions involved in these calculations must be computed along directions to fit the anisotropies of the geological bodies and their preferential locations in space. Figure 48(d) shows an example of directional dependency issued from the case study of this paper. North-South and vertical transitions are similar, while the transition is different in the West-East direction. Practically, the directional quantities  $P(\rightarrow j | i \rightarrow)^{\text{dir}}$ ,  $P_i^{\text{dir}}$  and  $P_j^{\text{dir}}$  are based only on the pairs of samples  $(i,j)$  which respect the directional constraint.

## 4.4 TOOLS TO IDENTIFY TRANSITIONAL BOUNDARIES

### 4.4.1 Preferential relationship schemes

Séguret (2012) developed preferential relationship schemes. The method of Seguret was developed to detect preferential contacts, (i.e. only positive preferentiality values) and to assess the dominant behaviors of the several domains based on the theory of spatial transition. The idea is the mutual behavior of the geological units while analyzing transitions between the pairs  $(i,j)$ , for the whole extent of the ore deposit.

Therefore, Equation (23) is calculated in the three main directions and the pairs with positive Preferentiality Values  $\text{Pref}(i \rightarrow j)$  are retained as defined by Equation (25).

To identify the mutual behavior on geological units in the case study, the variogram ratios ( $\left| \frac{\gamma_{ij}(h)}{\gamma_i(h)} \right|$ ) are shown for three main directions (North-South, East-West and Vertical) in Figures 49 to 51. Variogram ratios make it possible to separate the units in contact with each other from those that are not and distinguish those with large contact zones. The number of the variogram plots is 25 because we have five geological units and variogram ratios are calculated in three directions separately.

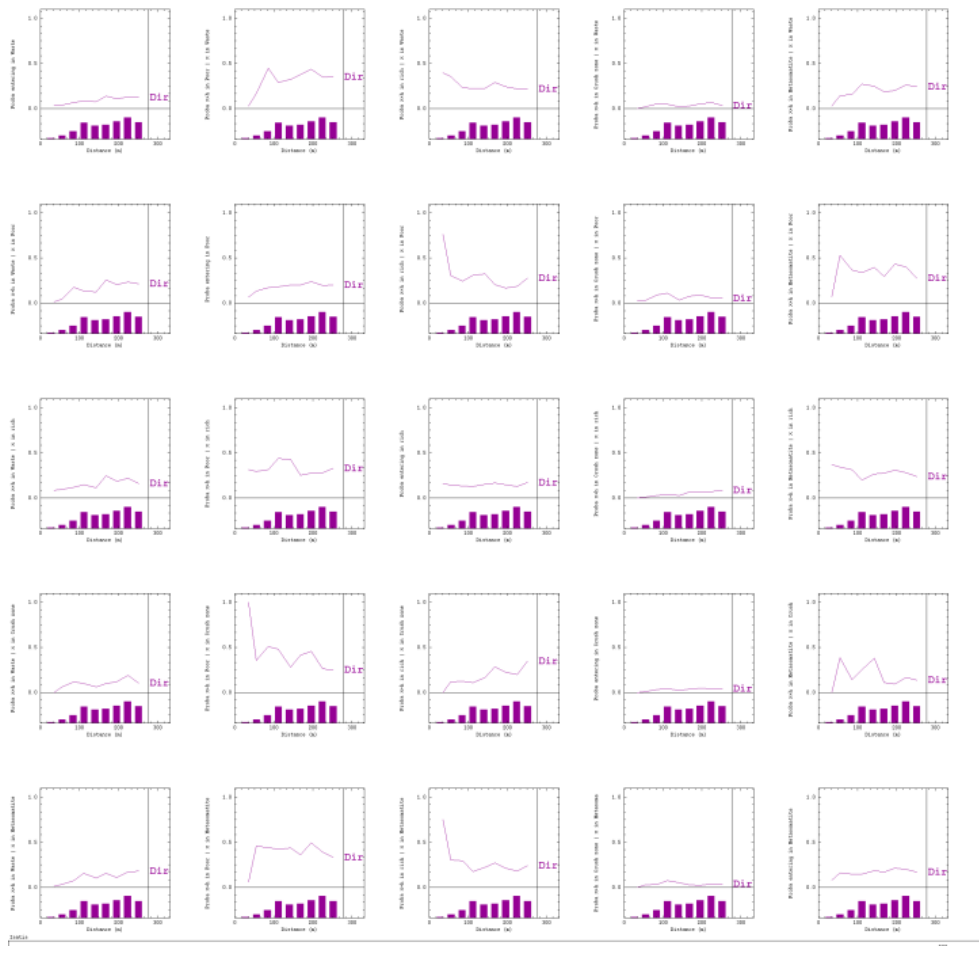


**Figure 49.** Cross indicator variogram divided by a single indicator variogram along the North-South direction

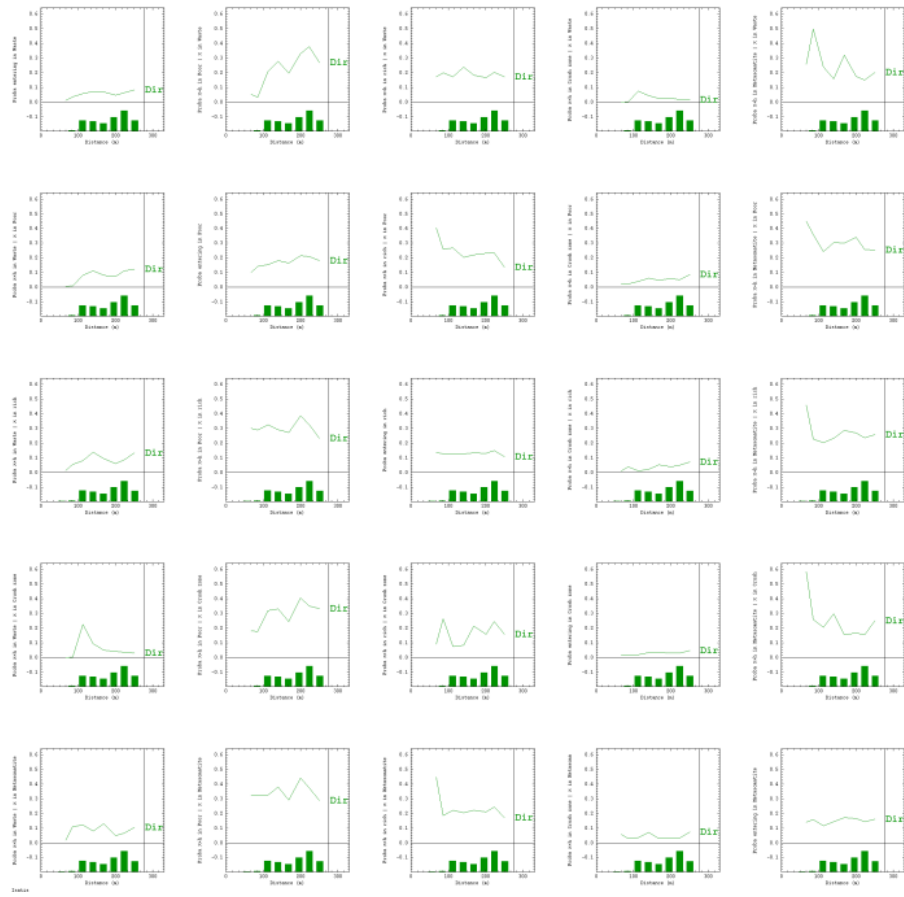


**Figure 50.** Cross indicator variogram divided by a single indicator variogram along the East-West direction

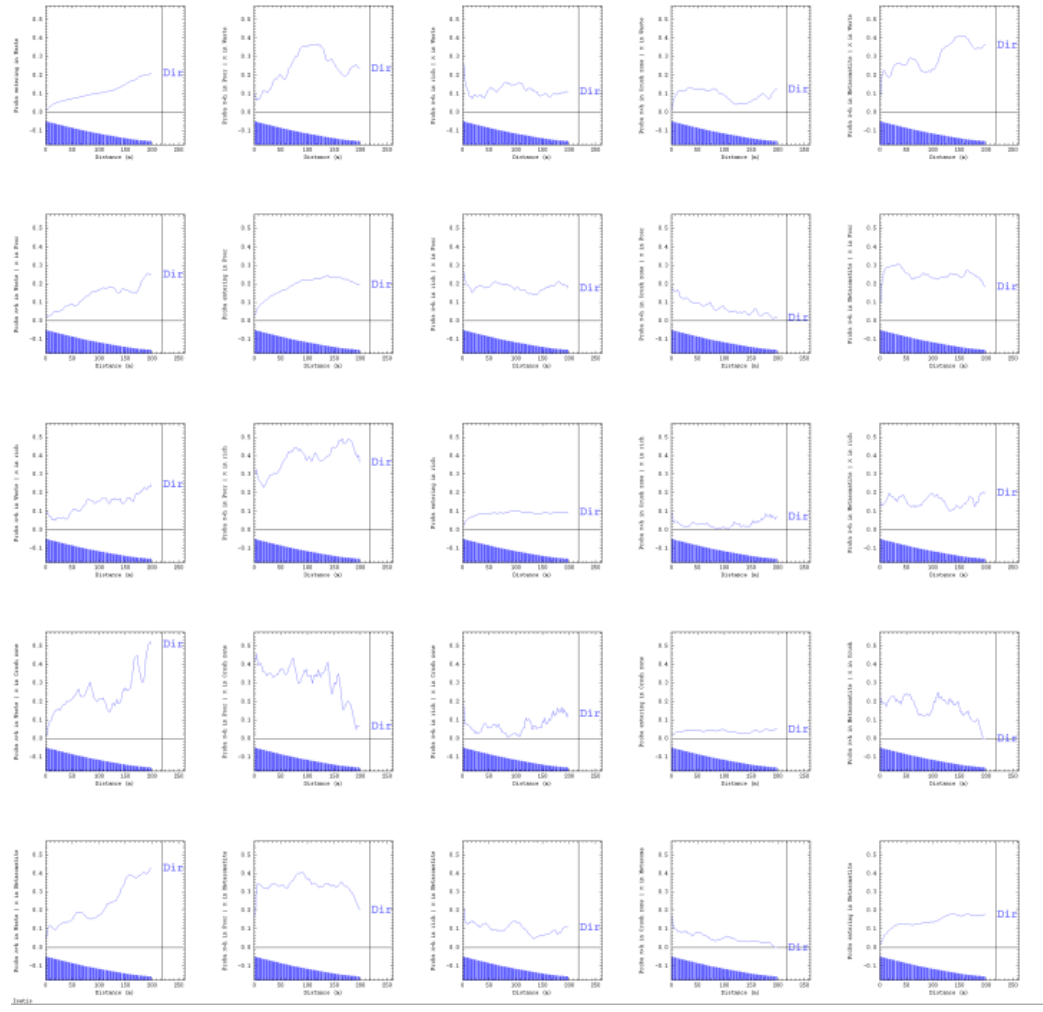


**Figure 51.** Cross indicator variogram divided by a single indicator variogram along the vertical direction

To calculate the preferentiality,  $\left| \frac{\gamma_{ij}(h)}{\gamma_i(h)} \right|$  as the first point (1) (Figure 47) and (

$\frac{P_j}{1-P_i}$ ) as the second point (2) (Figure 47) are extracted from Figures 49 to

51. The preferentiality values  $\text{pref}(i \rightarrow j)$  (Equation 25) are calculated and showed in Table.16.

**Table 16.** Preferentiality values; each cell contains one value per direction from top to bottom: N-S, W-E and vertical directions

From/To	1=Waste	2=Poor	3=Rich	4=Crush Zone	5=Metasomatite
1=Waste	Dir-1	-0.25	0.05	0.30	0.50
	Dir-2	-0.24	-0.20	0.00	0.00
	Dir-3	-0.34		0.00	-0.18
2=Poor	-0.30	Dir-1	0.40	-0.10	0.10
	-0.14	Dir-2	0.26	-0.10	0.12
	-0.12	Dir-3	-0.22	-0.08	0.20
3=Rich	-0.15	0.30	Dir-1	0.00	-0.05
	-0.28	0.18	Dir-2	-0.16	-0.14
	-0.28	-0.34	Dir-3	0.00	-0.18
4=Crush Zone	0.45	-0.25	-0.15	Dir-1	0.25
	0.20	0.28	-0.16	Dir-2	0.00
	-0.24	0.12	-0.16	Dir-3	-0.02
5=Metasomatite	0.00	0.05	0.25	0.00	Dir-1
	-0.12	0.24	0.08	0.00	Dir-2
	-0.18	-0.14	-0.10	0.00	Dir-3

To detect the preferential contacts, only positive values (Figure 48) from Table 16 are considered and classified into four classes and schemes are drawn up for each direction showing the relationships (Figures 52, 53 and 54). An arrow represents a spatial transition, and its color the magnitude of the transition.

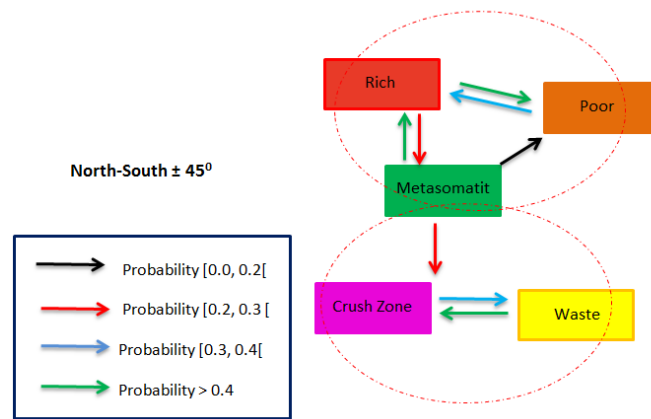


**Figure 52.** Preferential relationship schemes obtained after classification of positive preferentiality values, transitions in North-South direction, upper part recalls units above cut-off ( $\text{Fe} > 20\%$ ) and lower part recalls units below the cut-off ( $\text{Fe} < 20\%$ )

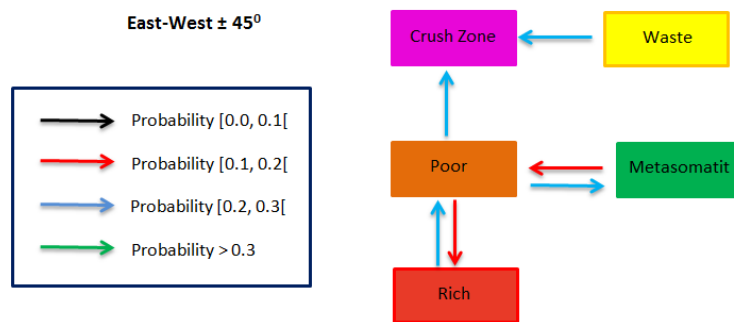


**Figure 53.** Preferential relationship schemes obtained after classification of positive preferentiality values, transitions in east-west direction

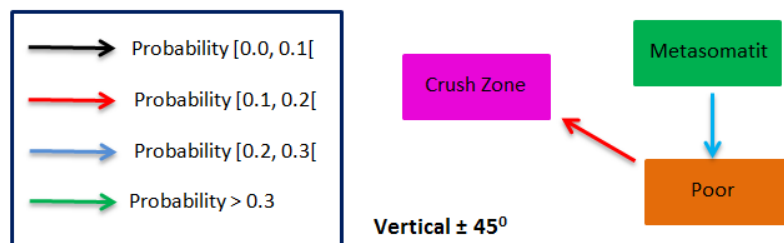


**Figure 54.** Preferential relationship schemes obtained after classification of positive preferentiality values, transitions in vertical direction

These schemes are not connected with geological location in space, and the only importance of the figures is presented by the colored arrows showing the mutual behavior and their probabilities between geological units. According to the preferential schemes obtained by the use of the variogram ratio, it is possible to detect if there is or not the spatial transition. This method allows assessing if there is a mutual transition and provide enough information to choose the appropriate estimation method. As shown in Figures 52 to 54, the variogram ratio interpretation show three main subsets of units with the maximum probability (in two directions) of mutual transition and will be named the “transition zone” (Séguret, 2012).

According to cutoff value of the deposit (Cut-off = 20% Fe), the geological subsets in Figure 52, can be classified into two groups: geological units above the cutoff grade and the geological units below the cutoff grade. Therefore, as shown in Figure 52, there is an important mixture between poor and rich units with metasomatite and collecting enough information about the metasomatite unit is fundamental. However, at the time of sampling, the mining sector almost decided to stop mining in the metasomatite part. With this method, it is possible to improve the spatial discrimination of the units giving accurate information about the expected grade of un-mined parts.

#### 4.4.2 Contact plots

The Contact plots application calculates and displays the mean value of a variable in a geological unit as a function of the distance in a reference direction of the samples to the contact with another unit. The mean value is calculated on

samples along a core line by class of distance. The general form of the contact plot for both soft and hard boundaries are shown in Figure 55 as the second tool to determine the mutual behavior of boundaries. Plot can be classified as one of these four types based on the slope of expected value line and the width of 90% probability interval. For example, one could conclude that no boundary is present when the expected value at zero distance for each domain is within the range of variability at zero distance for the other domain. A hard boundary is likely present when the expected value at zero distance for at least one domain falls outside the range variability for the other domain. This hard boundary is considered as stationary when neither domain exhibits a strong trend near the boundary. The hard boundary would be considered non-stationary when a significant trend is present. A soft boundary is present when the grade within one or both domains exhibits a strong trend near the boundary with no significant change in grade (Wilde and Deutsch, 2012).

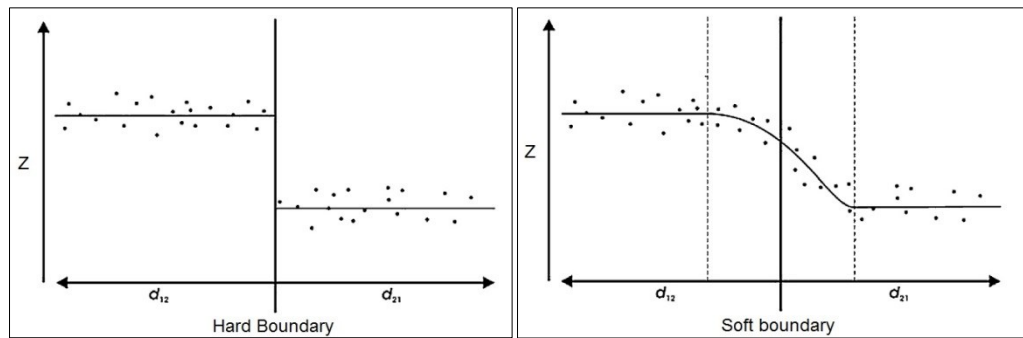


**Figure 55.** The general form of contact plots for a hard and soft boundary

Contact plots are performed for all geological units of the case study, and four of them are shown in Figures 56 and 57. However the number of samples

should be enough to show the continuity of the variable Fe (%) near boundaries.

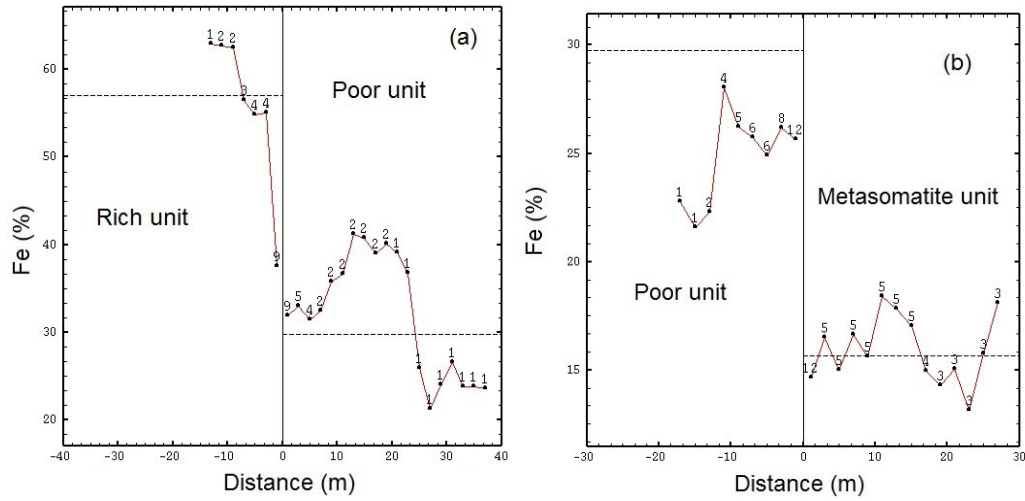


**Figure 56.** Contact plot showing the mean value of Fe (%) in rich domain (left) and poor domain (right) at a distance (a) and contact plot showing the mean value of Fe (%) in poor domain (left) and metasomatite domain (right) at a distance (b)

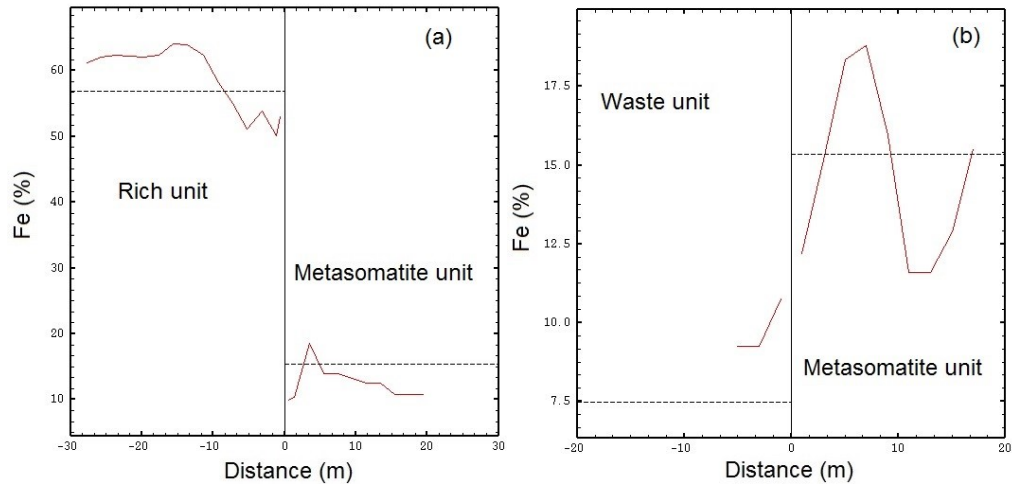


**Figure 57.** Contact plot showing the mean value of Fe (%) in rich domain (left) and metasomatite domain (right) at a distance (a) and contact plot showing the mean value of Fe (%) in waste domain (left) and metasomatite domain (right) at a distance (b)

According to the lack of iron data Fe (%) in some geological units (such as waste, crush zone) contact plots could not be calculated for mentioned geological units. In addition, the number of pairs in long distances is not enough to have precise contact plots. Hence, to sum up with the preferential relationship schemes, it can be concluded that the main geological units are poor, rich and metasomatite, which show the most transitional areas.

## 4.5 BORDER EFFECTS

While working with indicator functions (Equations 16 and 17), according to Equation 17, when the sum of indicator function is multiplied by the grade  $Z(x)$ , the proportion of a variable through an indicator (for instance a geological unit) is calculated within the following equation.

$$Z(x) = Z(x) \sum_{i=1}^n l_i(x) \forall x \quad (26)$$

By inverting the sum sign, products of the grade by the indicators appear:

$$Z(x) = \sum_{i=1}^n Z(x) l_i(x) \forall x \quad (27)$$

These products define the partial grades  $Z_i(x)$  (Séguret 2011):

$$Z_i(x) = Z(x) l_i(x) \forall x \quad (28)$$

Then the cross variogram between the indicator of  $i$  unit and its partial grade  $Z_i(x)$  defined by Equation (28) is

$$\gamma_{iZ_i}(h) = \frac{1}{2} E[(l_i(x+h) - l_i(x))(Z_i(x+h) - Z_i(x))] \quad (29)$$

The equation is not null if  $\{x+h \notin i, x \in i\}$  or  $\{x+h \in i, x \notin i\}$  so we obtain

$$\begin{aligned} \gamma_{iZ_i}(h) &= \frac{1}{2} E[Z(x)|x+h \notin i, x \in i]P(x+h \notin i, x \in i) + \\ &\quad \frac{1}{2} E[Z(x+h)|x+h \in i, x \notin i]P(x+h \in i, x \notin i) \\ &= E[Z(x+h)|x+h \in i, x \notin i]\gamma_i(h) \end{aligned}$$

So another ratio intervenes

$$\frac{\gamma_{iZ_i}(h)}{\gamma_i(h)} = E[Z(x+h)|x+h \in i, x \notin i] \quad (30)$$

This ratio shows how the average grade increases or decreases when moving inside the  $i$  unit. This property is named “**Border Effect (BE)**” by Rivoirard (1994). If this ratio depend on  $h$ ,  $\gamma_{iZ_i}(h)$  is proportional to  $\gamma_i(h)$ , leading to a model where the partial grade is defined. In the presence of BE, the method named “Partial Grade” can be performed (Séguret 2011).

## 4.6 PARTIAL GRADE

Given samples informed by a categorical variable and a grade, another method to estimate the average grade with a focus on transitional areas is the “**Partial Grades**” (PG) method (Séguret 2011). This method leads to an isotopic CK system based on the indicators of the units and their products with the grade.

The definition of the PG for a variable  $Z(x)$  and indicator  $l_i$  is:

$$Z(x) = \sum_{i=1}^n Z_i(x) \times 1_i(x) \quad \forall x \quad (31)$$

Where  $1_i(x)$  is the indicator function for each unit  $i$ , and  $Z(x)$  is the variable.

These products define the PG:

$$Z_i(x) = Z(x) \times 1_i(x) \quad \forall x \quad (32)$$

By this approach, the optimal estimation of the grade at the scale of a production block  $V$  is performed by CK based on the PG that is equal to a sequence of partial-grade cokrigings:

$$Z(V)^{CK} = \sum_{i=1}^n Z_i(V)^{CK} \quad (33)$$

This method can be useful in the case where the border effect is present (Séguret 2012). The cross variogram between indicator  $i$  and its partial grade  $Z_i$  divided by the  $i$  indicator variogram is simply the way the average grade increases or decreases while crossing different geological units (Equation 30). Hence, by the help of variogram ratios is possible to quantify the enrichment or impoverishment when moving inside the unit. It means that when crossing from one geological unit into another, (Figure 58-left) for instance from poor into rich, if there is an increase in the iron grade Fe (%), this shows the BE between poor and rich units. In this case study, the variogram ratios were performed for all geological units, however as it is shown in Figure 58, the BE exists only between poor, rich and metasomatite.

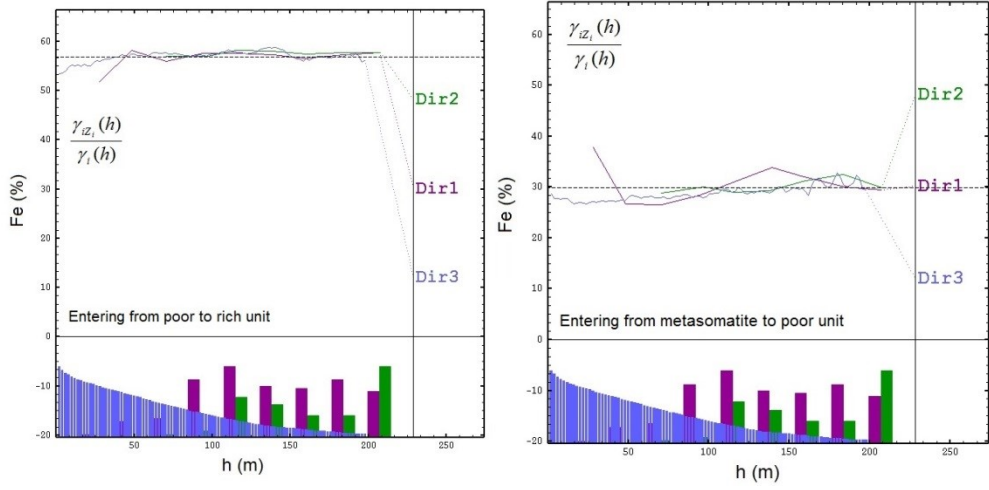


**Figure 58.** Cross variogram between indicator and partial grade divided by indicator variogram

Figure 58, represents the way the grade decreases or increases while entering unit  $i$  (entering to rich and poor units). Based on the existing of border effect between the three main geological domains of this case study (poor, rich and metasomatite), and as preferential relationship schemes highlighted, PG Co-Kriging is performed on three main domains of the ore body. Direct and cross variograms and their models are shown in Figure 59. Variogram models are used to perform between indicators and partial grades.

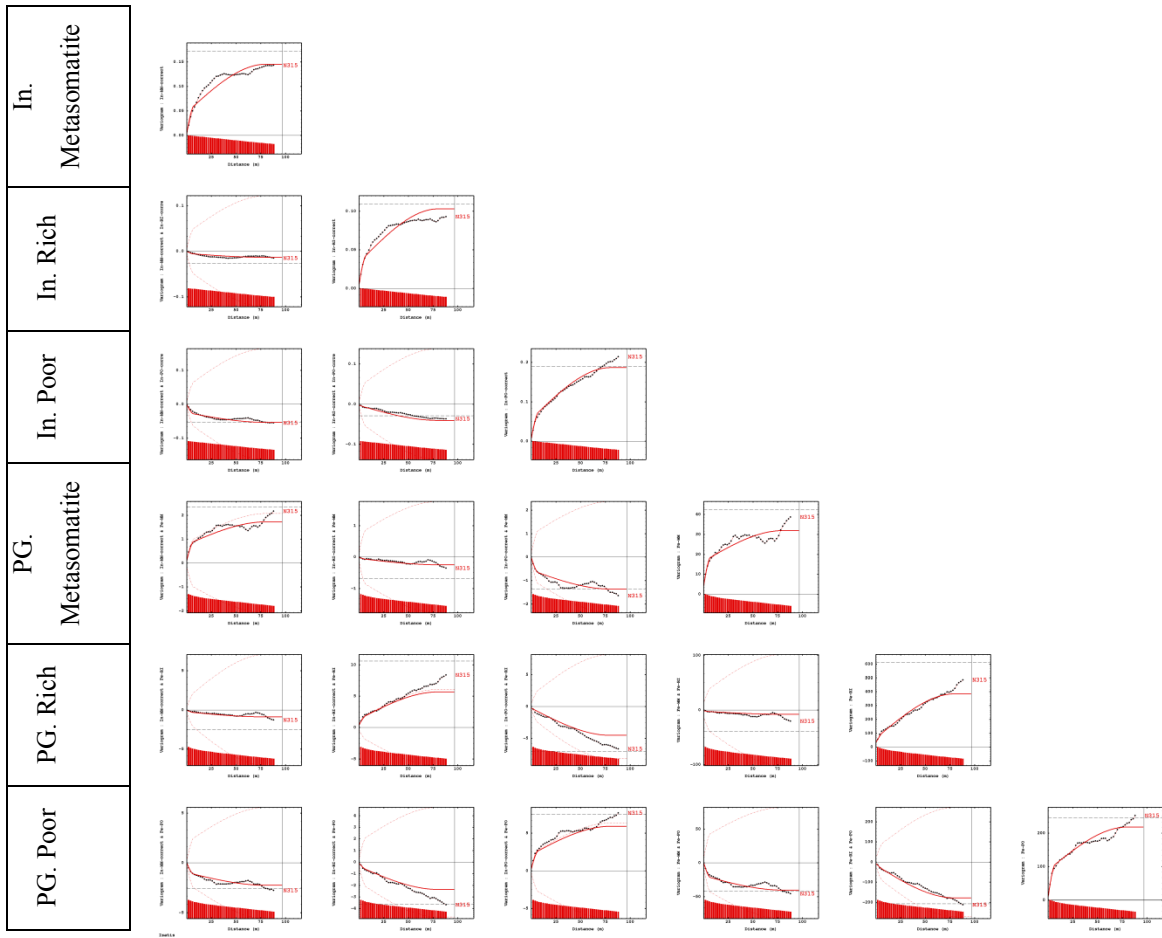


**Figure 59.** Cross variogram between indicator and partial grade divided by indicator variogram

Note that partial grade method (Equation 32) considers the proportion of each geological unit within one block. As cross-validation performs for a point variable (for example a borehole sample), cross-validation of partial grade is skipped for poor, rich and metasomatite models. Based on the definition of PG method Equation 33, because the results are the sum of three main geological units (poor, rich and metasomatite) and the method is performed for a block, it is possible to skip cross-validation. However, the validations of estimation results were compared for different methods.

The important step for choosing the most coherent estimator among all mentioned methods, Kriging (OK and UK), Co-kriging (CK and UCK) and PG, is to validate estimation results when real data are available. In this case study there are 10 excavated benches with blasthole data, which can be considered as the values of blocks. Hence, the estimation results can be compared with blasthole data to validate the estimators.

## 4.7 VALIDATION OF ESTIMATIONS

In geoscience applications, if real data are available the estimation results can be validated. For instance in mining studies, evaluations made from limited information (such as boreholes) can be validated by the real grades of blocks, approximated by the mean of blast holes (Chiles and Delfiner, 2012). The long road that leads to the opening of the mine is marked by drilling, to achieve the block model that will condition the exploitation at large scale as well as for medium- and long-term planning. Typically, kriging and Geostatistics are used to build the model at this stage. In addition, the blast holes are used for short term planning with no need of Geostatistics, a simple moving average is often used to estimate the block quantity of metal (Seguret 2015).

Due to blast holes data available from 10 excavation benches in Sechahun case study it is possible to evaluate estimation results. With the same block model used for all estimation procedures with the dimension  $25 \times 25 \times 25$  m<sup>3</sup> (height), the weighted average of blast hole samples inside each block are calculated and assumed as the true value of each block (Figure 60).

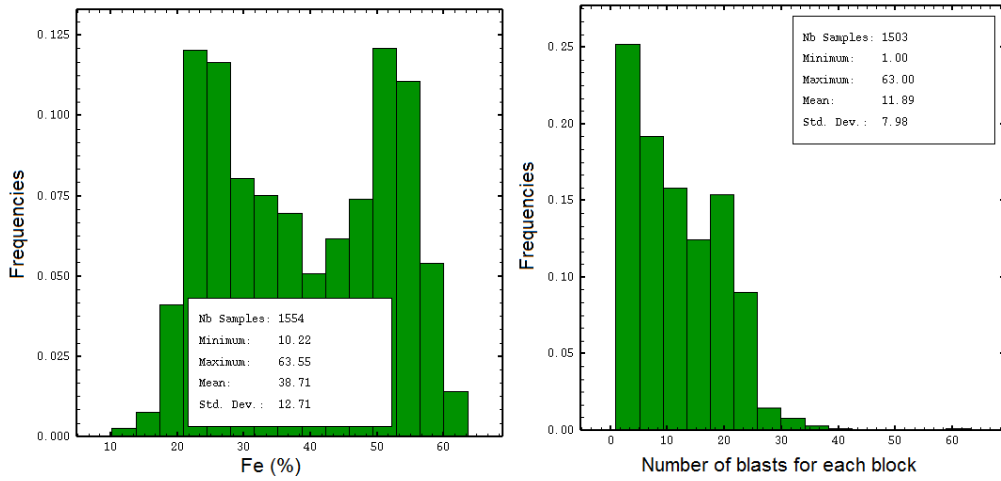


**Figure 60.** Histogram of true block values obtained from mean of blast holes (Left) and histogram of number of blast holes used for averaging block values

However, as the excavation of the ore body is still ongoing, the available data are from blast holes only from 10 excavated levels but not yet completed. To have reliable results, only blocks with more than 16 numbers of blast samples are considered for the validation (Figure 60). This number was chosen after some tests on block averaging, where with more samples, the average values were stable. Results are shown in scatter diagrams between true and estimated grades in Table 17, using the estimators as described in previous chapters. Statistical parameters relating to validation of estimators are shown in Table 18 to compare results obtained from the different methodologies.

**Table 17.** Scatter plots between real values (obtained from blast holes) and Fe (%) estimated by different kriging methods

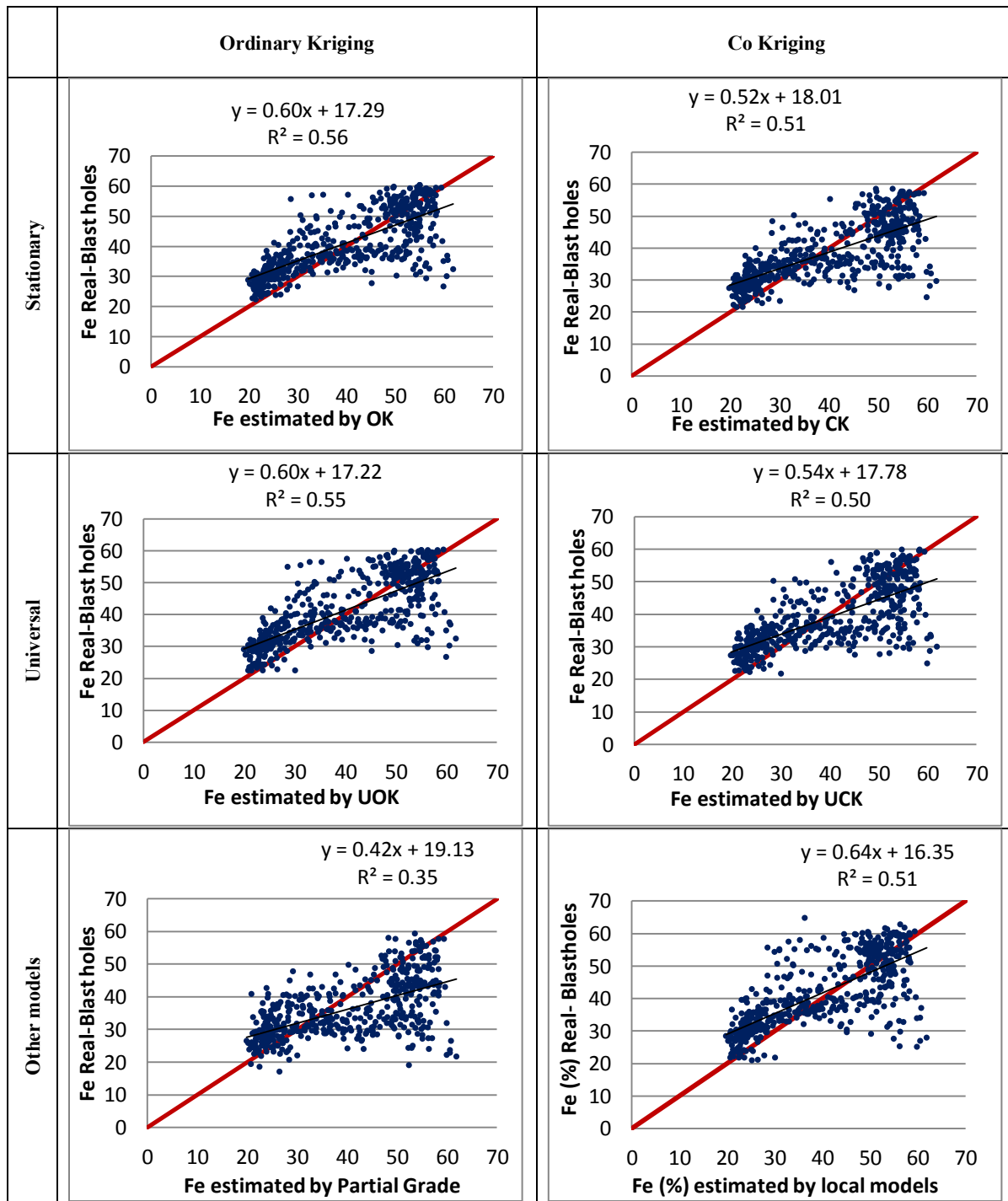


**Table 18.** Statistical parameters between real values (obtained from blast holes) and Fe (%) estimated by different kriging methods

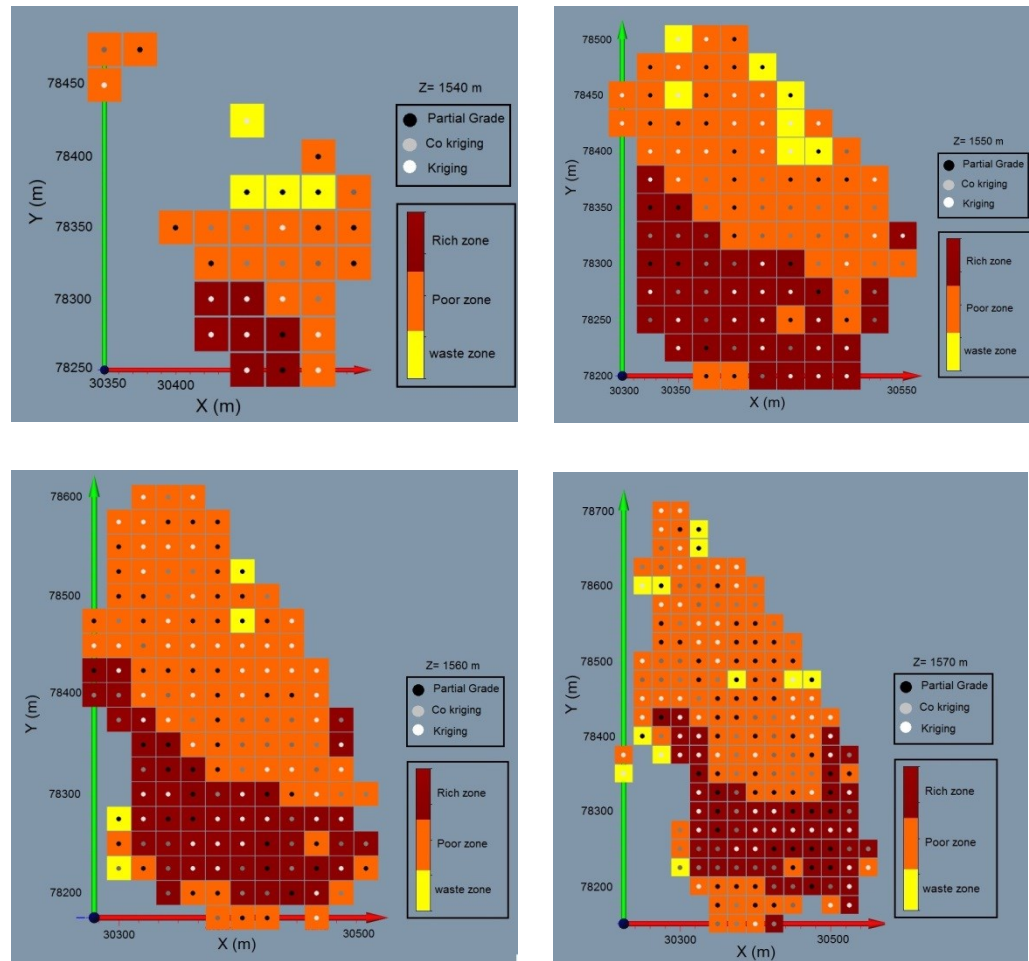
Methods	OK	UK	CK	UCK
<b>Mean of Error (%)</b>	-1.21	-1.50	<b>1.20</b>	0.69
<b>Variance of Error (%<sup>2</sup>)</b>	<b>71.19</b>	72.78	78.59	79.77
<b>Standardized Variance (%<sup>2</sup>)</b>	<b>1.41</b>	1.49	1.43	1.49
<b>Estimated variance (%<sup>2</sup>)</b>	<b>53.52</b>	50.53	59.36	56.59

According to the validation results shown in Tables 17 and 18, using a global model of spatial variability, OK has more coherent estimation results for the whole ore body. However, as mentioned before, focusing mainly on transitional boundaries it is necessary to highlight only those blocks located in transitional areas. Moreover, according to the non-homogenous geological domains of the case-study, it is important to assess how different methods or estimators are influenced by geology in different parts of the ore body and particularly in transitional areas. To identify the most coherent method in transitional areas, the error of each estimated block (true value-estimated value) is calculated within each method.

It was assigned a code value from 1 to 5 (1=OK, 2=UK, 3=CK, 4=UCK and 5=PG), for each block, to the best estimator (method with minimum error). Results show that best estimators are: Kriging, Co-kriging and Partial grade. Three groups are shown graphically for each level of excavation on true block values. True block values are calculated from blasts as described and for a clearer graphical representation, are classified into three main domains: poor, rich and waste. This classification is performed according to the mining exploitation plan:

- Waste: Fe (%) < 20 (yellow color)
- Poor: 20 < Fe (%) < 45 (orange color)
- Rich: 45 < Fe (%) (red color)

Maps of true block values calculated by the blast holes, for each excavation levels, are coincident with the optimum estimation method (minimum error) shown in Figure 61. Based on maps in Figure 61, with statistically accounting blocks with optimum method (minimum error), it is possible to interpret the most coherent method in three main geological domains with transitional areas.



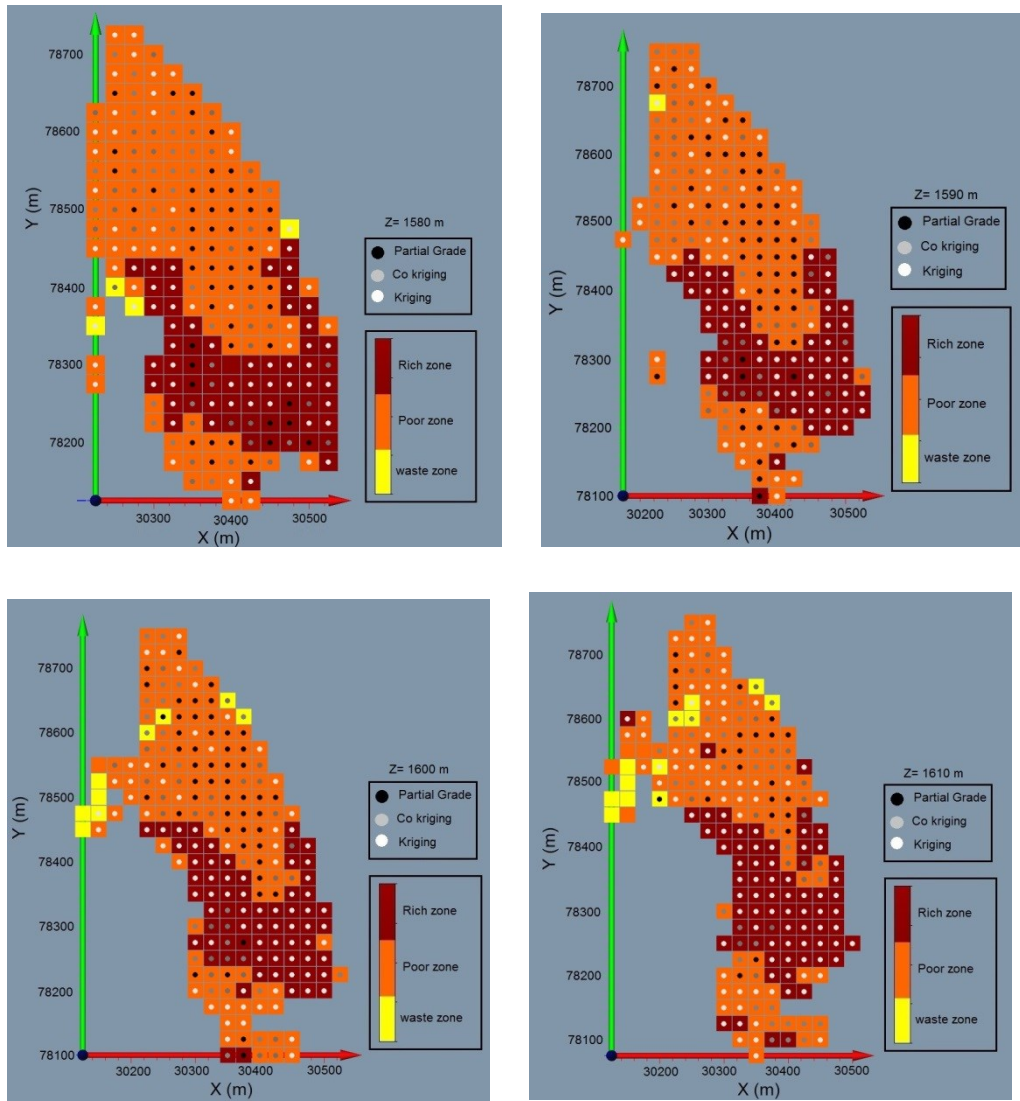


**Figure 61.** Maps of real block values obtained from mean of blast holes with optimum estimation method

To demonstrate the coherency of the optimum methods in Figure 61, the number of blocks is counted in each geological domain classified by blast holes (rich, poor and waste) according to three main estimators:

- Kriging (K) consists of OK and UK;

- Co-kriging consists of CK and UCK (method using geological information as indicators);
- Partial grade (PG) using proportion of geological information according to the grade of Fe(%).

Results of statistical counting of blocks are shown in Table.19:

**Table 19.** Comparison of number of blocks with optimum estimation methods for three main geological domains; poor, rich and waste (include metasomatite zone)

Levels (m)	total number of Blocks	Rich zone (Num.Blocks)			Poor zone (Num.Blocks)			Waste zone (Num.Blocks)		
		K	CK	PG	K	CK	PG	K	CK	PG
<b>Z=1540</b>	31	5	0	2	5	8	7	1	0	3
<b>Z=1550</b>	100	18	14	7	17	17	20	4	0	3
<b>Z=1560</b>	145	19	18	13	34	22	35	0	1	3
<b>Z=1570</b>	183	24	17	17	35	38	41	4	1	6
<b>Z=1580</b>	203	46	8	10	40	50	45	3	1	0
<b>Z=1590</b>	203	52	12	4	39	43	52	1	0	0
<b>Z=1600</b>	203	58	9	2	41	40	48	1	3	1
<b>Z=1610</b>	189	64	6	0	50	40	22	2	4	1

Based on the results of Table 19, in each excavation levels, for rich domain mainly Kriging is the optimum method for estimation, while in poor domain it changed into the partial grade method. For waste domain, the number of available blocks with enough samples is so low and it is not easy to make a precise interpretation.



# **5 CONCLUSION**

## **5.1 DISCUSSION**

Geostatistical estimations and modeling by use of the available information and comparison of different methods, a complex ore deposit with transitional boundaries was estimated. A compositing method such as regularization helped to use all available samples with accurate models close to the theoretical punctual model as the most coherent model. Moreover, adding geological information through indicators makes it possible to incorporate different geostatistical approaches (for instance IK, CK, PG) to promote the knowledge about the complexity of the ore body.

Theoretically, the punctual model shows improvement compared to the part of data with the same support. With given sources of information, the accuracy of the model depends strongly on the amount of data available, its nature and quality and its dispersion over the area of interest, which through the theoretical punctual model is optimum. However, in this study, the regularized samples have very close results to the theoretical punctual model, making it possible to use the regularized samples. This makes all procedures of estimation and validation results easier and less time consuming using the classical procedure of kriging with available software (ISATIS).

Based on different tools used in this study to identify the types of boundaries, (such as contact plots and preferential relationship schemes), it showed that in some cases it is necessary to test both tools according to different number of samples in various geological domains. Geological boundaries in the deposit under study are not ‘hard’ and are associated with gradational transitions in the

mean iron grade, except maybe the boundary between dikes and crush zones (faults) but, because of the reduced number of data it was not possible to demonstrate it through contact plots.

As showed in the results of the validation, when an ore body has complex geological domains like the case study of this work, it is fundamental to test different approaches and in the case of the presence of the trend, using non-stationary methods.

Partial grade method uses both the spatial grade and the geometry of the domain. In this ore deposit, considering transitional areas with important border effect, CK of partial grade is performed. As far as is our knowledge (December 2016), the application of the method on a mining case is a novelty. The estimation results validated with blast holes samples considering as real data (Table 20). Comparing different methodologies is an appropriate way to test different geological hypotheses and select the most plausible method.

**Table 20.** Optimum estimation method (minimum error) for three main geological domains; poor, rich and waste (include metasomatite zone)

Geological units	Optimum Method
Rich zone	Kriging
Poor zone	Partial Grade
Waste	Partial Grade

According to Table 20, the kriging approach with global model provides the best results (minimum error) for the rich zone. This is because the rich domain is more homogenous. Homogenous domain here means having the same spatial continuity of grades inside the domain, and similar geological features such as lithology, mineralogy and alteration.

However, in poor domain partial grade method has less error for estimation, due to the proportion of geological domains for estimating each block. As other

tools (for instance preferential schemes and contact plots) also noted, poor domain is non-homogenous with transitional areas. For waste domain, instead as excavated procedures are not continued in this zone (because of economic reasons) there are not enough blocks to recognize the optimum estimator.

In order to distinguish the rich, poor and metasomatite contacts in Sechahun deposit, the estimated probability map of each previously extracted bench is overlaid to the optimum estimators (minimum error). Estimation results from UK and OK methods. Maps are shown in the levels which have maximum number of blocks to perform validation,  $Z=1570$  m and  $Z=1580$  m.

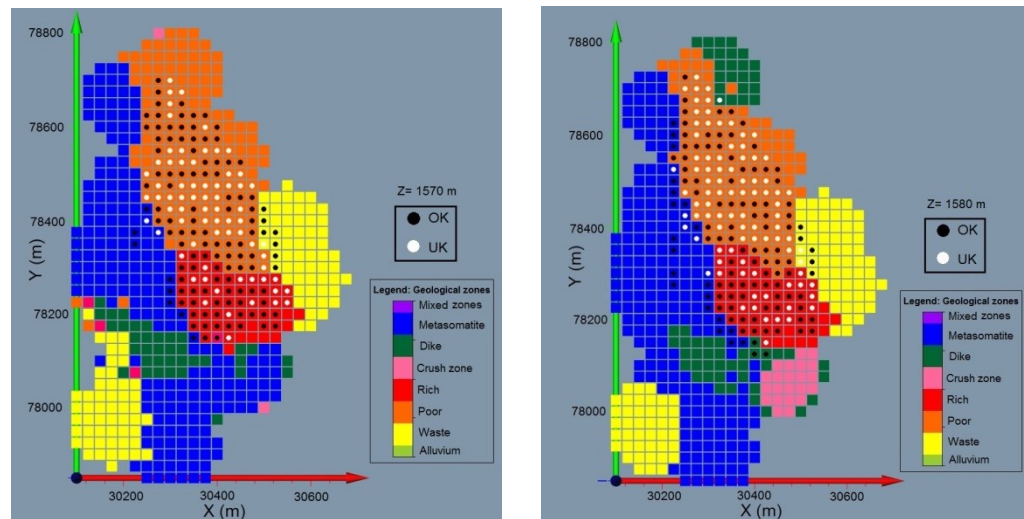


**Figure 62.** Maps of ICK results with optimum estimation method for two excavated levels

As Figure 62 showed, in rich zone, which is more homogenous, OK has minimum error while in poor zone UK is the optimum method.

However, as it is shown in Figures 61 and 62, geology of the ore body is too complex and according to this complexity of units, different estimators can be used for estimating the ore deposit but one estimator as the optimum with minimum error.

Hence, due to the mentioned advantages and disadvantages of each estimation method, sometime relating to the complexity of the ore body, a combination of methods should be used to have a coherent estimation results. This point highlights the sensitivity of reserve estimation to different estimator methods particularly with transitional areas.

## 5.2 FUTURE DEVELOPEMENTS

The overall methodologies for modeling and for geostatistical estimation in the case of transitional boundaries are performed in this thesis. A number of details could be further investigated as they are likely to generate sizeable incremental improvements over the presented studies:

- 1) The method of CK of partial grade can be performed in the case of non-stationarity and compared with the demonstrated results;
- 2) As in this work, geostatistical estimation methods are deeply studied; it would be a benefit to test geostatistical simulation methods particularly methods for simulating geological units such as gaussian truncated simulation;
- 3) Based on the simulated geological units, estimating grade can be performed inside each domain in order to compare the results of estimation and simulation.



## **Part II**

# **6 FEASIBILITY OF GEOSTATISTICAL STOCKPILE CHARACTERIZATION**

## **6.1 INTRODUCTION**

Since the beginning of the mining activities, stockpiles are formed by dumping wastes or low-grade materials, considered unvalued at the time of excavation. Generally, stockpiles are located beside the open pit area without any economic benefits. However, advances in recovery and processing technology have helped to re-consider stockpile as a new source for feeding the processing plans. Depleting the in-situ reserves and increasing the need of using lower grade materials are additional reasons to consider stockpiles as recoverable resources. Recently environmental aspects caused a strong push for more effective managements of stockpiles in many mining sites. Some companies and environmental institutes have developed and put on the market proprietary technology allowing remediation for tailings and stockpiles, that is harmless to humans and environmentally friendly. Therefore, these aboveground stockpiles have to be quantified and classified and a reliable expected-revenue model developed to assess the feasibility of production.

There are a large number of studies applied on stockpiles or mostly tailings due to completely divergent targets (Lèbre et al. 2016, Sracek et al, 2006, Guezennec et al, 2015, Alcolea ed al, 2015, Abrosimova et al, 2015, Castillo et

al, 2013, Márton et al. 2016). Among the others, we can mention the topic of characterization of environmental issues related to mine wastes. Some studies refer to the evaluation of the acid drainage production potential related to Sulphur mine waste (Sracek et al, 2006, Guezennec et al, 2015); some others refer to the characterization of the contaminated mine wastes and their effects on soil or other environmental aspects (Alcolea ed al, 2015, Abrosimova et al,2015, Castillo et al, 2013). Moreover, focusing on reutilizing stockpiles as economical sources -which are the direct products of mining procedures before the processing plans -causes more considerations on characterization of the grade of the mineral that is inside the stockpiles. The cut-off grades are dynamic, changing in time during mining operation (Ataei and Osanloo, 2003, Bascetin and Nieto, 2007, Osanloo et al., 2008, He et al., 2009, Meagher et al., 2008). This implies the existence of low-grade ore stockpiles that although uneconomical to process in the past years, nonetheless contain sufficient metal grade to justify mining and refining later on (King 2001). Some authors have estimated stockpile grade-tonnage curves from the set of geostatistical simulated ore body realizations in order to establish possible long-term stockpiles (Asad and Dimitrakopoulos, 2012). In other cases, different methodologies are applied on stockpiles to figure out the blending opportunities of the different possibilities for building and reclaiming (Jupp et al., 2013). Moreover, geostatistical simulation methods are applied to optimize stockpile designs using sparse samples. Therefore, using the distribution of the variables the uncertainty at un-sampled locations is estimated (Kumral, 2006, Marques et al. 2009).

Characterization of stockpiles requires adequate sampling, if possible by integrating existing data with new sampling. According to the sampling problems -sampling of compact solids and particulate solids- and different errors influenced in sampling procedure (Gy, 1982) in the cases with different

size of materials, errors of samplings may be negatively notable (Gy, 1982). Hence, sampling in extensive stockpiles containing rocks with different size can be cumbersome and costly. Huge stockpile size and the consequent difficulty of access to all parts of piles for sampling, along with grain size variety are some of the reasons why sampling may be complicated. However, at the prefeasibility stage of the study, sampling can be dispensed with numerical modeling using data from the exploited ore body and then reconstructing the piling procedures, namely: ore selection, haulage and piling. The spatial correlation of natural mineralization will be significantly modified with respect to the piling procedure in the stockpiles, or even disappear (on the point of artificial aspect of stockpiles). Hence, stockpiles will show significant disruption with respect to the original spatial correlation of natural mineralization. On the other hand, the time sequence of blocks excavations and piling them - or part of them- in nearby locations as stockpiles following the same time order, may lead to, in some way, maintain the natural spatial correlation of the main ore deposit. This is because stockpiles are part natural and part artificial, and they are located in the main deposit. Considering this point, initial data must be obtained regarding stockpile grade (as a variable) characterization and regarding selection from the main ore deposit and the stockpiling procedure. Stockpile construction method will determine the spatial variability of the grade. Back reconstruction of the exploitation flows of the main resource, the waste selection process, their transportation and disposal can provide predictions regarding stockpile variable distribution and spatial variability inside the stockpile.

In this Chapter, a short study is presented on stockpile grade distribution and their variability estimation based on primary data from the main ore body. The case study is related to two stockpiles in an iron mine where sampling was considered economically and physically unfeasible. The iron and phosphate

grade distribution of stockpiles are estimated using numerical modeling. The iron and phosphorus grades, contained in a given piling volume – equal to the contents of a single truck – were estimated by CK. Reconstruction of the haulage process allowed calculation of stockpile grade distribution.

In all reconstructing the haulage-piling procedures, it is fundamental to consider the same support for stockpiles and their main resource. The support varies widely from site to site and should be identified since it is a key for comparison between the main source and pile structure. Figure 63 summarizes the procedural steps.

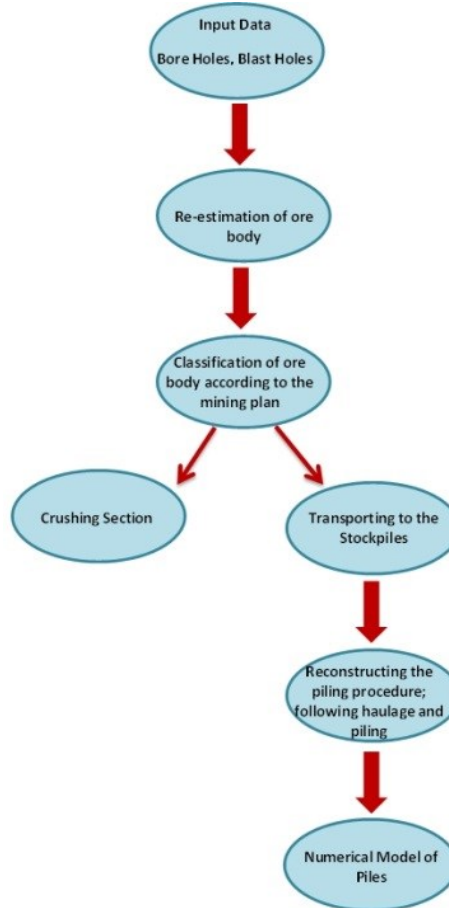


**Figure 63.** Simple chart of numerical modelling procedure of stockpiles

## 6.2 INTRODUCTION OF THE CASE STUDY: CHOGHART IRON ORE MINE

The Iranian Choghart iron-ore mine has been operational since 1975. The first project was to exploit a large iron-ore deposit in the region of Bafgh, approximately 125 km southeast of the city of Yazd, Iran (Figure 64).



**Figure 64.** Choghart iron ore mine in Iran and the Google map of the ore deposit and stockpiles

Initially, the Choghart ore body was a prominent iron ore outcrop measuring  $800 \times 300 \text{ m}^2$ , standing 150 m above the surrounding plain, itself some Z=1257 m above sea level (Moor and Modabberi, 2003). The iron ore is low in Sulphur, 90% of the ore body being non-oxidized (magnetite ore). Over 65% of the reserve is of the low phosphorous type (Torab and Lehman, 2006). However, a huge quantity of high-grade, high phosphorous ore (average above 0.6% phosphorous) and low-grade ore (average less than 50% iron) has been

removed from the pit and stored in high phosphate (HP): [Fe% $\geq$ 50%, P $\geq$ 0.6] and low grade: (LG) [Fe<50%] stockpiles for possible future beneficiation. The construction of a processing plant at Choghart able to produce 3.2 Mt of iron concentrate has made exploitation of the piles potentially economically viable (Gholamnejad and Kasmaee 2012).

Exploitation at Choghart is open cast, with 10 m high blasting benches. Each blasting panel is almost 25m $\times$ 25 m $\times$ 10 m (height) and blast-holes lie in a regular pattern of 5 m $\times$ 5 m $\times$ 10 m (height). The blasted rocks are shoveled onto trucks and transferred to a 250 m<sup>3</sup> crushing plant. The high phosphorous and low-grade iron ore are transported to separate stockpiles. Open pit operations entail five stages: drilling, blasting, loading, hauling and crushing. Loading and transporting is via a truck- shovel system.

The two main - HP and LG - stockpiles were started in 1993 using 35-ton-capacity trucks. Materials have been disposed in sequential horizontal layers, with each stockpile section being filled over 30 days. In both cases, stockpile construction followed all mining plan operations (drilling, blasting, loading and hauling to the two different locations) with the exception of the crushing stage (Figure 65).

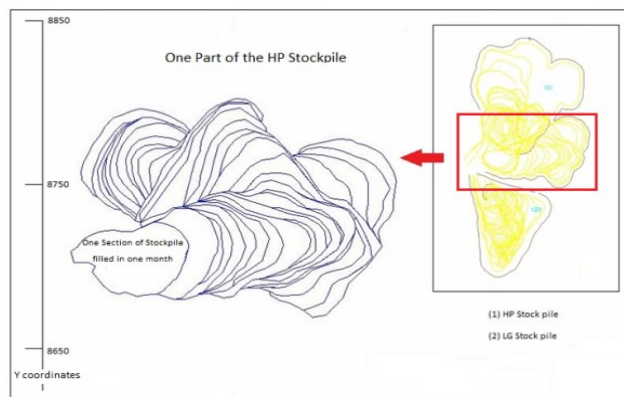


**Figure 65.** HP and LG stockpiles

Each stockpile is almost 400 (X) m×500 (Y) m× 20 (Z) m high and includes rocks with completely different grain dimension. Their huge size and wide rock grain dimension make sampling both difficult and costly. However, the availability of complete blast-hole data as well as the regular piling sequences from identified mine panels allow reliable prefeasibility studies to be carried out prior to embarking on costly sampling operations. Moreover, since stockpiles were built up in layers of material from specific areas of the mines, stockpile grade variability can also be estimated. As a result, preliminary main ore deposit data and structural analysis of preferred variability (iron and phosphorous) can be used to assess stockpile characterization and predictions. The first step is to make a direct link between deposit and pile, identifying the selection support from the primary blasted panels. The study considered blast hole data for low grade and high phosphorous blocks at level Z=1140 m of the Choghart mine. Figure 66 shows the base map of the selected panels with blast-hole samples classified according to feeding destination: crusher (CR) or the different stockpiles (HP, LG).

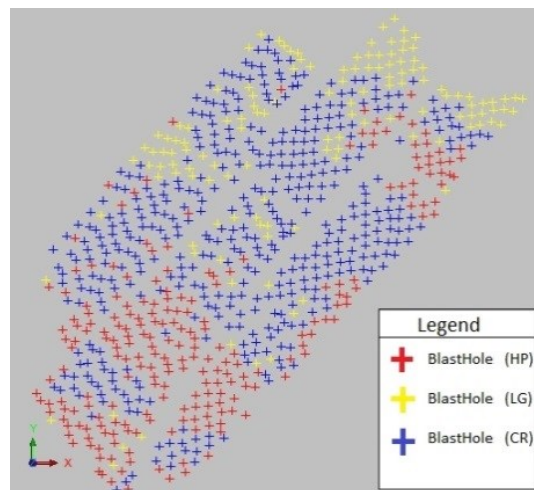


**Figure 66.** Base map of blast hole data for five panels, classified according destination (High Phosphorous stockpile: Red; Low Grade stockpile: Yellow; Crusher Feed: Blue)

The numerical modeling of the iron distribution of the deposit can be carried out employing geostatistical method CK for obtaining block estimates along with estimation variance. These estimates are further used to predict stockpile grade variability.

### 6.3 ORE DEPOSIT MODELLING

Conventional statistical data analysis was performed prior to determine the basic characteristics of sampling. Figure 67 shows the summary statistics for Fe and P distributions, respectively.

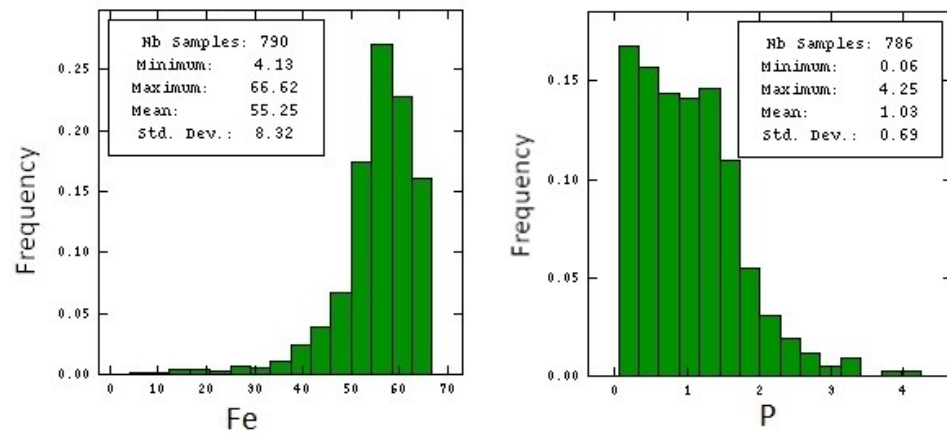


**Figure 67.** Histograms of Fe (left) and P (right) concentration (%) for blast hole data from 5 panels

Blast hole data of five panels (numbers: 478, 480, 482, 484 and 486) at level 1140 containing low grade ( $\text{Fe} < 50\%$ ) and high phosphorous ( $\text{Fe}\% \geq 50\%$ ,  $\text{P} \geq 0.6$ ) were considered as an example. Iron and Phosphor grades in the ore body (from mentioned panels) were found to be spatially structured and negatively correlated as shown by the direct and cross variograms (Figure 68) where a

linear coregionalisation model (nugget + exponential with range 20 m) was fitted. Depending on block shape - 5 panels (Figure 68) - the maximum distance of variography is equal to the length of 2 panels (less than 100 meters). As the spatial variability is same in all the directions, no significant anisotropy was observed in any two directions. An omni-directional variogram was used for modelling the deposit. Based on the grid size, a lag distance of 5.0 meters with a lag tolerance of 2.5 meters is used for the variogram calculation.

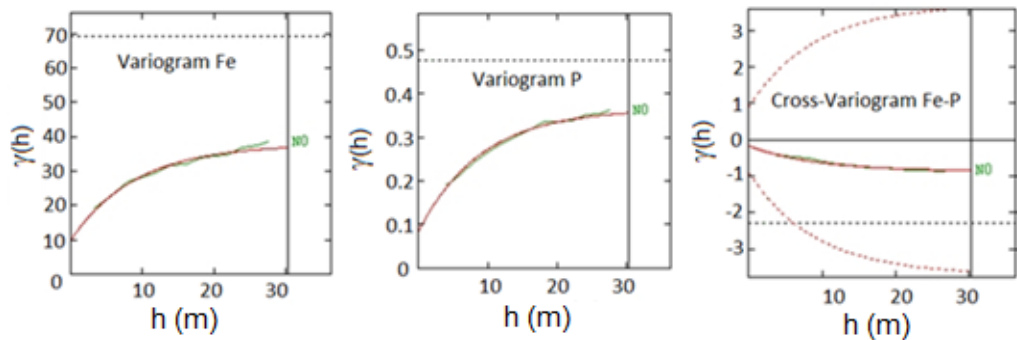


**Figure 68.** Experimental and cross variograms of Fe and P obtained from blast holes of five panels

A comparison between the grade spatial variability in stockpile and deposit can be based on the ore sent to stockpiles, which is a portion of the main deposit that has been determined by cut-off selection (grade selection for PH and LG). Stockpile grades considered by the procedure; refer to the elementary unit (cell) that constitutes it, in other words, to a not-punctual support. The reconstruction of the ore flow from deposit to stockpile requires the identification of an elementary unit (a unique volume named support) of in situ ore corresponding to the piling unit, which is conditioned by truck capacity (35 tons). After regularization of support, stockpile grade spatial variability is significantly different from the grade of the original samples. With reference to variograms, after regularization, one would expect theoretically, the variable has a lower sill and increased range (Chiles and Delfiner, 2012). Depending on the dimension of the blasted panels ( $25 \times 25 \times 10 \text{ m}^3$ ), the selected unit - in other words, the

elementary volume transported and piled (support) - is 10 (height)  $\times$ 2.5 (X)  $\times$ 1.4 (Y) m<sup>3</sup>. These dimensions have been chosen with reference to:

- i) bench, the 10 m height level of the mine to be exploited;
- ii) volume, corresponding to truck capacity;
- iii) shovel bucket width.

As previously mentioned, each stockpile was fed only by a selected part of the deposit. In compliance with Choghart's long-term production strategy, high-grade rocks ( $\text{Fe}\% \geq 50\%$ ,  $P \geq 0.6$ ), and low-grade material ( $\text{Fe} < 50\%$ ) were consigned to HP and LG stockpiles. Selection of stockpile materials in the main ore body requires estimation of the selected units or blocks (support of 10  $\times$ 2.5  $\times$ 1.4 m<sup>3</sup>) inside the blasted panels. A linear coregionalisation model was used for CK of the iron and phosphate sample grades. After estimation, the selected procedure was applied to separate the high and low-grade phosphorous parts of the panels. Then the structural analysis in the selected parts of the blocks and stockpile grade variability is performed.

Since kriging is a linear averaging, kriging estimates can be expected to be less dispersed than the data (Chiles and Delfiner, 2012) and with lower variogram sill. The cut-off grade criteria modify means, variances and variogram ranges (Matheron, 1982). Figures 69 and 70 show the direct and cross variograms of a specific portion of the estimated blocks (separated by cut-off for LG, HP). Note that the sign of the cross-variogram for the blast holes changes from negative to positive in the case of the cross-variograms of estimated selected blocks in both the LG and HP parts of the ore body. This reveals two different homogeneous populations of iron and phosphorous, which are in fact positively correlated. In addition, it is possible to interpret the result of the different composition and degree of oxidation, which is the basis for the classification of Choghart iron

ore into different groups (Torab, 2008). The stockpile characterization using data from different zones may prove to be quite different from that of one single zone estimated separately.

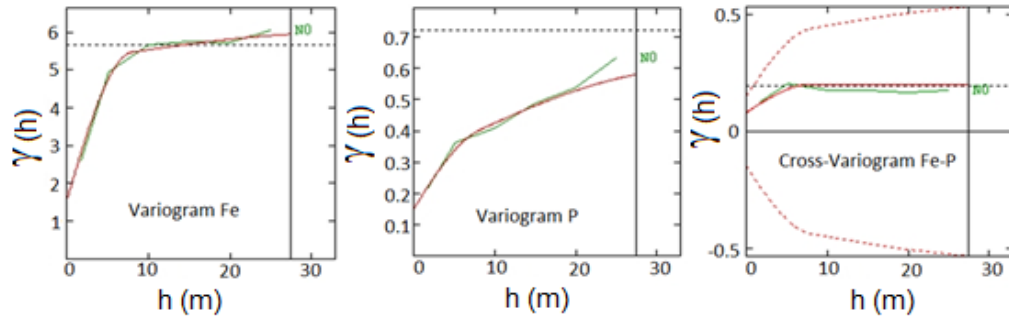


**Figure 69.** Structural analysis of HP (estimated) blocks from 5 panels

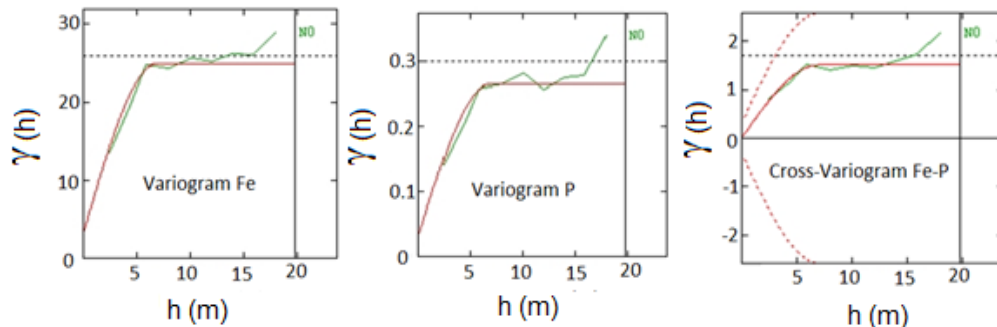


**Figure 70.** Structural analysis of LG (estimated) blocks from 5 panels

In fact, in the HP portion of the deposit, the sill of the variogram obtained from block estimated grades shows P and Fe to be more homogeneous, with a variance 28% lower than samples in the LG part of the deposit. Only the Fe grade has a variogram sill 30% lower than the variogram obtained from samples, while the P variograms maintain almost the same sill.

## 6.4 STOCKPILE MODELING

As mentioned above, parts of the excavated blocks, selected according to the cut-off grade were considered for piling in an area near the pit (Figure 64). The piling procedure was considered in order to follow grade flow from ore deposit to stockpiles. In particular, exact information from mine face to ship loading, haulage and dumping in the specific area should be gathered. Selected parts of the blasted panels were carried at regular intervals to specific locations within the HP and LG stockpiles and dumped separately (schematically in Figure 71). For the haulage construction, the volume transported was equated to a 35-ton truck capacity, which amounts to about 1/3 of estimated block volume. Therefore, the elementary stockpile model is conditioned by truck width and height, and so block dimension is considered 1 m high, 3 m large and 4 m long. Finally, based on the original information and blast-hole samples regularized over a length of 10 m (Figure 71), it was assumed that the 3 cells (as blocks) and cells were comprising the blocks delivered to the stockpiles with the equal grade.

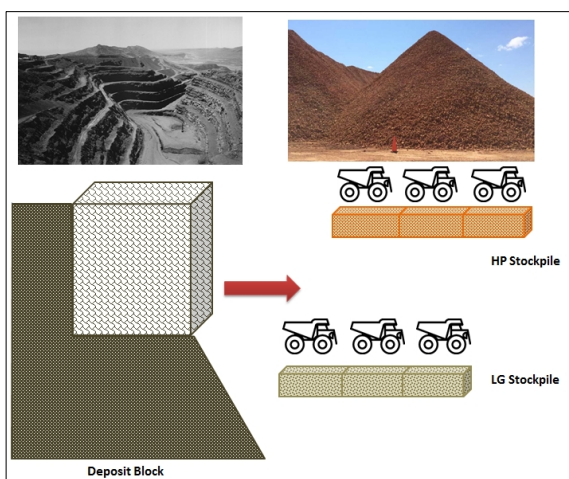


**Figure 71.** Simplified flowchart of piling modelling from ore deposit

Regarding stockpiles geometry, construction of the piling procedure considered that a level is filled by parallel lines, and when one line is completed, a new line is piled up. When one level is filled, a new level is started. Since the excavated benches are a constant height (10 m), the heights of each pile sequence (line/level) produced due to the height trucks can make (about 1 m). Subsequently, grade spatial variability in the reconstructed stockpiles (built up with the same support) can be compared with the specific part of the ore body excavated and transported to the stockpiles (main 5-panel ore body). The experimental and model variograms of piling cell grades along and across the piling directions are shown in Figures 72 and 73. Lag distance is about 5.0 (m).

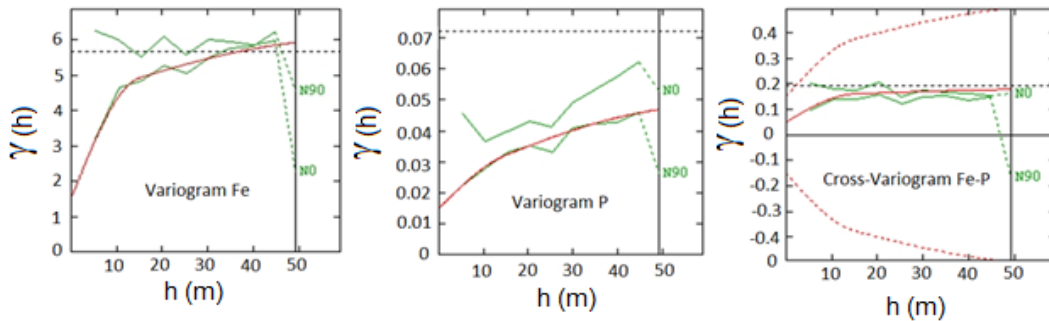


**Figure 72.** Structural analysis of cells grades of simulated HP pile in two orthogonal directions, N0 and N90

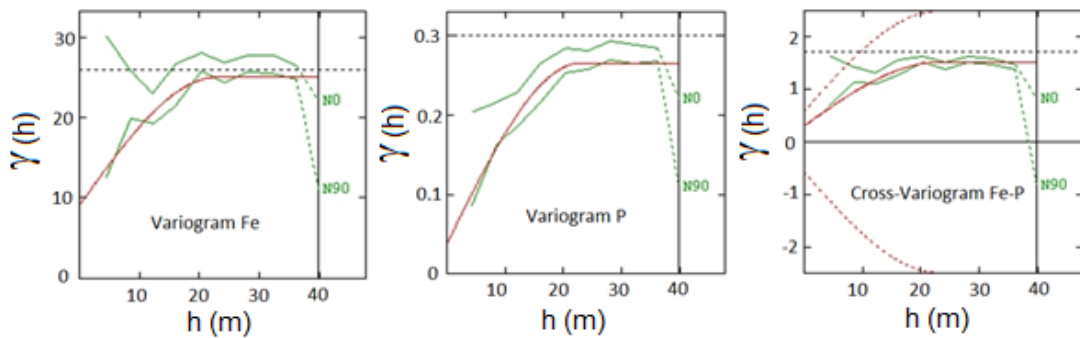


**Figure 73.** Structural analysis of cell grades of simulated LG pile in two orthogonal directions, N0 and N90

According to the experimental variograms, no orthogonal spatial correlation was found for Fe in North-South direction (N0) because of the particular ore disposal process. In contrast, P grades did show some orthogonal spatial correlation to the piling lines, both for HP and LG stockpiles. Further investigation should be carried out to verify and explain this finding, which is probably linked to the long-range structure observed in deposit block grades.

As the main East-West direction (N90) coincides with the direction of stockpile material disposal, stockpile variograms might be expected to have the same spatial behavior as the main 5-panel resource (from ore body) but no orthogonal spatial behavior. The fact that stockpiles are artificial constructions built up in a series of different layers with selected panels placed in proximity to each other is one of the reasons for the lack of orthogonal structure. The variograms in Figures 72 and 73 show the complete absence of Fe spatial correlation in direction N0 (orthogonal to material disposal). In contrast, P grades in HP and LG stockpiles still maintain some orthogonal spatial correlation to piling lines. In addition, the finding of one ore body panel placed in three stockpile sequences (Figure 71) requires further investigation and verification of its probable link to the long-range structure observed (Figures 72 and 73). Since the regular piling sequences maintain the spatial correlations along the direction of disposal, the range of structures in HP and LG stockpiles increases.

## 6.5 CONCLUSION

Numerical modeling of Choghart stockpile using estimated data from stockpiles allows the assessment and the comparison of piling design sequences with

selected parts of the deposit. This modeling technique also produces comparisons of spatial variability of the grade distribution of the main variables (Fe and P) of the two stockpiles. This can be performed by comparing structural analyses of the stockpiles and main ore body (selected panels).

A simple, rapid verification method is a grade spatial variability coherence check in the stockpiles. Figures 72 and 73 show the results of a check from stockpile cell grade variability. According to the piling process construction, the mean of grades and variance of estimated grades of selected blocks should be constant in the piling procedure. This statement is strongly supported by the study because the results of the CK estimation are directly used for stockpile reconstruction. In addition, the horizontal variability along truck discharge lines may be expected to remain unaltered. The same spatial structure was observed within an increased range of a couple of meters (Figure 72 and 73) and with differentiable behavior near the origin due to the artificial homogeneity introduced by giving the same grade to three sequential cells in stockpiles. As mentioned in Section 6.4 (Stockpile modeling), as expected, variability without spatial correlation (nugget) was in fact observed in the direction orthogonal to piling disposal (Table 21). This is due to the fact that, once a row is finished, the next one is started either with materials from the same block (now deposited at the initial position) or from a subsequent block (Figure 74).

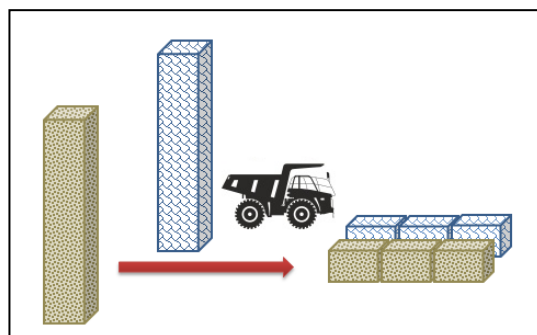


**Figure 74.** Scheme of stockpiling procedure from the panels

Table 21 shows the proper expectations (or predictions) in the case of spatial structure comparisons. The spherical spatial models are followed with a larger range in the stockpiles (because the materials from one panel of stockpiles are more widely spread out into three larger but thinner layers in stockpiles) (Figures 71, 74, and Table 21). In the case of HP, for example, adding the nugget effect to the sill of the Fe variograms in the HP blocks (the HP part of the estimated panels), the variance will be equal to  $6 (\%)^2$  ( $3.7 (\%)^2$ ) the first structure sill +  $0.8 (\%)^2$  the second structure sill +  $1.5 (\%)^2$  nugget effect of Fe variogram). The result is equal to the Fe variance in variograms of the HP stockpile ( $2.8 (\%)^2$ ) the first structure sill +  $1.7 (\%)^2$  the second structure sill +  $1.5 (\%)^2$  nugget effect of Fe variogram).

This proves that in this case study, the stockpiles have the same (spherical) model as the selected part of the deposit, with the same variance and a larger range. The same method can be applied for the LG stockpile with same variance equal to 25 for the Fe variable:

The Fe sill (equal to  $22(\%)^2$ ) + nugget effect of Fe variogram (equal to  $3(\%)^2$ ) in the LG blocks in comparison to the Fe sill (equal to  $16(\%)^2$ ) + nugget effect of the Fe variogram in the LG pile (equal to  $9(\%)^2$ ) from Table 21.

**Table 21.** comparison of variogram parameters of structured (spherical/spherical) components in stockpiles and deposit blocks

Variogram	Model	Range(m)	Sill-Fe (%) <sup>2</sup>	Sill-P (%) <sup>2</sup>	Sill Fe/P (%) <sup>2</sup>	Nugget Fe (%) <sup>2</sup>	Nugget P (%) <sup>2</sup>	Nugget Fe/P (%) <sup>2</sup>
HP-blocks	Spherical	8	3.7	0.005	0.06	1.5	0.150	0.12
		35	0.8	0.028	0.00			

HP-pile	Spherical	15	2.8	0.008	0.10	1.5	0.150	0.05
		60	1.7	0.025	0.03			
LG-blocks	Spherical	7	22.0	0.235	1.51	3.0	0.030	0.00
LG-pile	Spherical	23	16.0	0.228	1.21	9.0	0.037	0.30

This comparison is also applied to P modeling and Fe/P cross variograms.

Comparing the result of variogram modeling of piles with the geostatistical parameters of selected blocks from the main deposit allows approximation of pile grade spatial distribution and variability without resorting to extra sampling. Piling sequences can be reconstructed, referencing the data of the volumes transported to specific pile locations. Figure 75 shows Fe (%) distribution in HP and LG stockpiles after piling reconstruction.

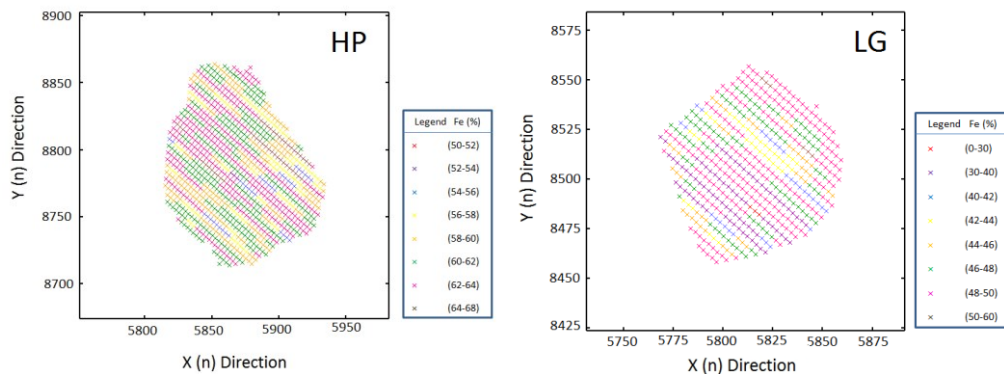


**Figure 75.** Map of Fe (%) variability in HP (left) and LG (right) stockpile obtained by construction piling procedure

Assessing Fe (%) variability in stockpiles (Figure 75) allows mine planning decisions, regarding future stockpile excavation, processing feasibility, sampling advisability and most appropriate excavation site.

Stockpile reserves and grade variability can also be evaluated using the Grade-Tonnage curves. Figure 76 gives the grade-tonnage curves only for iron in LG and HP stockpiles. Curves and pile grade variability are considered to be of assistance to managing decisions regarding sampling with a view to stockpile exploitation and the economic feasibility of waste materials as a new source.

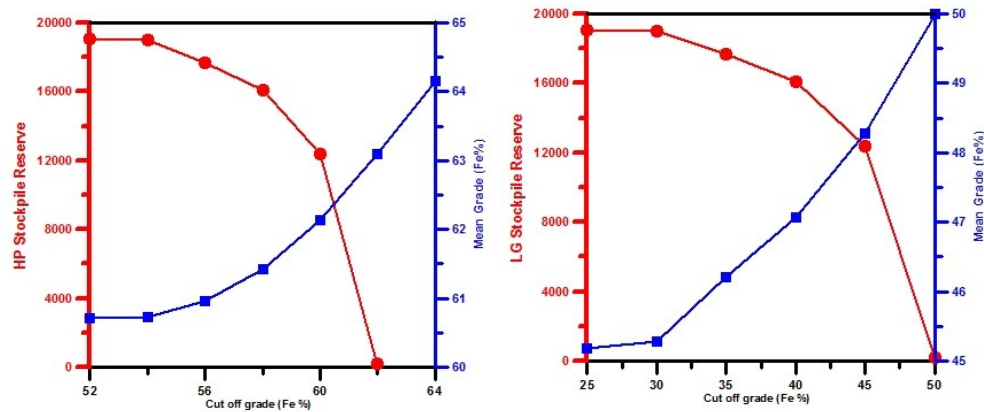


**Figure 76.** Grade-Tonnage curve for two simulated stockpiles

The methodology of stockpiles reconstruction from selected parts of ore body is simple; it can be implemented in a short “macro”<sup>2</sup> of Excel and may be of use especially when stockpile sampling is not an immediate or appropriate option.

---

<sup>2</sup> The macro of the reconstruction procedure is particular to the case study; according to the piling procedure it can be change from each case to another.



## References

- Abrosimova N, Gaskova O, Loshkareva A, Edelev A, Bortnikova (2015), Assessment of the acid mine drainage potential of waste rocks at the Ak-Sug porphyry Cu–Mo deposit, *Journal of Geochemical Exploration*, doi:10.1016/j.gexplo.2015.05.009.
- Alcolea A, Fernández-López C, Vázquez M, Caparrós A, Ibarra I, Garcíac C, Zarrocad M, Rodríguez R, (2015) An assessment of the influence of sulfidic mine wastes on rainwater quality in a semiarid climate (SE Spain), *Journal of Atmospheric Environment*, doi:10.1016/j.atmosenv.2015.02.028.
- Asad MW A , Dimitrakopoulos R (2012), Optimal production scale of open pit mining operations with uncertain metal supply and long-term stockpiles, *Journal of Resources Policy*, doi:10.1016/j.resourpol.2011.12.002.
- Ataei M, Osanloo M (2003), Methods of calculation of optimal cut off grades in complex ore deposits. *Journal of Mining Science*, doi:10.1023/B:JOMI.0000029314.42174.d9.
- Atkinson. P, and Tate. N, (2000), Spatial scale problems and geostatistical solutions: a review, *The Professional Geographer*, Vol. 52 , Iss. 4.
- Armstrong, M., (1998), *Basic Linear Geostatistics*. Berlin, Heidelberg: Springer Berlin Heidelberg, 154pp.
- Bascetin A and Nieto A, (2007), Determination of optimal cut-off grade policy to optimize NPV using a new approach with optimization factor, *Journal of South African Institute of Mining and Metallurgy*. ISSN 0038–223X/3.00 + 0.00.

Bassani, M. A. and Costa, J., (2016), Grade estimation with samples of different length Grade estimation with samples of different length. *Journal of Applied Earth Science*, 0(0), 1–6.

Bonyadi, Z., Davidson,G. J., Mehrabi, B., Meffre, S., Ghazban, F., (2011), Significance of apatite REE depletion and monazite inclusions in the brecciated Se-Chahun iron oxide–apatite deposit, Bafq district. Iran: *Journal of Insights from paragenesis and geochemistry*. *Chemical Geology* 281 P253–269.

Borook D.M., Kesler S.E., Boer R.H. and Essene E.J. (1998), The Vergenoeg magnetite-fluorite deposit, South Africa: support for a hydrothermal model for massive iron oxide deposits, *Economic Geology*, 93: 564-586.

Cairns. R.D. and Shinkumab. T, (2004), The choice of the cutoff grade in mining, *Journal of Resources Policy*, Volume 29, Issues 3–4, Pages 75–81, <http://dx.doi.org/10.1016/j.jrpol.2004.07.001>.

Calcagno, P., Chiles, J.P., Courrioux, G., Guillen,A, (2008), Geological modelling from field data and geological knowledge. Part I. Modelling method coupling 3D potential field interpolation and geological rules. *Physics of the Earth and Planetary Interiors*.

Carrasco.P., Chiles J., Seguret.S, (2008), Additivity, metallurgical recovery and grade. 8th international Geostatistics Congress, Dec 2008, Santiago, Chile.

Castillo S, de la Rosa J D, Sánchez de la Campa A M, González-Castanedo Y, Fernández-Caliani J C, Gonzalez I, (2013), Contribution of mine wastes to atmospheric metal deposition in the surrounding area of an abandoned heavily polluted mining district (Rio Tinto Mines, Spain), *Journal of Science of the Total Environment*, 449 (2013), pp. 363–372.

Chiles J. P. and Delfiner.P., (2012), Geostatistics Modeling Spatial Uncertainty, 2th Edition, WILEY, ISBN: 978-0-470-18315-1, 734pp.

Clark, I., (1977), Regularization of a semivariogram, Journal of Computers and Geosciences, Vol. 3, pp341–346.

Daliran F, (1999), REE geochemistry of Bafq apatites, Iran; implication for the genesis of Kiruna-type iron ores. In: Stancly et al. (Eds.) Mineral Deposits; Processes to Processing. Balkema, Rotterdam, pp. 631-634.

Daliran, F., (2002), Kiruna-type iron oxide-apatite ores and “apatitites” of the Bafq district, Iran, with an emphasis on the REE geochemistry of their apatites, in Porter, T.M. ed., Hydrothermal iron oxide copper-gold & related deposits: A global perspective: PGC Publishing, Adelaide, v. 2, p. 303-320.

Des FitzGerald, Chilès, J.P., Guillen, A., (2009), Delineate 3D Iron Ore Geology and Resource Models Using the Potential Field Method. The Iron Ore Conference 27-29 July.

Dimitrakopoulos R, Dagbert M (1993), Sequential modeling of relative indicator variables: Dealing with multiple lithology types. In: Soares A (ed) Geostatistics Tr’oia ’92. Kluwer, Dordrecht, The Netherlands, pp 413–424.

Dowd, P.A., and Pardo-Ig’uzquiza, E., (2005) Estimating the boundary surface between geologic formations from 3D seismic data using neural networks and Geostatistics,Geophysics,VOL. 70, NO. 1; P. P1–P11, 12 FIGS.10.1190/1.1852783.

Emery,X, J.M. Ortiz, and A.M. C ceres, (2008), Geostatistical modeling of rock type domains with spatially varying proportions: application to a porphyry copper deposit, The Journal of The Southern African Institute of Mining and Metallurgy, Volume 108.

FORTRAN software, website: <http://www.pgroup.com>.

Frietsch R. (1978), On the magmatic origin of the iron ores of the Kiruna-type. *Ibid.*, 73: 478-485.

Förster, H. and Jafarzadeh, A., (1994), The Bafq mining district in Central Iran - a highly mineralized Infracambrian volcanic field: *Economic Geology*, v. 89, p. 1697-1721.

Glachen, I.M. and Snowden, D. V., (2001), Mineral resource estimation, Melbourne, The Australasian Institute of Mining and Metallurgy, 2001: 189–198.

Gossage, B., (1998), The Application of Indicator Kriging in the modeling of geological data , Symposium on Beyond Ordinary Kriging, West Perth WA Australia.

Gholamnejad,J., Ansari,A.H., Yarahmadi Bafghi, A. and Taqizadeh, M., (2010), Determination of Ore/Waste Contacts by Using Indicator Kriging, Case Study: Choghart Iron Mine of Iran, *International journal of engineering*. Vol. 23, Nos. 3 & 4.

Gholamnejad J, Kasmaee S (2012), Optimum blending of iron ore from Choghart stockpiles by using goal programming, *Journal of Centre of South University*. doi: 10.1007/s11771-012-1112-4.

Guarascio. M, Raspa.G, (1974) Valuation and production optimization of a metal mine, Proceedings of the 12 International APCOM Symposium. Vol II, Golden, Colorado, pp.50-64

Guezennec A G, Bru K, Jacob J, Hugues P (2015), 2-Co-processing of sulfidic mining wastes and metal-rich post-consumer wastes by bio hydrometallurgy, *Journal of Minerals Engineering*, doi:10.1016/j.mineng.2014.12.033.

Gy PM (1982), Sampling of Particulate Materials: Theory and Practice, Elsevier Scientific Pub. Co. New York .pp. 23-33.

He Y, Zhu K, Gao S, Liu T, Li Y (2009), Theory and method of genetic-neural optimizing cut-off grade and grade of crude ore, Journal of Expert Systems with Applications. doi:10.1016/j.eswa.2008.09.018.

ISATIS software, website: <http://www.geovariances.com>.

Journel, A.G., (1983), Nonparametric estimation of spatial distributions, Journal of Mathematical Geology, 15(3): 445–468.

Journel, A.G., Huijbregts.C.J., (1991), Mining Geostatistics. Academic Press, London, 600 pp.

Jupp K., Howard T. J. and Everett J.E, (2013), Role of pre-crusher stockpiling for grade control in iron ore mining, J Applied Earth Science ; 122(4), 242-255, doi: <http://dx.doi.org/10.1179/1743275814Y.0000000045>.

Kameshwara Rao.V, Narayana1. A. C., (2015), Application of nonlinear geostatistical indicator kriging in lithological categorization of an iron ore deposit, Current science, Vol. 108, NO. 3.

Kasmaee. S., Torab. F., (2014), Risk reduction in Sechahun iron ore deposit by geological boundary modification using multiple indicator Kriging. Journal of Central South University, 21(5).

King B, (2001), Optimal Mine Scheduling Policies. Dissertation, Royal School of Mines, Imperial College, London University, UK.

Krige, D. G., (1951). A statistical approach to some basic mine valuation problems on the Witwatersrand. Journal of the Chemical, Metallurgical and Mining Society of South Africa, December, 119\_139.

Kumral O.M, (2006), Bed blending design incorporating multiple regression modelling and genetic algorithms, Journal of Southern African Institute of Mining and Metallurgy, vol. 106, no. 3, pp. 229-236. ISSN 0038-223X/3.00 + 0.00.

Larrondo P. F. and Deutsch C. V., (2004), Methodology for Geostatistical Model of Gradational Geological Boundaries: Local Non-stationary LMC. In Centre for Computational Geostatistics, volume 6, Edmonton, AB.

Lèbre, E., Corder, G.D., Golev, A., (2016), Sustainable practices in the management of mining waste: A focus on the mineral resource, Journal of Minerals Engineering, <http://dx.doi.org/10.1016/j.mineng.2016.12.004>.

Lillah,M., Boisvert, JB., (2012), Stochastic Distance Based Geological Boundary Modeling with Curvilinear Features, International Association for Mathematical Geosciences, DOI 10.1007/s11004-012-9426-1.

Marinoni, O., (2003), Improving Geological Models Using a Combined Ordinary–Indicator Kriging Approach. *Engineering Geology* 69. 37–45.

Marques D.M, Costa J. F., Ribeiro D., and Kopp J. C., (2009), The evidence of volume variance relationship in blending and homogenisation piles using stochastic simulation, in Proceedings of the 4th World Forum on Sampling and Blending, Fourth World Conference on Sampling & Blending, Journal of Southern African Institute of Mining and Metallurgy, pp. 235-242.

Márlon A. Longhi, M.A., Rodríguez, E.D., Bernal, S.A., Provis, J.L., Kirchheim, A.P, (2016), Valorization of a kaolin mining waste for the production of geopolymers, *Journal of Cleaner Production*, Volume 115, Pages 265–272.

Matheron G., (1982b), La déstructuration des hautes teneurs et le krigeage des indicatrices, Technical Report N.761, Centre de Géostatistique, Fontainebleau, France.

Matheron, G., (1971), The Theory Of Regionalized Variables And Its Application. École Nationale Supérieure des Mines de Paris, Mathematical Statistics, 211pp.

Meagher C, Dimitrakopoulos R, Avis D., (2008), A new approach to constrained open pit pushback design using dynamic cut off grades, COSMO Research Report, Department of Mining and Materials Engineering, McGill University, doi: 10.1134/S1062739114040140.

Moor FM, Modabberi S., (2003), Origin of Choghart Iron oxide deposit, Bafgh Mining district, central Iran: new isotopic and geochemical evidence. Journal of Sciences Islamic Republic of Iran, University of Tehran 14(3): 259-269, ISSN 1016-1104.

Mücke, A. and Younessi, R., (1994), Magnetite-apatite deposits (Kiruna-type) along the Sanandaj-Sirjan zone and in the Bafq area, Iran, associated with ultramafic and calcalkaline rocks and carbonatites: Mineralogy and Petrology, v. 50, p. 219-244.

National Iranian Steel Corporation, (1975), Report on detailed exploration of Se-Chahun iron ore deposit in Central Iran. National Iranian Steel Corporation (NISCO), Tehran.,117 pp.

Nyström J.O. and Henriquez F., (1994), Magmatic features of iron ores of the Kiruna type in Chile and Sweden: ore textures and magnetite geochemistry. Economic Geology, 89: 820-839.

Oliver, M., Webster, R., (2014), A tutorial guide to geostatistics : Computing and modelling variograms and kriging., Journal of Catena, 113, 56-69.

Ortiz, J.M., Emery, X., (2005), Estimation of mineral resources using grade domains: critical analysis and a suggested methodology, The Journal of The Southern African Institute of Mining and Metallurgy, Volume 105.

Ortiz, J.M., Emery, X., (2006), Geostatistical estimation of mineral resources with soft geological boundaries: a comparative study, The Journal of The Southern African Institute of Mining and Metallurgy, Volume 106.

Osanloo M, Rashidinejad F, Rezai B., (2008), Incorporating environmental issues into optimum cut off grades modeling at porphyry copper deposits. Journal of Resources Policy . doi:10.1016/j.resourpol.2008.06.001.

Rivoirard J., (1987), Two key parameters when choosing the kriging neighborhood, Journal of Mathematical geology, Vol.19, No.8.

Rivoirard J. (1994), Introduction to Disjunctive Kriging and Non-linear Geostatistics. Oxford University Press, Oxford.

Samani, B., (1993), Saghand formation: A riftogenic unit of upper Precambrian in central Iran, Geoscience Scientific Quarterly Journal of Geological Survey of Iran, 2(6): 32–45.

Serra J., (1982), Image Analysis and Mathematical Morphology. Academic Press, London.

Séguret S. A., (2011), Block model in a multi facies context – Application to a porphyry copper deposit. In Beniselli J, ed. Proceedings of Geomin2011- Second International Seminar on Geology for the Mining Industry, Gecamin, Santiago, Chile.

Séguret, S.A., (2012), Analysis and estimation of multi-unit deposits: Application to a porphyry copper deposit 1, (September 2012), 1–42. <http://doi.org/10.1007/s11004-013-9475-0>.

Séguret, S.A., (2015), Geostatistical comparison between blast and drill holes in a porphyry copper deposit, 7<sup>th</sup> world conference on sampling and blending, Bordeaux, France.

Soares A., (1992), Geostatistical estimation of multiphase structures: Math. Math Geol 24(2):149–160.

Sracek O, Gélinas P, Lefebvre R, Nicholson R.V., (2006), Comparison of methods for the estimation of pyrite oxidation rate in a waste rock pile at Mine Doyon site, Quebec, Canada Journal of Geochemical Exploration, doi:10.1016/j.gexplo.2006.03.002.

Torab FM. and Lehman BL., (2006), Iron oxide-apatite deposits of the Bafq district, central Iran: an overview from geology to mining, World of Mining Surface and Underground, Mineralogical Magazine, doi:10.1180/minmag.2007.071.3.347.

Torab FM, (2008), Geochemistry and metallogeny of magnetiteapatite deposits of the Bafq Mining District, Central Iran, Doctoral Thesis, Clausthal University of Technology, Germany.

VOXLER software, <http://www.goldensoftware.com/products/voxler>)

Wackernagel,H, (2003), Multivariate Geostatistics An Introduction With Applications. Berlin, Heidelberg: Springer Berlin Heidelberg.387 pp.

Wilde, B.J and Deutsch, C.V., (2012), Kriging and simulation in presence of stationary domains: developments in boundary modeling, DOI: 10.1007/978-94-007-4153-9\_23.

Xinbiao, L. and Pengda, Z., (1998), Geologic anomaly analysis for space-time distribution of mineral deposits in the middle-lower Yangtze area, southeastern China, journal of Natural Resource Research, Volume 7, Issue3, pp 187–196, 7: 187. doi:10.1007/BF02767669.

Zharikov, V.A., Pertsev, F, Rusinov, V.L., Callegari, E., and Fettes, D.J., (2004), Metasomatism and metasomatic rocks, Recommendations by the IUGS Subcommission on the Systematics of Metamorphic Rocks: Web version 01.02.07.